מכון ויצמן למדע
WEIZMANN INSTITUTE OF SCIENCE

Thesis for the degree
Doctor of Philosophy

עבודת גמר (תזה) לתואר
דוקטור לפילוסופיה

Submitted to the Scientific Council of the
Weizmann Institute of Science
Rehovot, Israel

מוגשת למועצה המדעית של
מכון ויצמן למדע
רחובות, ישראל

By
Zhana Haimon

מאת
ז'אנה חימון

ניתוח טרנסלטום מיקרוגליאלי במצב יציב ובמודל עכברי של דלקת מוחית אוטואימונית דלקתית של טרשת נפוצה חוזרת ונשנית.

Microglia Translatome Analysis in Steady State and in a Murine Relapsing-Remitting Model of Multiple Sclerosis

Advisor:
Prof. Steffen Jung

מנחה:
פרופ' שטפן יונג

September 2020

תשרי תשפ"א

Acknowledgments

First and foremost I would like to thank my supervisor and the person that gave me the opportunity to do great science in one of the best places in the world, Prof. Steffen Jung. Thank you for giving me the freedom to think and explore, thank you for teaching me how to think and how to criticize science and for being an inspiration for outstanding curiosity-driven science. Thank you for your support even in personal issues in difficult times. Thank you for always being available by having your door and zoom links open. It was not always easy to convince you, but as a challenge lover it was fascinating for me and taught me a lot, it made me build my independence and confidence as a researcher.

Who always stood there as the light at the end of the tunnel every day are my husband Ariel, and the product of our love – Meir and Hallel. Thank you for giving me the motivation to get up in the morning, thank you for putting a smile on my face every single day. Thank you for celebrating the happy moments, and especially thank you Ariel for wiping my tears and lifting me up during hard times when my self-confidence was at the lowest point, thank you for believing in me and pushing me.

I wouldn't be here if not for my parents, Boris and Sofia, who made me who I am, who educated me to always do my best, work hard (and fast, thanks mom), strive forward and always learn from others.

In this journey I was escorted by so many lab members that have left while I was there and new people that came along, some of which became good friends. Thanks to Louise who was my loyal lab-roommate and friend for almost 5 years, Masha who so quickly became my good friend and confidante, and Biana for always consulting me from one step ahead. Finally, the most stable pillar in the lab, thanks to Sigalit who was always there to say what I don't want (but need) to hear and for all the philosophical and fruitful scientific and non-scientific discussions we had.

Declaration

I hereby declare that this thesis summarizes my independent research.

We collaborated with the lab of Dr. Igor Ulitsky in the Weizmann Institute of Science and his student Binyamin Zuckerman performed the analysis of splicing efficiency, localization and length of RNA in the first part of the thesis (Figure 5D, 5E).

Dr. Shifra Ben-Dor (probably the fastest person in the world) from the Weizmann Institute designed the CRISPR guide RNAs and the genotyping primers and helped with the analysis of the sequences of the mutant mice.

Dr. Rebecca Haffner-Krausz from the Weizmann Institute generated the mutant SJL mice.

Dr. Louise Chappell-Maor performed all the RNA-Sequencing, and served as my 3rd and 4th hands in many of the experiments.

Table of contents

List of abbreviations

CNS - Central nervous system

BBB - Blood-brain barrier

EMP - Erythro-myeloid precursors

YS - Yolk sac

TREM2 - Triggering receptor expressed on myeloid cells 2

AD - Alzheimer's Disease

WT - Wild type

BM - Bone marrow

HSC - Hematopoietic stem cell

WAS – Wiskott-Aldrich syndrome

MS - Multiple sclerosis

EAE - Experimental autoimmune encephalomyelitis

MIA - Maternal immune activation

MOG - Myelin oligodendrocyte glycoprotein

PLP - Proteolipid Protein

MHCII - Major histocompatibility complex class II

IFNγ – Interferon gamma

LPS - Lipopolysaccharide

TF - Transcription factor

TBI - Total body irradiation

BMT - Bone marrow transfer

DEG - Differentially expressed genes

PCA - Principle component analysis

SPF - Specific-pathogen-free

APC - Antigen presenting cell

DC - Dendritic cell

TAK1 - Transforming growth factor β activating kinase 1

SC - Spinal cord

KO - Knockout

GM-CSF - Granulocyte macrophage colony-stimulating factor

JAK - Janus kinase

STAT - Signal transducer and activator of transcription

i.p. - Intra-peritoneal

IP - immunoprecipitation

HA - hemagglutinin

RPL - ribosomal protein large subunit

HSCT - Hematopoietic stem cell transplantation

BAM - Barrier-associated macrophages

TCR - T cell receptor

ROS - Reactive oxygen species

RRMS - Relapsing remitting multiple sclerosis

RR-EAE - Relapsing remitting experimental autoimmune encephalomyelitis

PPMS - primary progressive multiple sclerosis

GWAS - Genome wide association studies

IL - interleukin

EBV - Epstein bar virus

PTx - Pertussis toxin

CFA - Complete Freund's adjuvants

MBP - Myelin basic protein

Th - T helper cell

RORγt - RAR-related orphan receptor gamma

Foxp3 - Forkhead box P3

TLR - Toll-like receptor

MAPK - Mitogen-activated protein kinase

NLRP3 - NLR family pyrin domain containing 3

UTR - Untranslated region

TAM - Tamoxifen

Treg - T regulatory cells

Abstract

Microglia are the resident mononuclear phagocytes of the central nervous system (CNS) parenchyma, sequestered behind the blood brain barrier (BBB). Microglia research has exponentially surged in the past decade as advanced genetic and omics tools are being constantly refined. However, exact functional contributions of microglia in CNS pathologies remain unclear due to difficulties in discriminating resident microglia from infiltrating monocyte-derived macrophages. In my first PhD project, I implemented a new powerful tool by utilizing the RiboTag method, which enables the pulldown of ribosome-attached mRNA from microglia in *Cx3cr1*^{CreER}*:Rpl22*^{HA} mice. A side-by-side comparison of microglia translatomes to total transcriptomes obtained from sorted microglia showed that the RiboTag allowed to discriminate isolation-related artifacts, as well as non-translated and phagocytosed mRNA originating from neighboring cells. In my second main project, I then used the RiboTag for a longitudinal analysis of microglial translatomes throughout the stages of a Relapsing-Remitting Experimental Autoimmune Encephalomyelitis (RR-EAE) model of multiple sclerosis (MS) in (SJL*B6) F1 hybrid mice challenged with PLP peptide. We provide evidence that microglia functionally contribute to remission and transient recovery. Specifically, using advanced image-stream analysis, multicolor immunofluorescence and flow cytometry, we found, evidence for cognate microglia interactions with T cells, and preferentially T regulatory (Treg) cells. Depletion of microglia in *Cx3cr1*^{CreER}:*Rosa26*^{iDTR} mice impaired remission and led to accumulation of T cells in the brain. Microglia-specific gene deletion of the Wiskott-Aldrich Syndrome gene led to a similar delay in recovery. To further pinpoint the mechanism of microglia-T cell interactions and its implications in RR-EAE we used CRISPR-Cas9 mutagenesis to generate mice that harbor microglia-specific deletions of MHC-II and IFNγR1. Collectively, our data suggest that microglia act as critical local antigen presenting cells (APC) that promote Treg proliferation and activity, and allow for remission.

Introduction

Microglia in homeostasis

Microglia are the tissue resident macrophages of the central nervous system (CNS)[1]. As part of their homeostatic functions, microglia use highly ramified processes to constantly scan the surrounding extracellular space[2,3] and communicate with neurons and astrocytes. Microglia have been recognized as critical players in CNS development, homeostasis, and nearly all CNS pathologies. Intrinsic microglia deficiencies can result in neuropsychiatric or neurologic disorders. More specifically, during development microglia engulf neuronal precursor cells, regulate the size of the progenitor pool in the developing cerebral cortex and thereby orchestrate cortical development[4,5]. Accordingly, factors that alter the number or activation state of microglia *in utero*, for instance during maternal immune activation (MIA), are believed to affect neural development and affect behavior[6,7]. Microglia also regulate neuronal circuit plasticity by digesting synapses, a process called synaptic pruning[8]. The latter is important for proper brain development as it controls the number of neuronal synapses. Disruption of these interactions can have a severe negative impact on CNS development and function[9].

Microglia ontogeny

Microglia are derived from myb-independent primitive macrophages that emanate from the embryonic yolk sac (YS) during development (prior to embryonic day 8.5, (E8.5)) and enter the brain rudiment via the circulatory system[10,11,12]. These progenitors surround the neuro-epithelium of the developing brain around E9.5 and one day later enter and colonize the CNS parenchyma[13].

In the adult CNS, sequestered behind the blood-brain barrier (BBB), microglia are characterized by relative radio-resistance and longevity, and are maintained by self-renewal[14,15,16] with no contribution of adult hematopoiesis and circulating blood monocytes. For example, upon their depletion, microglia repopulate from the internal residual pool, but not from blood monocytes[15]. Microglia and CNS border associated macrophages (BAMs) are unique with this respect among tissue macrophages, which receive varying contributions form a second hematopoietic wave and even adult HSC[16], like the gastrointestinal tract[17]. Nevertheless, HSC-derived cells, including monocytes, can infiltrate the CNS under specific experimental settings (irradiation and bone marrow transplantation (BMT)) or under disease

conditions (multiple sclerosis (MS) and other neuropathological disorders). In the murine MS model, Experimental autoimmune encephalomyelitis (EAE), for example, monocytes infiltrate the parenchyma but do not persistently contribute to the microglial compartment[18]. However, upon irradiation and BMT, when the BBB is compromised, CX_3CR1^{neg} hematopoietic precursors enter and seed the brain and finally differentiate into microglia-like cells. The latter cells persist and acquire characteristic microglia morphology and relative radio-resistance, but remain transcriptionally and epigenetically distinct from microglia even after a prolonged CNS residency[19,20]. Microglia are thus a unique macrophage population of the CNS with distinctive developmental and functional characteristics that are either linked to their YS origin, or acquired early during their development in the CNS and cannot be mimicked by other immune cells.

Microglia in pathology

In the context of pathologies, microglia sense the damaged tissue and respond by retraction of their long processes, and transform into an activated amoeboid morphology[21]. Microglia proliferate in response to damage[22] and can migrate to sites of injury[3], where they phagocytose dead cells and cell debris, produce pro-inflammatory molecules and cytokines and start to express molecules allowing interactions with other immune cells, such as MHC-II and CD40[23]. In many pathologies microglia are considered neurotoxic, as their activation was found to correlate with degenerated neurons and demyelination[24], although this remains largely 'guilt by association'. In contrast, in demyelinating disorders, microglia need to phagocytose and clear dead cells and debris from the damaged tissue in order to enable remyelination[25]. In Alzheimer's Disease (AD), activated microglia co-localize with toxic amyloid beta plaques and degenerated neurons[26,27]. In multiple sclerosis (MS), activated microglia co-localize with lesions of demyelination and immune infiltrates[28,29]. However whether the activation of microglia is the cause or the consequence of the pathological conditions, and what is their relative contribution, remains to be determined[30].

Upon aging, microglia become dysfunctional, lose a part of their homeostatic molecular signature and show functional impairments, such as increased production of proinflammatory cytokines and impaired phagocytosis[31,32]. Moreover, the cells accumulate lipid droplets that interfere with their phagocytic function and lead to the secretion of ROS and pro-inflammatory cytokines[33]. Impaired phagocytosis of aging microglia has been linked to their expression of

CD22, blockade of which can re-stimulate phagocytosis by microglia and delay age-related cognitive decline[34].

Multiple sclerosis

Multiple sclerosis (MS) is the most common chronic inflammatory disease of the CNS and affects ~2.5 million people worldwide[35]. Clinical MS manifestations are diverse and include sensory and visual problems, fatigue, cognitive defects, and motor disturbances[35]. The variation in clinical manifestations correlates with the location of lesions within the CNS[36,37]. These lesions are a hallmark of MS and result from immune cell infiltration across the BBB that promotes inflammation, demyelination, gliosis and neuroaxonal degeneration, leading to disruption of neuronal signaling[38]. T cells appear early in lesion formation, and the disease is considered to be autoimmune, initiated by autoreactive lymphocytes that mount aberrant responses against CNS autoantigens, the precise nature of which, however, remains unknown.

The individual disease course of MS patients can considerably vary: the majority of patients (85%) display a relapsing-remitting (RR) form, where recurrent episodes of neurological dysfunction are followed by remission periods of clinical recovery[35]. Relapses are characterized by lesions of inflammation and demyelination in the CNS white matter. After years of RR episodes, damage gradually accumulates, resulting in secondary progressive MS with no recovery, where patients display atrophy of the CNS and decreased brain volume. About 10% of patients display primary progressive MS form (PPMS) that is characterized by gradual decline from onset with no recovery[35].

The exact etiology of MS is still unknown, but it is widely accepted to be induced by both genetic and environmental factors. Genome wide association studies (GWAS) identified more than 100 genetic regions to be associated with MS[39], many of which are related to the immune system. This includes the Major Histocompatibility Complex class II (MHC-II)[40], Interleukin-2 Receptor alpha (IL2RA)[41] and Interleukin-7 Receptor alpha (IL7R)[41], and collectively points at defects in central or peripheral tolerance and T cell functions. Potential environmental factors include viral of bacterial infections that might trigger autoreactive T cells through molecular mimicry. In addition, high levels of EBV-specific antibodies were found to correlate with increased risk of MS[42], and it was suggested that also B cell dysregulation during EBV infection might lead to T cell activation[43,44]. Surprisingly, some MS patients were for instance shown to significantly benefit from anti-CD20/ Rituximab mediated B cell depletion[45,46].

Infiltration of immune cells from the periphery, which is particularly prominent in the common relapsing-remitting form of the disease, has been the main target of currently available MS therapies[47]. Although these broad-spectrum immunomodulatory drugs reduce immune cell activity and entry into the CNS and decrease relapse frequency, they do not substantially halt the disease, and neurological damage as well as physical disability continue to accumulate and become permanent[47].

Experimental Autoimmune Encephalomyelitis (EAE)

Seminal work of Avraham Ben-Nun at the Weizmann Institute and studies by others have led to the establishment of a mouse model for MS: Experimental autoimmune encephalomyelitis (EAE) [48,49,50].

EAE is induced by peripheral immunization of mice with myelin-specific proteins or peptides in combination with complete Freund's adjuvants (CFA), and Pertussis toxin (PTx) injections[51]. EAE shares an autoimmune etiology with MS and is characterized by BBB disruption and infiltration of immune cell into the CNS[52,53,54]. EAE models vary with respect to mouse strains used (C57BL/6, SJL, NOD), and the regimen of the myelin component immunized with (proteolipid protein (PLP), myelin basic protein (MBP), myelin oligodendrocyte glycoprotein (MOG)), presenting different patterns of disease[55]. One of the most commonly used MS models involves the challenge of C57BL/6 mice (H-2^b) with MOG_{35-55} peptide that yields chronic EAE with no recovery. This model allows to investigate the underlying mechanisms of peripheral autoimmunity induction and disease onset. It enabled for instance to define the critical role of autoreactive Th17 and monocyte infiltrates for disease development[56,57]. However, the monophasic EAE observed in this model does not allow the study of mechanisms involved in recovery and relapse that are characteristic of MS. Study of these processes require alternative models that display a RR-EAE disease course, such as SJL (H-2^s) mice or (B6*SJL) H-$2^{b/s}$ hybrids, immunized with PLP peptide[58].

T cells in EAE

In EAE, naïve $CD4^+$ T cells are primed in peripheral lymph nodes, and differentiate locally into T helper (Th) subsets. Type 1 (Th1) cells are controlled by the transcription factor (TF) Tbet and produce IFNγ, while Th17 express the TF RORγt and produce IL-17. Pathogenicity of Th17 cells requires further differentiation into so-called Th17* cells[59], that produce GM-

CSF[57,60]. Generation of Th17* cells require interleukin-23 receptor (IL-23R) and IL-1R, but not IL-6R signaling for their maintenance and pathogenicity[57].

Both Th1 and Th17* cells have been linked to CNS autoimmunity in active MS lesions[61,62]. Transfer experiments of *in-vitro* primed $CD4^+$ T cells taken from lymph nodes of MOG immunized mice, as well as from naive mice harboring a MOG specific TCR transgene (2D2), revealed that both Th1 (primed with IL-12) and Th17 (primed with IL-23) individually encompasses pathogenic potential to infiltrate the CNS and induce EAE[63,64,65]. Interestingly, even though injections of IFNγ alone can cause EAE-like symptoms[66,67], IFNγ is not essential for this process, since IFNγ KO mice were not only able to develop EAE, but actually developed an exacerbated disease[68,69,70,71]. This suggests a more complex role of IFNγ in EAE[72,73]. In contrast, GM-CSF produced by pathogenic Th17* cells has a non-redundant encephalitogenic property by promoting recruitment of monocytes and neutrophils that further enhance tissue destruction[56,57].

The control of inflammation is largely mediated by T regulatory (Treg) cells[74]. Treg depletion in 2D2 mice triggers EAE[75]. Treg cells can be generated in the thymus or induced peripherally in the course of T cell activation[76]. Both thymic and peripherally-induced Treg (tTreg, pTreg) are controlled by the Foxp3 transcriptional program and are characterized by the ability to control inflammation, partially by producing the anti-inflammatory cytokine IL-10. Recently it was shown that $Foxp3^+$ Tregs rely on the transcription factor Blimp1 in order to stabilize Foxp3 expression to enable the production of IL-10 for the control of EAE[77].

Following infiltration into the CNS, Tregs undergo TCR selection and clonal expansion[78,79]. In order to propagate regulatory functions, Treg cells depend on TCR signaling[80,81]. $Blimp1^+$ Treg cells are enriched in the CNS compared to the spleen and lymph nodes, further supporting the idea of local proliferation of these cells[77]. However, which local antigen presenting cells (APCs) mediate the Treg expansion and selection process and what molecular mechanisms govern Treg responses in EAE is not known.

The role of mononuclear phagocytes in EAE

The pathological features of EAE, i.e. the demyelination and ensuing neurodegeneration, are known to be caused by autoreactive T cells[82]. However, also pro-inflammatory monocytes are crucial for EAE development, as depletion of these cells prevents or delays EAE induction[83,84]. As monocytes infiltrate the CNS, they differentiate into macrophages and become with time indistinguishable from resident microglia with respect to morphology and

cell surface markers[85]. For this reason histopathology analysis, but also genetic targeting of myeloid cells, generally failed to differentiate between microglia and monocyte-derived macrophages[28], despite the fact that the two are distinct with respect to ontogeny and function[16]. This led to the probably erroneous assumption that microglia are pathogenic, since microglia/macrophages co-localized with degenerated neurons, secreted proinflammatory molecules and seemed to present antigens, which were considered to reactivate T cell in the CNS[86]. In addition, microglia/macrophages could also be found in nodules in MS patients and were associated with degenerated neurons[87]. However it remains unclear whether these nodules are the cause or the consequence of the degeneration, whether they comprise microglia or monocyte-derived macrophages, and what are the specific contributions of the latter two cell types.

Microglia in EAE

As the resident myeloid cell in the brain parenchyma and with the ability to present antigen and secrete cytokines and chemokines[88], microglia are a natural prime suspect for involvement in MS pathology. The main challenge in studying microglia specific contributions in EAE and MS, is their discrimination from infiltrating monocyte-derived macrophages[89].

Histological examination of CNS tissues of MS patients indicate that focal lesions of active demyelination and neurodegeneration are characterized by microgliosis[28]. TMEM119^{+} microglia can be found at the rim of active MS lesions, and microglia are proposed to be responsible for phagocytosis of myelin debris and dead cells, an essential process to enable remyelination[90]. Activated microglia can also be found in normal appearing white matter as clusters, termed as “microglial nodules”, associated with degenerated neurons and are therefore proposed to be pre-active lesions[87].

In mice, microglia-specific ablation of the MAPK kinase TAK1, that is critical for IL1 and TLR signaling, was shown to attenuate EAE development[91], suggesting a pathogenic role of microglia. Beneficial microglia contributions are suggested by the fact that microglia-specific ablation of the deubiquitinating enzyme A20, that controls NFκB activation, worsened EAE through hyperactivation of the NLRP3 inflammasome and enhanced IL-1b secretion[92]. Moreover, phagocytosis of myelin debris and dead cells by microglia is important for remyelination[25].

The upregulation of MHC-II expression and expression of costimulatory molecules upon activation of microglia, suggested that microglia might act as local APC that re-activate

pathogenic T cells upon entry to the CNS[93]. However, our laboratory established that microglial MHC-II is dispensable for EAE induction in the chronic model in C57BL/6 mice[94].

Collectively, the role of microglia in EAE and MS remains to be defined. Questions remain as to whether microglia are more than just phagocytes? Whether, as the only CNS immune cells and keepers of brain homeostasis, microglia interact with immune infiltrates to shape immune responses? And if so, what is their specific contribution? For instance, it is yet to be determined if microglial MHC-II has a role in EAE at later stages, and whether microglial antigen presentation is critical in the context of recovery.

Limitations of bulk and single cell transcriptome profiling

In the recent years, there has been an exponential growth of single cell (sc) transcriptome data in the field of microglia in pathologies and specifically in EAE[95,96,97,98,99,100] and concomitantly "new" sub-populations of microglia or "new" myeloid cell populations have emerged. However, despite the detailed gene expression data, so far little evidence for functional significance of these findings is available. Of note, transcriptomics, including the single cell approach, encompass several technical shortcomings: (1) transcriptomes reflect the mRNA repertoire but not the protein expression; (2) not all of the mRNAs contained in the cell are translated, rather some are sequestered in organelles, such as the nucleus or processing bodies (P-bodies), and therefore do not necessarily reflect a functional contribution[101]; (3) when analyzing phagocytes, such as macrophages, the cellular mRNA can include 'foreign transcripts' originating from phagocytosed material[102]; (4) particularly, single cell (sc) RNAseq analysis is technically limited with the depth of sequencing, with often only ~10% of the cellular mRNA sequenced, resulting incomplete coverage[103,104]; (5) bulk and sc transcriptomics of specific primary cells require cell isolation, which induces cell activation[105,106]. The above concerns have led researchers to develop alternative technologies, such as TRAP and RiboTag[107,108], that take advantage of genetic approaches to isolate *bona fide* translated, ribosome-associated mRNAs, i.e. the translatome, from tissue context without prior cell isolation.

In this work we aimed to better characterize microglia and study their specific role in EAE, an autoimmune demyelination and neurodegeneration disease modeling MS. In the first part of our study, we implemented the RiboTag approach, a method for the isolation of ribosome-attached translatome[107], to more specifically characterize the microglial expression profile. In

this (published) work[102] we show the superiority of RiboTag translatome analysis over classical transcriptome directed strategies that encompass non-translated and engulfed mRNA. In the second part of this thesis, we took advantage of the additional genetic fate map feature of the RiboTag approach to profile microglia throughout the stages of a relapsing and remitting EAE disease. The translational profile of microglia strongly suggested interactions of the cells with T cells, a notion that is also supported by immune-histochemistry and advanced flow cytometry. To directly probe for functional contributions of microglia to remission and relapse, we have generated mutant mouse lines that enabled specific conditional deletion of *Mhc-II*, *Ifngr1* and *Was.* Analysis of these animals is in progress.

Objectives

1. **Implementation of RiboTag-based translatome analysis of microglia.**

   Current sort-based mRNA-sequencing strategies allow the retrieval and sequencing of whole cell transcriptomes. The latter include, on top of the translated mRNA, regulatory long-non-coding (lnc) mRNAs, as well as incompletely spliced nuclear pre-mRNAs. In addition, and in particular in phagocytic cells such as microglia, transcriptomes are contaminated by mRNA from ingested neighboring cells. Isolation of cells from tissue context can be challenging, moreover tissue dissociation into single cell suspension, which is required for cell sorting, results in transcriptional changes and cellular reprogramming. All of the above can lead to misleading information when analyzing transcriptomes retrieved from sorted cells. We therefore decided to establish in our lab the RiboTag system, in which Cre recombinase-mediated recombination induces expression of HA-Tagged ribosomes in specific cells in the tissue, that can with their attached mRNA be immunoprecipitated from crude tissue homogenates. To establish the RiboTag approach for microglia research we used CX_3CR1^{CreER} mice and systematically compared retrieved translatomes to transcriptomes of sorted microglia, and studied the impact of cell dissociation on mRNA expression. The results of this study have been published. (*Haimon et al. Nat. Immunology, 2018*).

2. **Defining functional contributions of microglia in relapsing remitting EAE.**

   The role of microglia in multiple sclerosis (MS) and its mouse model experimental autoimmune encephalomyelitis (EAE) remains unclear. One reason for this is the difficulty to discriminate resident microglia from monocyte-derived macrophages (MoMf), that infiltrate the CNS in MS and EAE. Although these cells share some surface markers and are morphologically similar, microglia and MoMf differ with respect to ontogeny and function and their distinction is hence crucial for the understanding of the mechanisms that govern EAE and MS. The majority of MS patients display a relapsing and remitting form of MS, in which recurrent episodes of disability are followed by remission. Monocytes and monocyte-derived cells play a key pathogenic role in the initiation of EAE. Microglia/macrophages phagocytose cell debris and clear the environment from dead cells. However, microglia functions beyond

phagocytosis, and potential contributions in MS/EAE in relapse and remission remain to be defined. We used a relapsing-remitting model of EAE (RREAE), based on immunization of (SJL*B6) mice with $PLP_{151-179}$ peptide. The use of Tamoxifen-treated *Cx3cr1*^{CreER}:*Rpl22*^{HA} F_1 mice and their fate map feature allow us to analyze the translatome of microglia throughout the different stages of EAE, including remission and relapse. The detailed analysis of microglial translatomes during the RR-EAE pathology will provide insights into the mechanisms that govern EAE, and might enable the design of more accurate therapeutics for MS.

Results

Part I: Re-evaluating Microglia Expression Profiles Using RiboTag and Cell Isolation Strategies

Definition of cell type specificity of *Cx3cr1^{Cre}* and *Cx3cr1^{CreER}* transgenic mice

The RiboTag strategy is a two-component approach relying on the combination of a floxed *Rpl22^{HA}* allele with a cell type-specific Cre recombinase transgene[107]. Microglia display a unique high expression of CX_3CR1 and transgenic mice harboring a GFP reporter gene under the promoter of this chemokine receptor have been instrumental to study microglia morphology and dynamics[2,3,109]. GFP expression in brains of adult *Cx3cr1^{gfp}* mice is restricted to microglia and non-parenchymal macrophages[109]. More recently, we introduced two mouse strains that display Cre recombinase activity under the control of the *Cx3cr1* promoter, either constitutively (*Cx3cr1^{Cre}* mice), or following Tamoxifen (TAM) - mediated activation of an estrogen receptor-fused latent Cre recombinase (*Cx3cr1^{CreER}* mice)[110] (**Figure 1A**). To implement the RiboTag method for the study of microglia, we generated *Cx3cr1^{Cre}:Rpl22^{HA}* and *Cx3cr1^{CreER}:Rpl22^{HA}* mice. We then performed high-throughput RNAseq on mRNA isolated from whole brain tissue (input), and mRNA retrieved by immunoprecipitation (IP) of brain extracts with either a control isotype IgG (IP IgG) or with a specific anti-HA (IP HA), from the two mouse strains (**Figure 1B**). To assess the cell type specificity of the obtained translatomes, we compared them to published neuron and glia-specific gene expression signatures[111]. Translatomes retrieved from *Cx3cr1^{Cre}:Rpl22^{HA}* and TAM-treated *Cx3cr1^{CreER}:Rpl22^{HA}* mice showed an enrichment for mRNAs encoding microglial proteins, such as Sall1, Csf1r, Trem2, Aif1 (Iba-1) and CD11b, that represent a small fraction in the total input, confirming rearrangement of the 'floxed' *Rpl22^{HA}* allele in microglia (**Figure 1C**). Conversely, key astrocyte and oligodendrocyte transcripts, such as *Gfap*, *Aldh1l1*, *Aqp4* and *Mbp*, *Mog*, *Olig1*, *Plp1*, respectively, were de-enriched in both translatomes as expected (**Figure 1C**). Translatomes retrieved by ribosome IP from brain homogenates of *Cx3cr1^{Cre}:Rpl22^{HA}* but not TAM-treated *Cx3cr1^{CreER}:Rpl22^{HA}* mice, also exhibited a prominent neuronal signature, including mRNAs encoding Calbindin 2, CX_3CL1 and CELF (**Figure 1C**). This suggested activation of RPL22-HA expression in neuronal cells of *Cx3cr1^{Cre}: Rpl22^{HA}* mice. Histological analysis of *Cx3cr1^{Cre}:Rosa26^{YFP}* animals that harbor a 'floxed' reporter allele revealed prominent neuronal labeling, comparable to that recently reported for LysM2^{Cre} mice[112] (**Figure 1D**). Moreover, immunohistochemical

analysis of *Cx3cr1^{Cre}:Rpl22^{HA}* animals detected neuronal staining by anti-HA antibodies in spinal cord and brain sections, including Purkinje cells in the cerebellum, in line with the observed *Calb2* expression (**Figure 1E**). In contrast, RPL22-HA expression in TAM-treated *Cx3cr1^{CreER}:Rpl22^{HA}* mice was restricted to microglia, as demonstrated by co-staining for IBA-1 (**Figure 1E**). Since *Cx3cr1^{gfp}* mice lack GFP labeling of adult neurons[109,113], rearrangements in *Cx3cr1^{Cre}* mice are likely due to a transient and further-to-be-defined window of *Cx3cr1* promoter activity during neuronal development. In support of this notion, one of the *Cx3cr1^{Cre}:Rpl22^{HA}* mice analyzed, also displayed astrocyte and oligodendrocyte transcripts, in line with the shared neuroectodermal origin of these glia cells and neurons (**Figure 1C**). Of note, rearrangements in neurons of *Cx3cr1^{Cre}:Rpl22^{HA}* animals were observed irrespective of whether the floxed allele and the Cre transgene went together through the germline (data not shown).

Cx3cr1^{CreER}:Rpl22^{HA} mice that were TAM-treated postnatally displayed brain macrophage-restricted activation of the RiboTag. Some enrichment for the microglia translatome was also observed without TAM treatment in these mice and rare YFP^{+} cells could be detected in non-treated *Cx3cr1^{CreER}:Rosa26^{YFP}* animals (**Figure 1C**, **1D** middle panel), corroborating reports of leakiness of the CreER system[114,115,116]. However, as confirmed by flow cytometric analysis (**Figure 1F**), robust rearrangement and microglial expression of the HA epitope-tagged ribosome subunit in *Cx3cr1^{CreER}: Rpl22^{HA}* mice were dependent on TAM induction in our facility.

Collectively, these data illustrate the value of the RiboTag profiling approach to assess the accuracy of Cre transgenic mouse models, and to investigate specific cell types, including fate mapping and conditional mutagenesis.

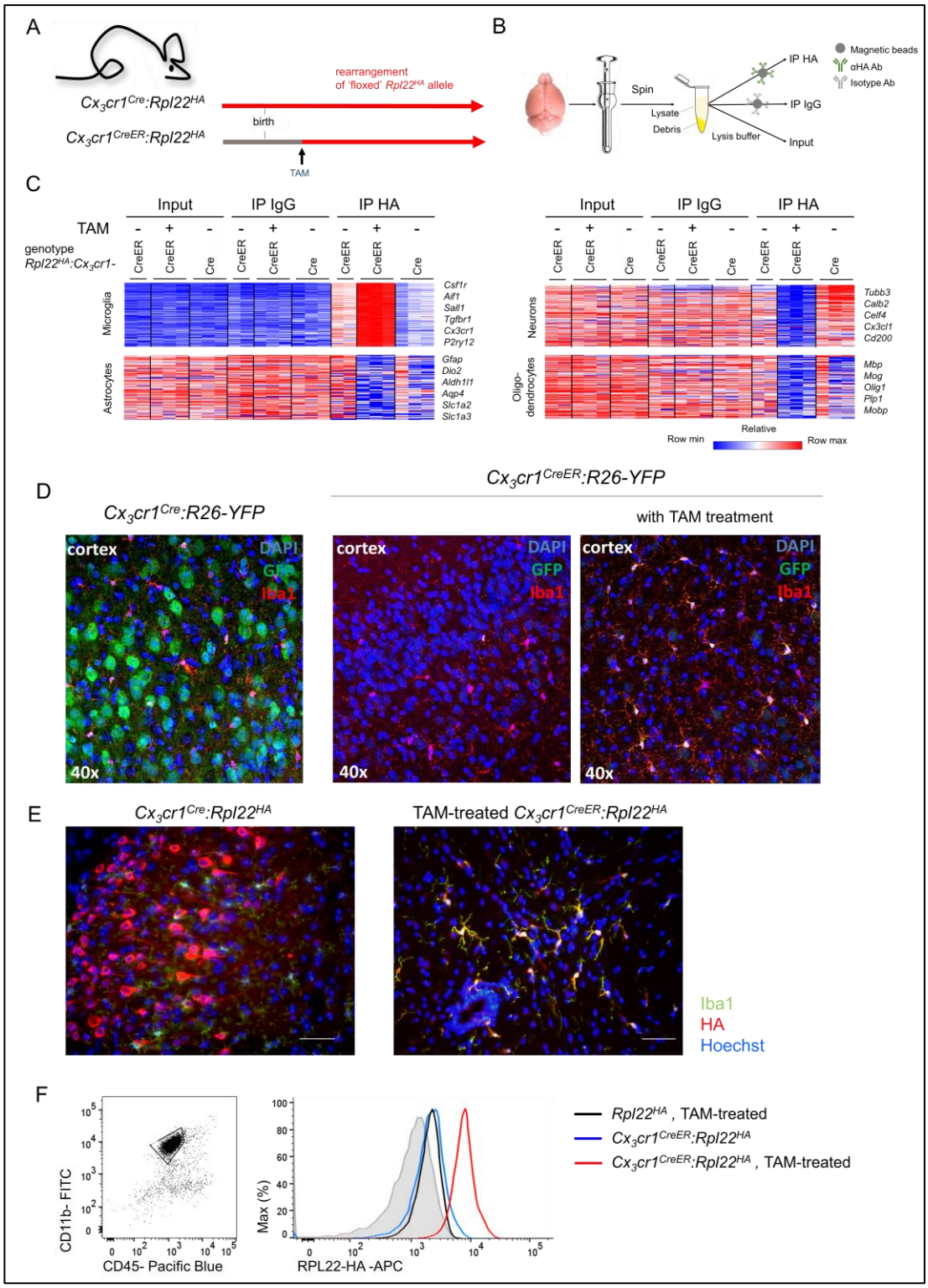

Figure 1. RiboTag analysis reveals that Cx3cr1^{Cre} mice but not Cx3cr1^{CreER} animals display rearrangements in neurons. **(A)** Scheme of Cx3cr1^{Cre} and Cx3cr1^{CreER} systems. **(B)** Scheme describing the immuno-precipitation protocol, including brain homogenization, centrifugation to remove cell debris and incubation with magnetic beads and relevant antibodies. **(C)** Heat maps of RNAseq data comparing IPs obtained from brains of Cx3cr1^{Cre}:Rpl22^{HA} and Cx3cr1^{CreER}:Rpl22^{HA} mice, represented by lists of genes of microglia (115), neurons (97), astrocytes (95) and oligodendrocytes (98) showing enrichment and de-enrichment of mRNAs of specific cell types in the different samples. Reference data sets[111]. Each column represents an individual mouse, n=2 for Cx3cr1^{CreER} no TAM, n=3 for Cx3cr1^{Cre} and Cx3cr1^{CreER} with TAM. **(D)** Microscopic analysis of cortex brain sections from Cx3cr1^{Cre}:R26-YFP mice (left panel) and Cx3cr1^{CreER}:R26-YFP mice (TAM treated (right panel) or untreated controls (middle panel)), stained for IBA-1, YFP and DAPI, showing neuronal expression of YFP in Cx3cr1^{Cre} brains and microglia-restricted YFP expression in Cx3cr1^{CreER}

brains. The animals analyzed are F1 offspring of the intercross of homozygote Cx3cr1^{CreER} or Cx3cr1^{Cre} animals and homozygote R26-YFP mice. Representative of 2 independent experiments. **(E)** Immuno-fluorescent staining of tissue sections of Cx3cr1^{Cre}:Rpl22^{HA} (left) and TAM-treated Cx3cr1^{CreER}:Rpl22^{HA} (right) mice, stained for IBA1, HA and Hoechst, showing neuronal expression of HA in Cx3cr1^{Cre} cortex, and microglia-restricted HA expression in Cx3cr1^{CreER} spinal cord. Scale bars: 200μm (left), 50μm (right) Representative of 2 independent experiments. **(F)** Flow cytometry analysis showing HA staining in microglia (CD11b^{+} CD45^{int}, gated on Ly6C/G^{-} DAPI^{-}) of Rpl22^{HA} TAM-treated mice (black line), Cx3cr1^{CreER}:Rpl22^{HA} mice, untreated (blue line) and TAM-treated (red line). Shadowed histogram represents isotype (IgG) control. Representative data of 3 repeats.

Comparison of RiboTag profiling to cell sort-based transcriptomics

Having established the value of *Cx3cr1^{CreER}:Rpl22^{HA}* mice, we next compared translatomes and transcriptomes of sorted and unsorted microglia. Specifically, individual brains of TAM-treated *Cx3cr1^{CreER}:Rpl22^{HA}* mice were divided: one hemisphere underwent direct tissue homogenization followed by IP with anti-HA (IP-HA) or an isotype control antibody to define the method-related background (IP-IgG). The second hemisphere was subjected to the classical microglia isolation protocol involving tissue digestion followed by cell sorting of microglial cells (defined as DAPI^{-} Ly6C/G (Gr1)$^{-}$ CD11b^{+} CD45^{int}) (**Figure 2A**). A fraction of the sorted microglia was taken for direct mRNA isolation to yield the whole transcriptome (Sort); another fraction was lysed and subjected to the anti-HA IP to retrieve the translatome of sorted cells (Sort-IP) (**Figure 2A**). This experimental set-up allowed comparison of translatomes of sorted and unsorted microglia alongside whole transcriptomes of sorted microglia from the same brain, and thus to investigate the impact of the isolation protocol on gene expression.

Unbiased K-means clustering of the significantly differentially expressed genes between at least two sample groups (IP-HA vs IP-IgG, IP-HA vs Sort, IP-HA vs Sort-IP and Sort vs Sort-IP, fold change>2, $p<0.05$), revealed 2508 differentially expressed genes, which could be divided into four clusters (**Figure 2B**).

Cluster IV was discerned as RiboTag method-related background, since mRNA reads in the non-specific IP-IgG were higher than in the specific IP-HA and absent from sorted samples. IP specific genes were selected for being significantly higher in IP-HA than IP-IgG (fold change>2, $p<0.05$), and all genes below this threshold were removed from the analysis.

Cluster I comprised 913 mRNAs enriched in the specific IP-HA compared with IP-IgG and present in both samples of sorted microglia. This cluster includes established microglia signature genes, such as *Aif1*, *Irf8*, *Sall1*, *Cx3cr1*, *Tgfbr*, *Tmem119* and *Hexb* (**Figure 2B**), indicating that the retrieval methods we used are comparable. Cluster II was represented by 525 mRNAs that were highly abundant in sorted samples (both in translatome and transcriptome), but not present in the direct IP-HA. Cluster III comprised 282 mRNAs prominently enriched in the direct IP-HA, but less abundant in the sorted microglia. Cluster II and III highlight

differences between the retrieval methods, as well as discrepancies between transcriptomes and translatomes and will be the focus of the remainder of this section.

Transcripts overrepresented in microglia translatomes

Cluster III (**Figure 2B**) is defined by genes highly expressed in 'IP-HA' samples relative to 'Sort' samples and could be further subdivided according to transcript abundance in the 'Sort-IP' samples (**Figure 2C**): Cluster III-a (72 mRNAs) were low in both samples of the sorted cells ('Sort' and 'Sort-IP'); Clusters III-b and III-c (210 mRNAs) were low in the 'Sort' samples but highly expressed in the 'Sort-IP' samples (**Figure 2C**).

Cluster III-a can be largely explained by the presence of non-parenchymal macrophage mRNAs. Non-parenchymal brain macrophages, including perivascular, meningeal and choroid plexus macrophages, can be discriminated from $CD11b^{+}$ $CD45^{int}$ microglia as $CD11b^{+}$ $CD45^{hi}$ cells and therefore be excluded by fluorescence-activated cell sorting (**Figure 2D**). CX_3CR1 is expressed both in microglia and in non-parenchymal brain macrophages (**Figure 2D**)[114]. Accordingly, both $CD45^{int}$ microglia and $CD45^{hi}$ macrophages of TAM-treated $Cx3cr1^{CreER}$*:*$Rpl22^{HA}$ mice express the HA-tagged Rpl22 isoform (**Figure 2E**). Moreover, some of the non-parenchymal brain macrophages are long-lived, similar to microglia, and hence do not lose the rearranged alleles as monocytes do[114]. Single cell transcriptomics have shown that non-parenchymal brain macrophages differ in gene expression from microglia[117]. Accordingly, cluster III-a included *Cd163, F13a1, Cbr2, Mrc1 and Lyve1* (**Figure 2F, 2G**).

The combined clusters III-b and III-c comprise mRNAs that are enriched in both IP-HA and Sort-IP translatomes over the whole transcriptomes, suggesting their functional importance for the cells. These include mRNAs encoding proteins related to metabolism (*Gpx1*, *Sdhc*), vesicular transport (*Clta, Kdelr1, Ykt6*), sphingolipid metabolism (*Gm2a, Psap*) and lipids (*Apoe*), as well as components of the GABA-receptor signaling cascade (*Gabarap, Gnai2*) (**Figure 2H**). Specific functions of these genes in microglia remain to be explored.

Collectively, these results highlight the value of a multifaceted approach, combination of the RiboTag and cell sorting strategies to improve cell type specificity. In addition, the RiboTag approach allows us to focus specifically on genes that are actively being translated and contributing to the cellular proteome at a particular time and location.

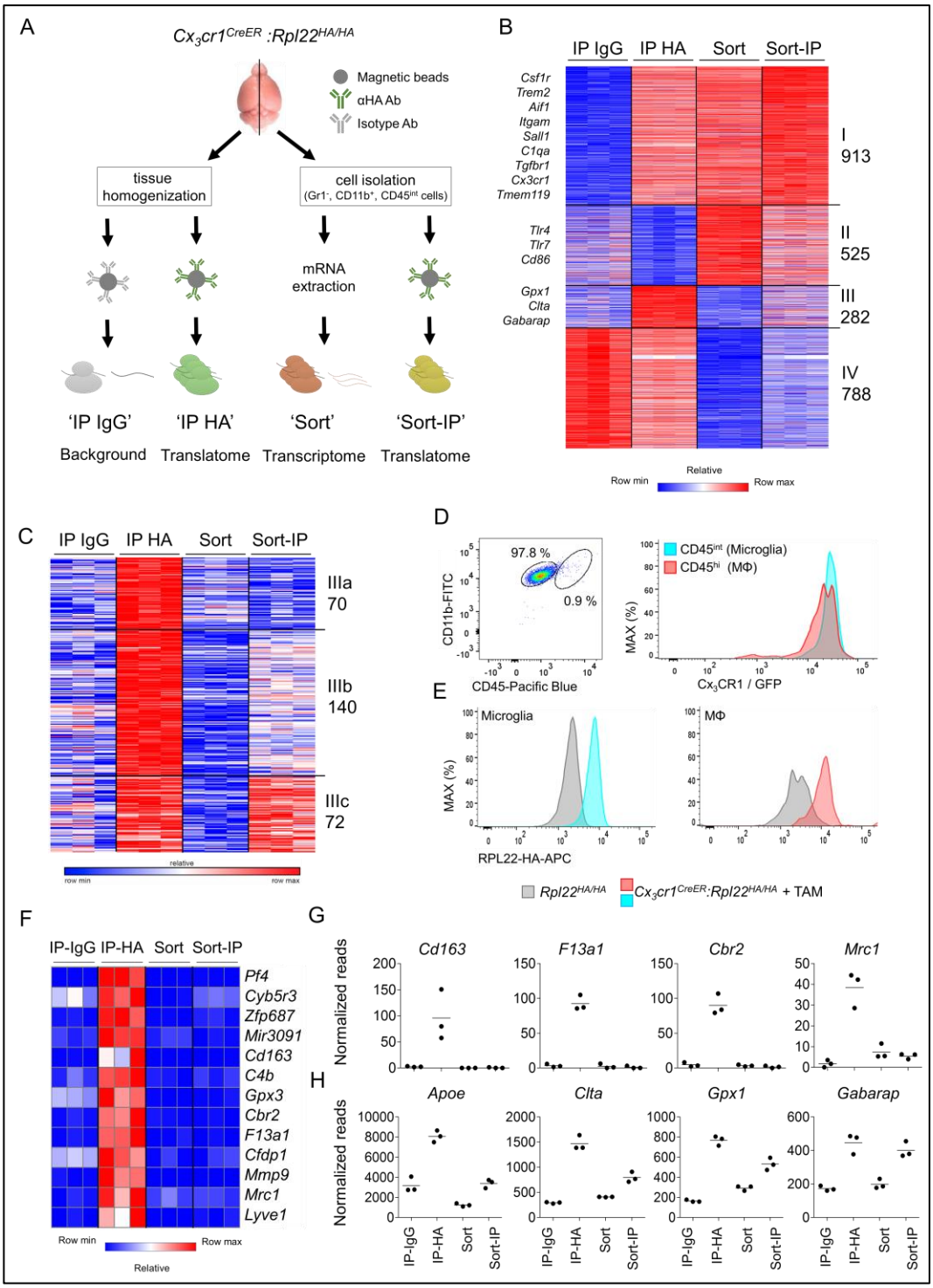

Figure 2. Comparison of cell sort-based protocol and the RiboTag method to profile microglia **(A)** Scheme describing the experimental protocol comparing RiboTag and cell sort-based strategies. **(B)** Heat map of RNAseq data of samples obtained in (A). Genes selected by maximum value>100 normalized reads (3,186 out of 17,406 genes), significantly changed (fold change>2, p-value<0.05) between: IP-HA vs IP-IgG, Sort vs IP HA, Sort-IP vs IP HA and Sort vs Sort-IP, Representing 2,508 genes. n=3, individual mice. Statistical test was part of the DESeq2 package, using p-adjusted. **(C)** Heatmap representing K-means re-clustering of genes from cluster III from Figure 2B, showing genes high in IP-HA and low in Sort samples. **(D)** FACS dot plot (left panel) showing separation of microglia ($CD45^{int}$) from other brain macrophages (MΦ) ($CD45^{hi}$) by flow cytometry. Histogram (right panel) of microglia and MΦ isolated from $Cx3cr1^{GFP}$ mice indicating high CX_3CR1/GFP expression in both populations. Representative of 3 independent experiments. **(E)** FACS histogram of HA staining in microglia (left panel) and other brain macrophages (MΦ) (right panel) in control $Rpl22^{HA}$ mice (grey) or TAM-treated $Cx3cr1^{CreER}$:$Rpl22^{HA}$ mice (blue/red). Representative of 2 independent experiments. **(F)** Heatmap of RNA-seq data of representative non-parenchymal brain macrophages genes,

showing enrichment in IP-HA, but not in sorted samples. **(G)** Graphs showing normalized reads of example genes from Figure 2F. Each dot represents an individual mouse, n=3, line represents mean. **(H)** Graphs showing normalized reads of example genes from cluster III-b and III-c in Figure 2C, showing functional genes enriched in IP and Sort-IP. Each dot represents an individual mouse, n=3, line represents mean.

Transcripts overrepresented in transcriptome cluster I: Isolation artifacts

Cluster II (**Figure 2B**) defines 525 mRNAs that were high in Sort, but low in IP-HA. This cluster can be further subdivided according to transcript abundance in the Sort-IP samples (**Figure 3A**). Cluster II-a comprised 190 transcripts similarly expressed in Sort-IP and Sort samples and was found to include mRNAs that are related to immune activation, such as *Cd86*, *Cd53*, *Tlr4*, and *Tlr7* (**Figure 3B**). Ingenuity Pathway Analysis (IPA) of significantly upregulated genes in Sort vs. IP-HA (>2 fold change, $p<0.05$) showed upregulation of pathways such as 'Production of NOS and ROS', 'Phagocytosis' and 'TLR signaling' (**Figure 3C**). Since these transcripts are high in both translatomes and transcriptomes of sorted cells, we assume that they reflect cell activation resulting from the isolation process, as recently reported from another system[118].

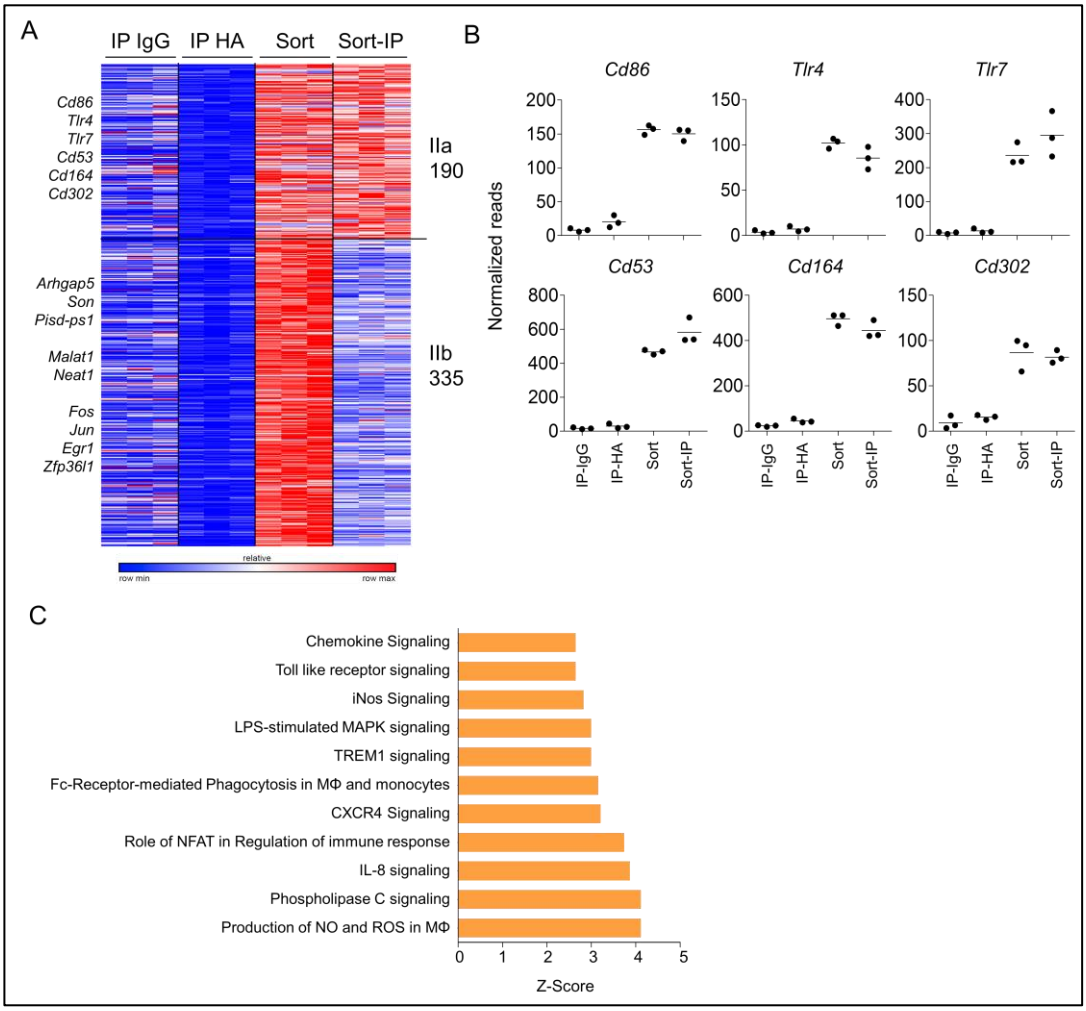

Figure 3. Microglia isolation results in cell activation. **(A)** Heatmap representing K-means re-clustering of genes from cluster II from Figure 2B, showing mRNAs high in Sort and low in IP-HA samples. **(B)** Graphs showing normalized reads of example genes from cluster II-a in Figure 3A, showing high level expression of immune-activation-related genes in sorted samples. Each dot represents an individual mouse, n=3, line represents mean. **(C)** Ingenuity Pathway Analysis (IPA) of genes significantly higher (>2 fold change, p-value<0.05, according to DESeq2 statistical analysis) in Sort compared to IP-HA (n=3), showing activated pathways related to immune response represented by activation Z-score as calculated by IPA software.

Commonly used macrophage isolation protocols, such as the one we applied for the microglia retrieval, include enzymatic tissue digestion at 37°C, i.e. a step that could cause cell activation and transcriptome alterations. Moreover, enzymes employed in these digests might contain endotoxin contaminations that could activate cells. To probe for the potential impact of these manipulations, we compared transcriptomes of sorted cells that were isolated from the same brain with or without collagenase and DNase digestion, and the RiboTag approach. Surprisingly, both isolation procedures resulted in comparable transcriptional profiles, indicated by differential expression of 472 and 267 genes (cluster II and III, respectively) as compared to the relevant IP samples (**Figure 4A**). Global correlation of gene expression of the

samples retrieved with or without incubation was high (r^2 = 0.99), as compared to the correlation of sorted and IP samples (r^2 = 0.1) (**Figure 4B**). Similarities were also apparent in a correlation matrix compiled from data of independent experiments (**Figure 4C**). Collectively, these data establish that the artifact is reproducible and suggest that it is introduced by extraction of the cells from their native environment, rather than subsequent manipulation.

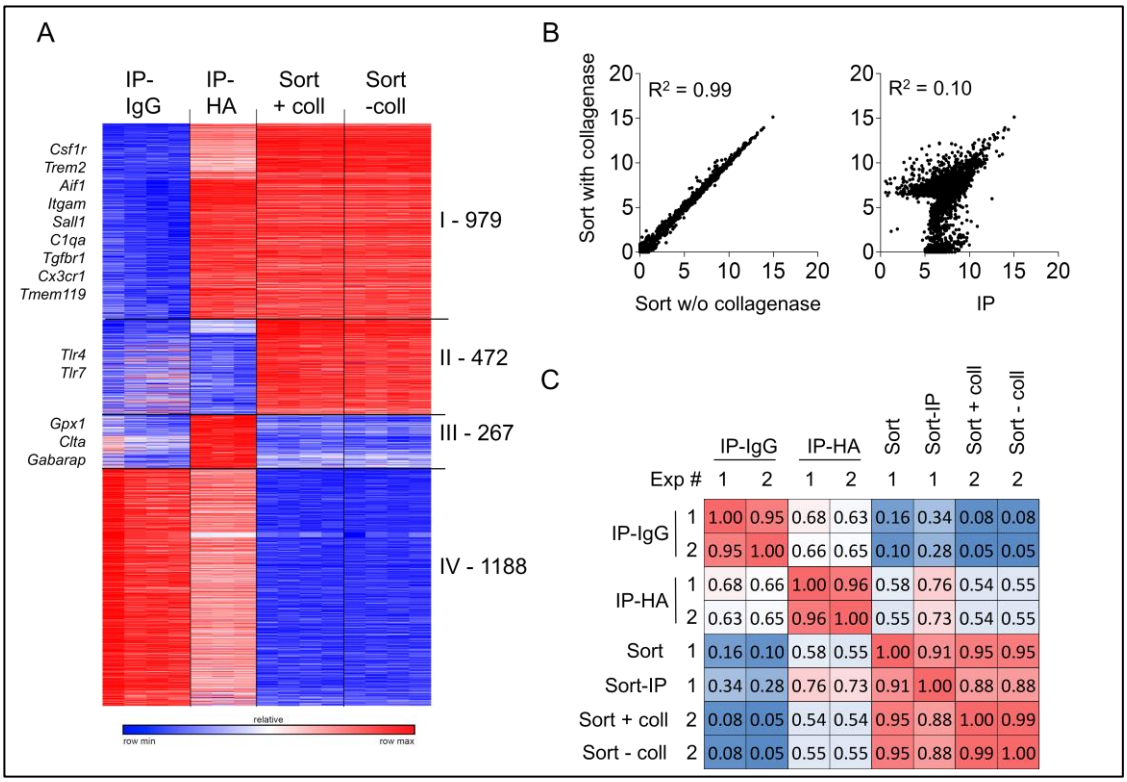

Figure 4. Microglia activation signature is robust, reproducible and induced by cell extraction form tissue
(A) Heatmap clustered by K-means clustering, comparing direct IP to whole mRNA retrieved from sorted cells extracted with (+coll) or without (-coll) enzymatic digestion in the isolation protocol, revealing 4 clusters similar to figure 2B. n=4 individual mice (one repeat of IP-HA was removed due to technical reasons). **(B)** Correlation plots of average of log2 normalized reads (n=4) plotting sorted cells with enzymatic digestion on the Y axis and sorted cells without enzymatic digestion on the X axis (left panel) or IP on the X axis (right panel). **(C)** Correlation matrix combining two independent experiments, showing high reproducibility of the results.

Transcripts overrepresented in the transcriptome cluster II: Cargo contaminants and sequestered RNAs

Cluster II-b spanned 335 genes that were low in the Sort-IP compared with Sort samples (**Figure 3A**), suggesting translatome-transcriptome differences.

Microglia are specialized phagocytes that like other macrophages take up dead cells and cell debris for clearance[118]. Although we did not formally rule out other sources of contaminations, whole cell transcriptomes could hence include genetic material from recently ingested neighboring cells. Indeed, almost half of the mRNAs in cluster II-b (157 out of 335 genes) are likely to be derived from such external sources (**Figure 5A**). Examples include *Arhgap5*, *Son* and *Pisd-ps1*, which are reportedly transcribed in astrocytes and neurons[111] (**Figure 5B**).

Long non-coding mRNAs (lncRNAs) were shown to be enriched in nuclei[119], where some of them act in transcriptional regulation. As expected, representatives of these lncRNAs, such as *Malat1* and *Neat1*, were identified in the whole cell transcriptomes, while absent from translatomes, and appeared in Cluster II-b (**Figure 5C**).

Gene expression is controlled at the level of transcription and translation. The latter comprises specific mechanisms that prevent mRNAs from their integration into ribosomes, including nuclear retention and sequestration into dedicated membrane-less cytosolic ribo-nucleoprotein complexes[120,121]. The content of these organelles, such as processing bodies (P-bodies) and stress granules is only beginning to be defined[101,121]. However, sequestered mRNAs have been reported to be longer and to comprise extended 3'UTRs, as well as to display lower splicing efficiencies[121,122]. When analyzed for these three parameters, mRNAs defined by Cluster II-b, showed significant presence of these hallmarks, as compared to all other clusters (**Figure 5D**). Moreover, transcripts of cluster II-b also showed significant overlap with the list of nuclear retained mRNAs reported for other cellular systems[123] (**Figure 5E**). Among the protein-coding mRNAs that seem sequestered from immediate translation, we found *Fos, Jun, Egr1* and *Zfp36l1* (**Figure 5F**), which are immediate early genes that have been described to be induced within minutes after activation. Of note, these mRNAs appear also in the translatome of the sorted cells, suggesting that they move to the ribosomes during the isolation procedure. Collectively, discrepancies we observed between microglia translatomes and whole cell transcriptomes can be explained by the inclusion of cargo-derived transcripts and mRNAs sequestered to nuclei or P-bodies (**Figure 5G**). These data highlight the value of the RiboTag approach to retrieve functionally relevant mRNAs.

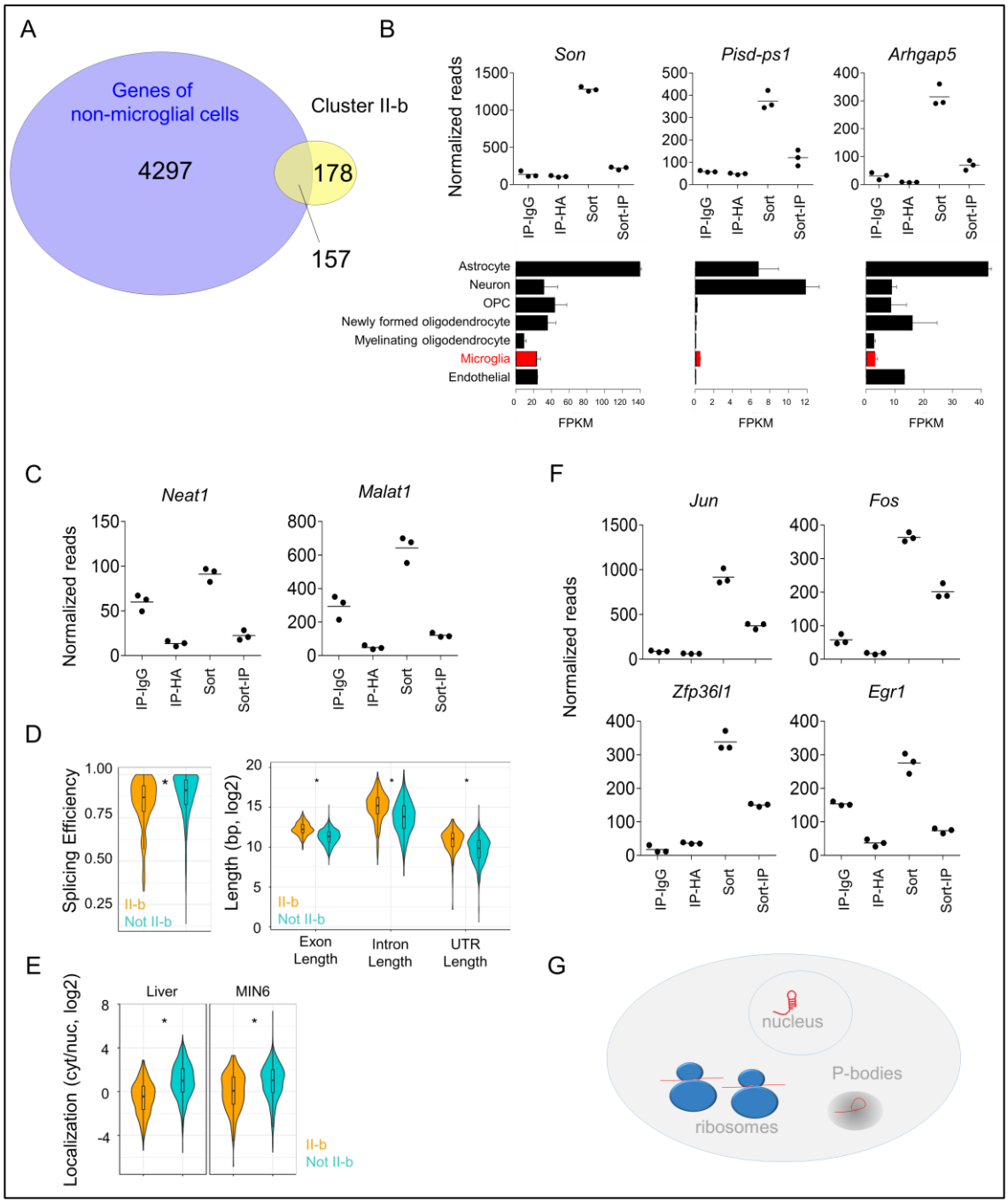

Figure 5 Microglia transcriptomes, but not translatomes include cargo-derived mRNAs and mRNAs sequestered in nuclei and P-bodies. **(A)** Venn diagram of overlapping genes of cluster II-b (Figure 2C) (yellow) with genes of non-microglial cells, as selected according to[111]. Non-microglia genes were selected by being with max value > 10, microglia reads < 30 and max value is > 3 fold change over microglia. Genes fitting these criteria represent cargo of ingested cells. **(B)** Graphs showing normalized reads of example genes from list of shared genes from Figure 4A, showing high levels cargo contamination in Sort samples, but not in IP. Each dot represents an individual mouse, n=3 (upper panels); Expression of genes above in different brain cells, data obtained from[111] (lower panels). FKPM, fragments per kilobase of exon per million reads mapped. (**C**) Graphs showing normalized reads of example genes of long non coding RNAs that reside within the nucleus and are presented only in Sort but not IP samples. Each dot represents an individual mouse, n=3, line represents mean. (**D**) Violin plot representing splicing efficiency (left panel) and gene length (right panel) of genes in cluster II-b (orange) compared to genes not in II-b (green), showing that genes in cluster II-b are less efficiently spliced and have longer genes and longer 3'UTRs compared with the rest of genes in the dataset, suggesting nuclear retention. Splicing efficiency was computed by comparing intron-spanning and intron-crossing reads [28]. Statistics was performed using Wilcoxon test, FDR correction was performed for right panel. * Splicing efficiency $p=4.124*10^{-7}$, exon length $p=6.636*10^{-63}$, Intron length $p=1.575*10^{-27}$, UTR length $p=1.865*10^{-35}$. **(E)** Violin plot representing cellular localization of genes in other tissues (left panel Liver, right panel – MIN6 pancreatic beta cell line) with established nuclear and cytoplasmic fractions. Genes in cluster II-b (orange) are more nuclear compared to

other genes (green). Statistics was performed using Wilcoxon test and FDR correction. * Liver $p=7.731*10^{-49}$, MIN6 $p=2.980*10^{-17}$. n (number of genes) = 316 (Liver 2b), 1970 (Liver not-2b), 306 (MIN6 2b), 1846 (MIN6 not-2b). Liver and MIN6 datasets were based on 2 independent experiments [22]. **(F)** Graphs showing normalized reads of immediate-early genes found in Sort but not in IP-HA (in cluster II-b, microglial genes), suggesting sequestration from translation in unsorted cells. Each dot represents an individual mouse, n=3, line represents mean. **(G)** Diagram representing different states of mRNAs in the cell: nuclear retention, sequestration from translation in P-bodies or active translation in the ribosomes.

RiboTag analysis of microglial response to peripheral LPS challenge

Arguably, method-related artifacts, like the ones associated with microglia isolation, could be neutralized, if controls and experimental samples are prepared using the same approach. However, this assumes that artifacts introduced by the isolation are not affected by biological treatments and challenges. To examine this issue, we performed the RiboTag protocol on TAM-treated *Cx3cr1*^{CreER}*: Rpl22*^{HA} mice following an intra-peritoneal lipopolysaccharide (LPS) injection (2.5 mg/kg). Brain hemispheres of individual LPS- and PBS-treated animals were subjected to either homogenization or microglia isolation and sorting, and processed (**Figure 2A**) and used to generate a summary heat map of the RNAseq data (**Figure 6**).

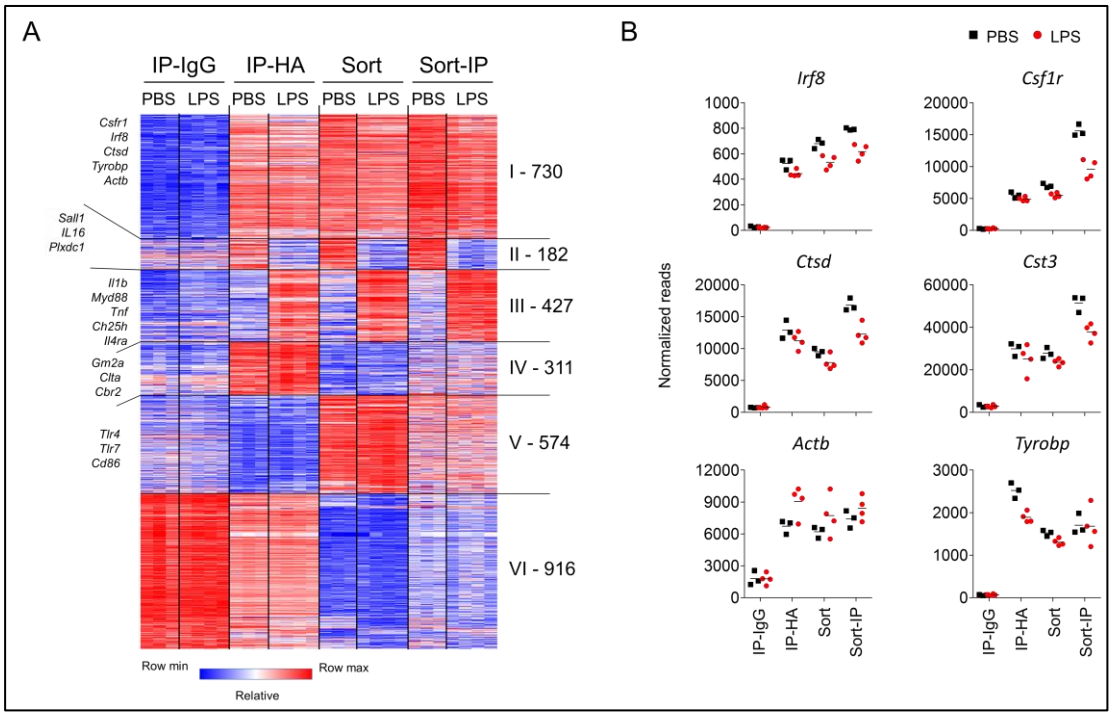

Figure 6. Analysis of microglia isolated from mice challenged with LPS. **(A)** Heatmap of RNA-seq data comparing RiboTag to sorting with LPS treatment, taking significantly changed genes (fold change>2, p-value<0.05, as calculated by DESeq2 statistical analysis). n=3 for PBS group, n=4 for LPS group. **(B)** Graphs showing normalized reads of example genes taken from cluster I from figure S6A, showing similar levels of microglia signature genes among samples. Each dot represents an individual mouse, n=3 for PBS group, n=4 for LPS group, lines represent mean.

To define the effect of the isolation method on microglia of LPS-treated and PBS-treated mice, we performed separate analyses for differentially expressed genes between PBS and LPS treatment in each method and then assessed the respective overlap. The majority of genes detected as up- or down-regulated by the endotoxin challenge in the IP sample were shared with the sorted samples (**Figure 7A, 7C**). Mutual genes correlated between methods, and showed a similar trend of up and downregulation (**Figure 7B, 7D**), indicating that bona fide LPS-induced changes are seen with both methods. Upregulated genes included *Il4ra, Ch25h* and *Il1b* (**Figure 7B**), while microglia signature genes such as *Tgfbr1, Sall1* and *Cx3cr1,* were down regulated (**Figure 7D**).

Notably, a considerable number of mRNAs changed upon LPS treatment only in the sorted samples, but not in the anti-HA IP from whole brain extract (46% of the upregulated and 71% of the downregulated genes) (**Figure 7A, 7C**). Transcripts that were detected as changed upon LPS treatment in sorted samples (both Sort and Sort-IP) but not in IP-HA included genes related to immune activation like *Il1a*, *Ccl2* and *Vcam1* that were upregulated (**Figure 7E**) and *Tlr4*, *Siglech* and *Cd48* that were downregulated (**Figure 7E**). Since they were found in the Sort-IP samples as well, these mRNAs are likely translated in sorted, but not in unsorted microglia. These data establish that the artifact introduced by the cell isolation is affected by the state of the animals from which the cells are retrieved. Moreover, mRNAs that are defined as 'cargo' contamination, due to their presence in the transcriptomes but absence from IPs of the sorted cells, changed following the LPS challenge (**Figure 7F**). For example *Pisd-ps1*, *Arhgap5* and *Tia1* were downregulated and *Ranbp2, Tet2* and *Gas5* were upregulated upon LPS challenge (**Figure 7F**). All of these genes were reported to be more highly expressed by other brain cells, rather than microglia (**Figure 8**)[111], and are absent from the translatomes of either sorted or unsorted microglia in our dataset.

Collectively, these results indicate that data retrieved from sorted microglia include false information that originates from sorting-related immune activation and cargo contamination of ingested cells. Importantly, our data establish that identical processing of control and test samples does not necessarily neutralize these artifacts, since they themselves are affected by the biological treatment. Taken together our study highlights the advantages and disadvantages of classical sort-based cell isolation protocols and the RiboTag approach (**Table 1**).

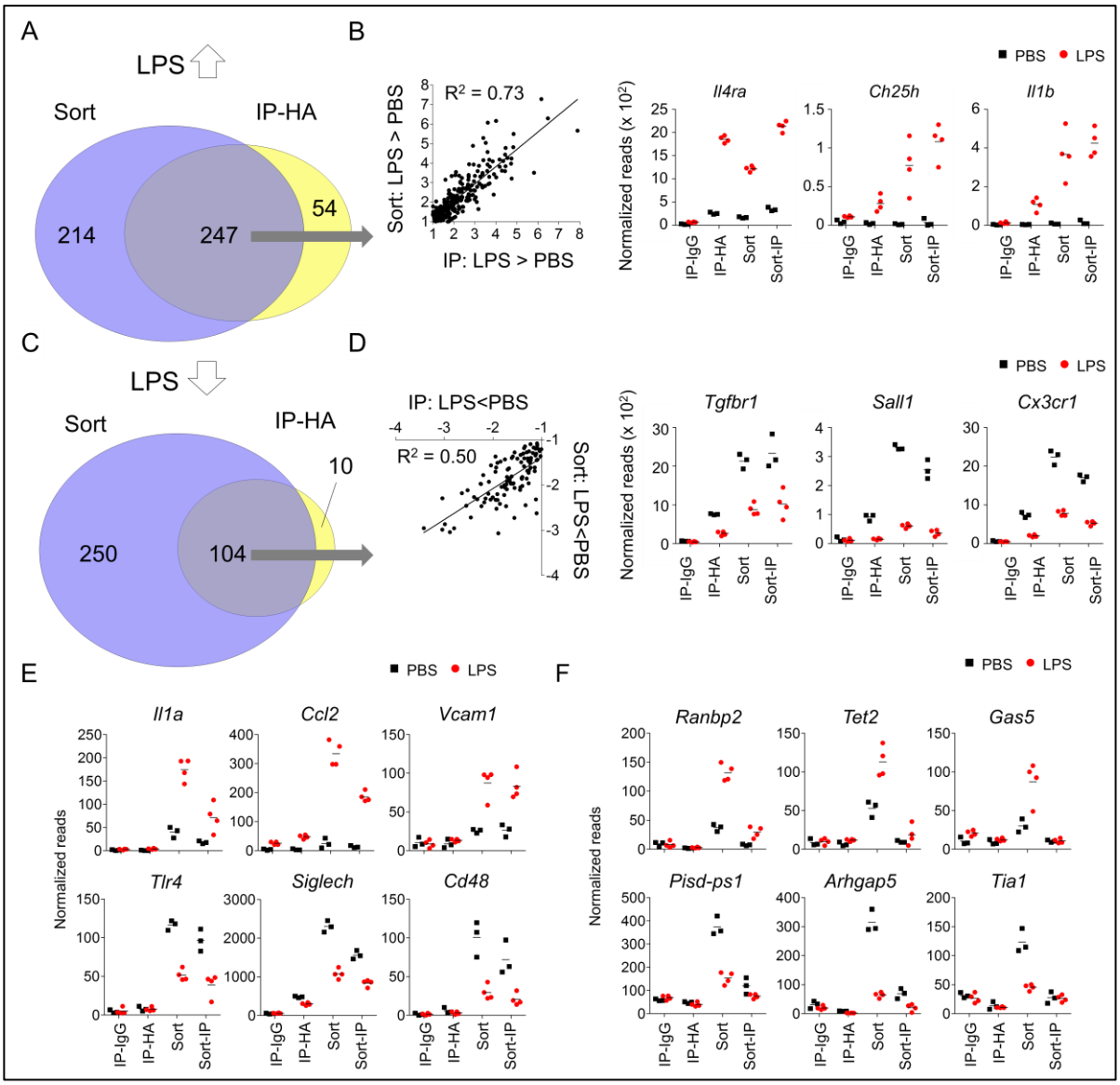

Figure 7. Analysis of microglia isolated from mice challenged with LPS. **(A)** Venn diagram of overlapping genes upregulated by LPS treatment in IP-HA (blue) and in Sort (yellow), showing 54 genes upregulated in IP-HA only, 247 genes shared between methods and 214 genes upregulated by sorting only. **(B)** Correlation analysis of 247 shared genes (from Figure 5A) upregulated due to LPS in both methods, representing log2 fold change of significantly changed genes (log2 fold change>1, pValue<0.05, as calculated by DESeq2 statistical analysis) in LPS vs PBS in each of the methods (left panel); Graphs showing normalized reads of example genes detected as upregulated with LPS by both methods (right panels). Each dot represents an individual mouse, n=3 in PBS group, n=4 in LPS group, line represents mean. For IP-HA genes were selected by first being enriched over control IP-IgG, and then by LPS>PBS. **(C)** Venn diagram of overlapping genes downregulated by LPS treatment in IP-HA (blue) and in Sort (yellow), showing 10 genes downregulated in IP-HA only, 104 genes shared between methods and 250 genes downregulated by sorting only. **(D)** Correlation analysis of 104 shared genes (from Figure 5C) downregulated due to LPS in both methods, representing log2 fold change of significantly changed genes (log2 fold change<-1, p-value<0.05, as calculated by DESeq2 statistical analysis) in LPS vs PBS in each of the methods (Left panel); Graphs showing normalized reads of example genes detected as downregulated with LPS by both methods (Right panels). Each dot represents an individual mouse, n=3 in PBS group, n=4 in LPS group, lines represent mean. For IP-HA genes were selected by first being enriched over control IP-IgG, and then by LPS<PBS. **(E)** Graphs showing normalized reads of example genes related to immune activation that were up- (upper panels) or down- (lower panels) regulated due to LPS treatment in sorted samples only but not detected in IP-HA, showing differential susceptibility of biologically treated samples to artifacts introduced by isolation method. Each dot represents an individual mouse, n=3 in PBS group, n=4 in LPS group, lines represent mean. **(F)** Graphs showing normalized reads of example genes originated from ingested cargo that were up- (upper panels) or down- (lower panels) regulated due to LPS treatment in Sort only but not detected in IP-HA or Sort-IP, showing that the whole translatome includes LPS-dependent changes that do not originate in microglia thus introducing false information. Each dot represents an individual mouse, n=3 in PBS group, n=4 in LPS group, lines represent mean.

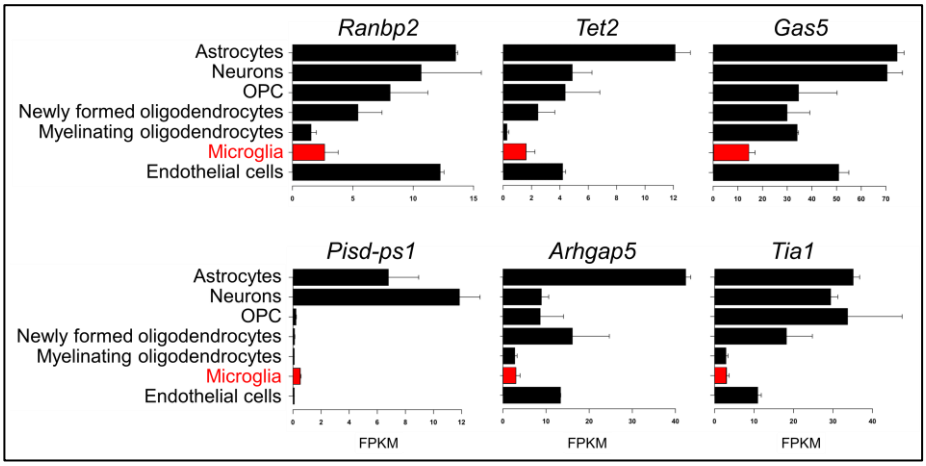

Figure 8. Expression profiles of selected genes across brain cell populations Non-microglia mRNAs suggesting cargo contamination Data obtained from (http://www.brainrnaseq.org/)[111].

Approach	Advantage	Limitation
Sort-based cell Isolation	*Independence from transgenic systems*	*Dependence on surface markers identifiable by antibodies*
		Restricted to cells that can be retrieved from tissue context
		Prone to be affected by isolation artifacts and biases
RiboTag approach	*Excludes 'cargo' contamination, particular relevant in case of phagocytes*	*Dependent on Cre recombinase transgenic systems and their specificity*
	Excludes mRNAs sequestered in nuclei (lncRNAs) and RNP complexes	
	Avoids tissue manipulation and extraction of cells from tissue context	
	Includes information closest to protein level	

Table 1*. Advantages and Limitations of the Ribotag approach and Cell-isolation based methods*

Part II: Probing the role of microglia in Relapsing- Remitting EAE

After establishing the RiboTag system for the study of microglia, and showing its superiority over sorting, we aimed to utilize it to tackle the long standing question of the role of microglia in EAE. Microglia were shown to be dispensable as APCs for the onset of MOG-induced EAE in C57BL/6 mice[94]. However, contributions of microglia to disease progression remain undefined.

Surprisingly, while the majority of MS patients display a relapsing and remitting form of disease, the most common mouse model used is the chronic model of EAE in C57BL/6 mice (B6, expressing the MHC-II haplotype H-2^b) that leads to a monophasic disease with no recovery. This model is appropriate to study mechanism of autoimmunity that control the induction of EAE. However, mechanisms that contribute to remission or relapse cannot be studied in this model. Immunization of SJL mice (expressing the MHC-II haplotype H-2^s) with myelin peptides results in RR-EAE, however the study of gene- or cell-specific contributions is challenging due to lack of appropriate genetic models in this strain. Crossing SJL to B6 mice allows to combine the advantages of the two mouse strains and utilize genetic models in the RR-EAE in the resulting H-$2^{s/b}$ F1 hybrids.

EAE development is associated with prominent monocyte infiltrates that critically drive the initial pathology[83,84,18]. Discrimination of monocyte-derived macrophages from activated microglia is crucial and challenging[85]. In the past years, our laboratory hence developed a number of new tools that allow to focus on the study of microglia and exclude monocytes and monocyte-derived macrophages. Using a TAM-inducible *Cx3cr1*^{CreER} approach, we take advantage of the longevity and self-renewal of microglia to permanently target these cells in adult animals[91,110]. By 6 weeks post TAM treatment, short lived monocytes that also express CX_3CR1 are replaced by WT cells, while only long lived cells will remain targeted throughout time[91,110]. It should however be noted that some non-parenchymal CNS border associated macrophages (BAMs) are long lived and are targeted as well[102,114]. Nonetheless, the proportion of long lived CNS BAMs is minimal compared to microglia and can therefore be mostly neglected.

Here, we use advanced genetic approaches to specifically dissect the contribution of microglia to RR-EAE. Along with RiboTag translatome data analysis, we provide insights into specific microglia / T cell interactions, as well as preliminary functional evidence that microglia contribute to recovery, using newly generated SJL KO mouse lines.

Longitudinal microglia analysis in a relapsing remitting EAE model

In order to establish the RiboTag in a relapsing-remitting EAE (RR-EAE) model, we crossed C57Bl/6 *Cx3cr1*$^{CreER/CreER}$:*Rpl22*$^{HA/HA}$ animals (B6, H-2^{b}) with WT SJL mice (H-2^{s}), and used their TAM-treated F1 *Cx3cr1*$^{CreER/WT}$:*Rpl22*$^{HA/WT}$ H-2$^{b/s}$ offspring 8 weeks post TAM treatment (**Figure 9A**). Immunization with $PLP_{139-151}$ peptide resulted in RR-EAE with full recovery being achieved after a first wave of disease, followed by a relapse (**Figure 9B**). We aimed to profile microglia over the entire course of RR-EAE, and collected brains from mice according to their clinical scores, at all stages of RR-EAE (i.e. initiation, max, remission, cure and relapse), as well as from TAM-treated non-immunized controls (**Figure 9B, C**).

Flow cytometry analysis of HA expression in immune cells revealed that microglia are the prominent cell type labeled, representing 90-100% of HA^{+} cells (**Figure 9D,** gating strategy in **Figure 10A, 10B**). In contrast, HA staining was absent from CD45^{hi} immune cells, including short-lived monocytes (**Figure 9D**). On top of that, the microglia population remained stable with ~100% of microglia expressing HA-tagged ribosomes throughout the RR-EAE disease course (**Figure 10C, 10D**). BAMs, namely perivascular, meningeal and choroid plexus macrophages, are targeted with the *Cx3cr1*^{CreER} system as well[102,114]. However, these cells are rare as compared to microglia and their turnover rate in EAE has not been described. It is therefore possible that BAMs are replaced by WT cells during RR-EAE. From our results we can conclude that microglia are the main population that is stably labeled with HA throughout RR-EAE.

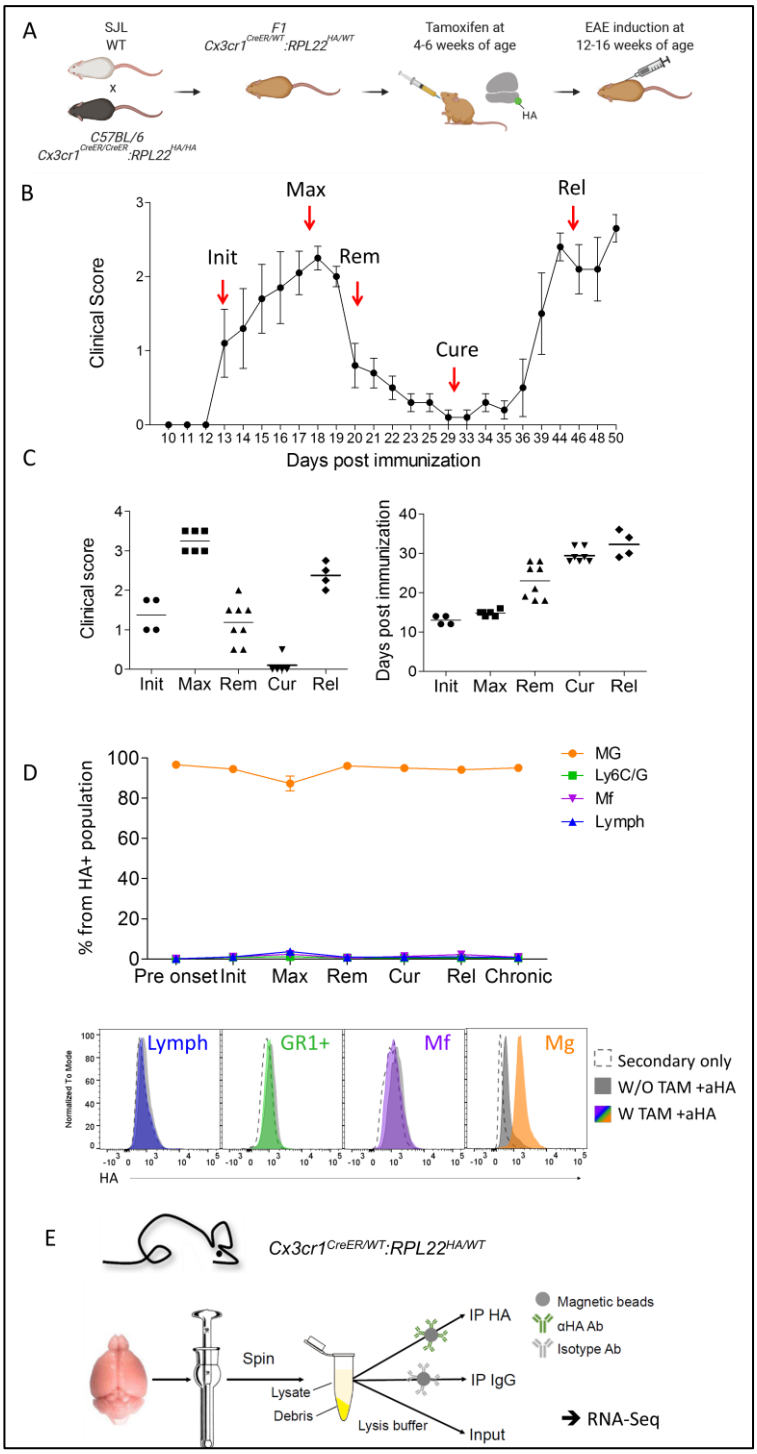

Figure 9. Establishing Relapsing-Remitting EAE in (B6*SJL) F1 RiboTag mice **(A)** Scheme describing mouse genotypes and crossing strategy **(B)** RR EAE course in F1 mice. Red arrows mark the stages at which mice were collected for RiboTag analysis. Init = initiation, Max = maximal score, Rem = remission, Cure = clinical recovery, Rel = relapse. **(C)** Clinical scores (left) and day post immunization (right) of individual mice at day of collection. **(D)** The prevalence of different populations from HA+ cells throughout RR-EAE stages, showing that >90% of HA+ cells are microglia. Pre = pre onset, Init = initiation, Max = maximal score, Rem = remission, Cure = clinical recovery, Rel = relapse, chronic = chronic stage, no recovery. Lower panels are representative histogram of each population stained for HA. Dashed line = secondary only control, filled gray = mice without TAM treatment stained with aHA antibody, color = TAM treated animals stained with anti HA antibody. N= 2-4 mice in each timepoint **(E)** Scheme of RiboTag immunoprecipitation (IP), with an anti-HA antibody (IP HA) or with isotype control (IP IgG), input is total brain lysate without IP.

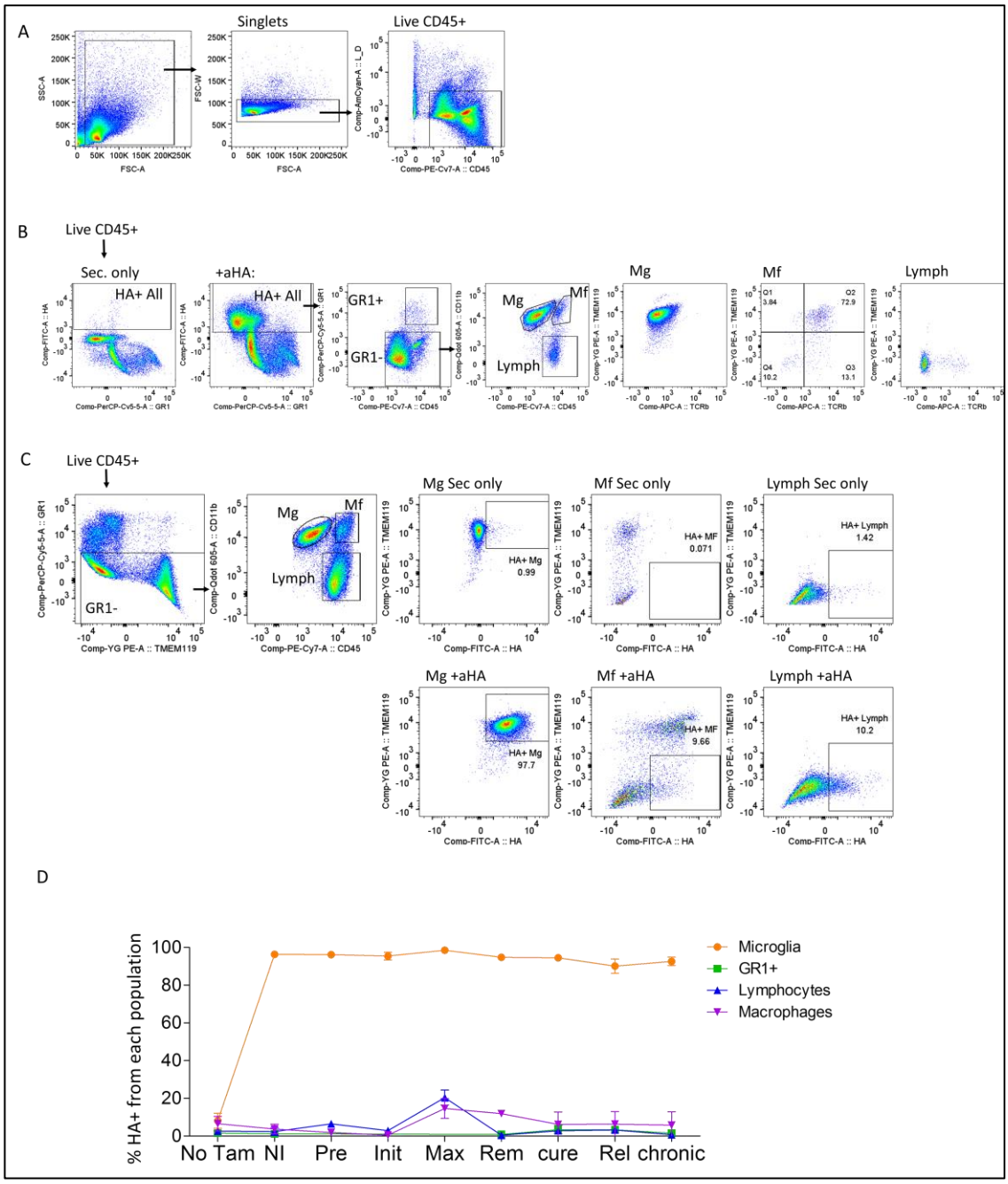

Figure 10. Analysis of RiboTag expression. **(A)** Gating strategy for live CD45⁺ population from which following gating in B and C is taken. **(B)** Gating strategy for Figure 1D, the percent of each population (GR1(Ly6C/G)⁺, Mg=Microglia, Mf = macrophages, Lymph = Lymphocytes) from total HA+ cells, gated from live CD45⁺. Most left panel shows the secondary only control (without aHA antibody). All other gating is from +aHA sample. **(C)** Gating strategy for S1D, calculating the percent of HA+ within each population. Upper three right panels are secondary only control for each population, compared to +aHA staining in lower three panels for each population. **(D)** Summary of HA+ cells from each population (as gated in S1C), at all stages as well as in non-TAM treated mice (No Tam). NI = non immunized, Pre = pre onset, Init = initiation, Max = maximal score, Rem = remission, Cure = clinical recovery, Rel = relapse, chronic = chronic stage, no recovery

Microglial translatome analysis

After confirming that microglia remain HA^+ throughout RR-EAE, and monocytes and their descendants are not labeled, we subjected brains to IP of ribosome-attached-mRNA with either a specific anti-HA antibody or an isotype IgG control, followed by RNA-seq alongside with the total input RNA (**Figure 9E**). By comparing the specific anti-HA pulldown to the IgG control and to the total input, we selected the IP-specific genes as significantly enriched in the anti-HA fraction. We focused our analysis on genes with a maximal value>50 (to exclude background genes with low reads), genes IP specific in at least one condition (log2fold-change>2, $p<0.05$ compared to IgG control and input), and finally significantly changed (log2fold-change>2, $p<0.05$) genes between the HA fraction of at least two conditions.

Selected genes from this stringent filter (716 genes) are represented in a heatmap showing the average of aHA-IP samples in each condition (**Figure 11A**). Genes were grouped using k-means clustering into 5 main clusters: **Cluster I** included microglial steady state genes (*Cst3, P2ry12, Siglech*) that are highly expressed in NI mice and are significantly downregulated throughout the disease (**Figure 11A, 11C**).

Expression of genes in **Cluster II** peaked at initiation and gradually decreased. As indicated by Gene Ontology (GO) enrichment analysis, this list mostly comprises genes related to proliferation (e.g. *Aurkb, Mki67, Top2a, Birc5, Pola2, Lig1*), (**Figure 11C, 11B** upper panel) and is in line with the earlier notion that microglia proliferate at the onset of EAE[14].

Cluster III is composed of genes that peak at the Max stage (score 3-3.5) and genes comprised in **Cluster IV** peaked at remission. GO term enrichment analysis of genes in the clusters III and IV together revealed pathways related to immune response, such as '*antigen processing and presentation'*, '*response to interferon gamma'* and '*leucocyte cell-cell adhesion'* (**Figure 11B**, lower panel). Interestingly, among the assigned GO terms for cluster III+IV, we found also '*negative regulation of immune response'* (**Figure 11B**). Closer inspection of cluster III revealed genes encoding chemokines, such as CXCL9, CXCL16, CXCL13, CCL8, CCL5, as well as immune synapse-related molecules, such as ICAM1, CD40, ICOS ligand and MHC-II (*H2-Ab1*). Intriguingly, microglia also translated mRNAs encoding molecules with established inhibitory activity, such as IL-18bp, Lag3, CD274 and the member of the leukocyte immunoglobulin-like receptor (LIR) family Lilrb4a, that might play a regulatory role (**Figure 11C**).

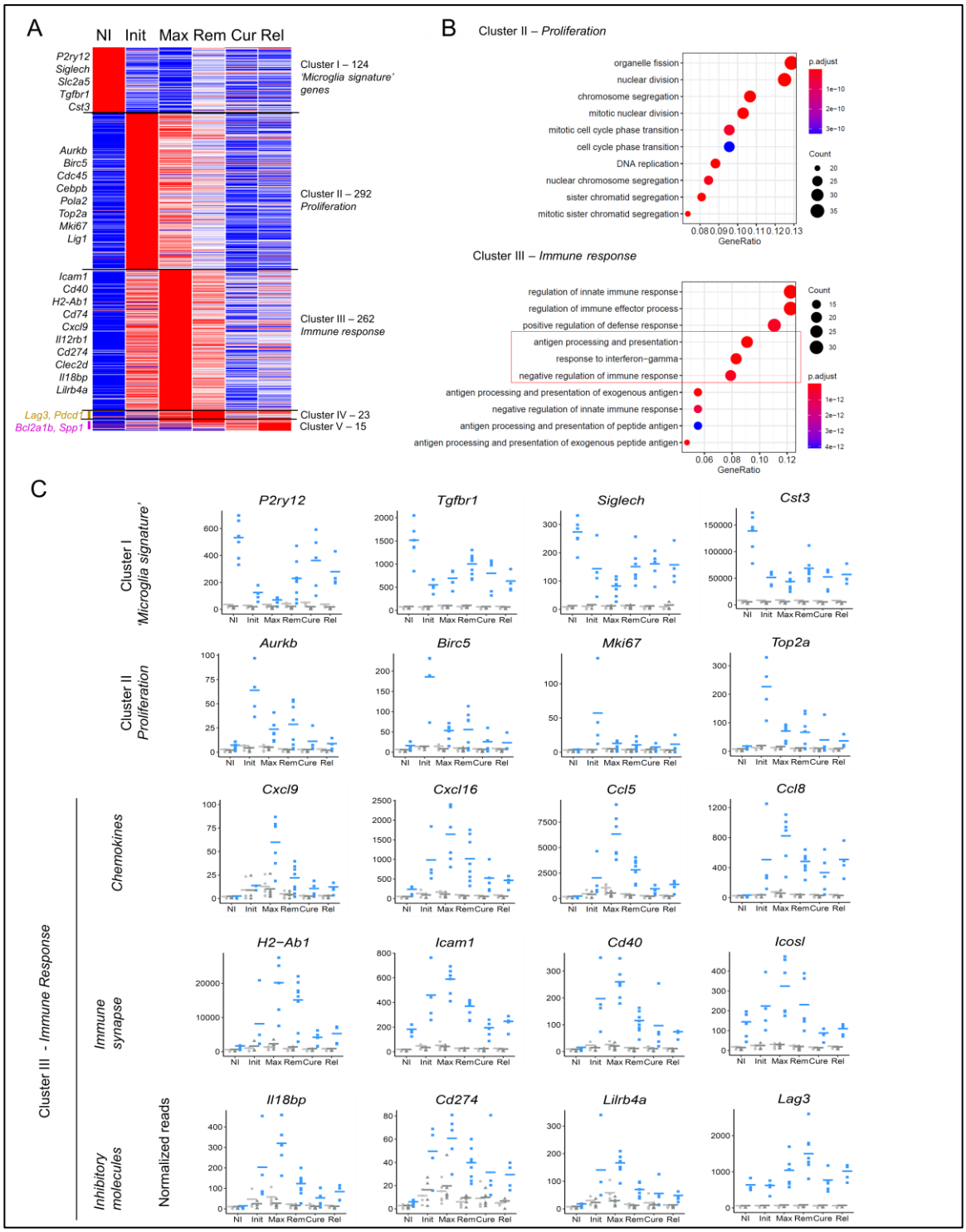

Figure 11. Microglial express immune-interaction and inhibitory molecules at the peak of RR-EAE. **(A)** Heatmap of 716 genes selected as maximal value >50, IP-specific (2 fold increase and p<0.05 of HA vs IgG and input in each stage) and differentially expressed (2 fold change and p<0.05) between each two IP-HA stages. Each column is an average of 4-8 individual biological replicate of the HA-IP. Genes were clustered using K-means clustering. **(B)** Metascape analysis of genes in cluster II (upper panel) and genes in cluster II+IV (lower panel), representing enriched GO terms and biological processes. **(C)** Representative genes from each cluster. Light gray circles = input, dark grey triangles = IP IgG, light blue squares = IP HA.

Microglia contributions to remission and relapse

The initial response of microglia to EAE was characterized by significant changes in gene expression, with 551 differentially expressed genes (DEG) between NI and initiation (**Figure 11, 12A**, left). In stark contrast, microglia essentially did not change their translatome in the second induction, with only 1 DEG between cure and relapse (**Figure 12A,** middle). Principal component analysis (PCA) of the data revealed that while microglia in diseased mice differed from that of NI mice with a spatial trajectory for the disease stages, it is evident that cure and relapse stages overlap (**Figure 12B**). These findings establish that microglia change significantly with the first induction of EAE, but are hardly responding in the relapse.

To better understand why microglia do not respond to the relapse, we compared the two clinically healthy states, i.e. 'NI' and 'Cure'. The PCA plot (**Figure 12B**) revealed that NI and Cure microglia cluster far from each other, with 193 DEG between the two groups (**Figure 12A,** right panel). The significantly downregulated genes in Cure vs NI (44 genes) were all related to cluster I (**Figure 12C**, lower panel), which represented microglia steady-state genes that were downregulated and not restored to steady-state levels – suggesting that microglia do not return to steady state even upon clinical recovery.

Interestingly, when we related the upregulated genes in Cure vs NI (149 genes) to the clusters originally compiled in the heatmap (**Figure 11A**), we found two thirds (100 genes) to be assigned to cluster III+IV that were related to *immune responses*, and 47 genes were assigned to cluster II, which was related to *proliferation* (**Figure 12C**, upper panel). Accordingly, GO enrichment analysis of these 149 genes revealed their relation to *cytokine signaling*, *response to interferon gamma* and *antigen presentation* (**Figure 12D**), indicating that microglia retain high expression of immune-related genes.

Closer examination of these genes by re-clustering clusters II and III generated in **Figure 11A**, revealed groups of genes, namely clusters 2a and 3a (**Figure 12E**), that although they were higher than NI, they were lower compared to initiation or max, i.e an intermediate expression between NI and max (or initiation). To conclude, even upon clinical recovery microglia do not return to ground state; rather they remain activated with an intermediate expression of immune molecules that is higher than at steady state, but lower than at the peak of EAE.

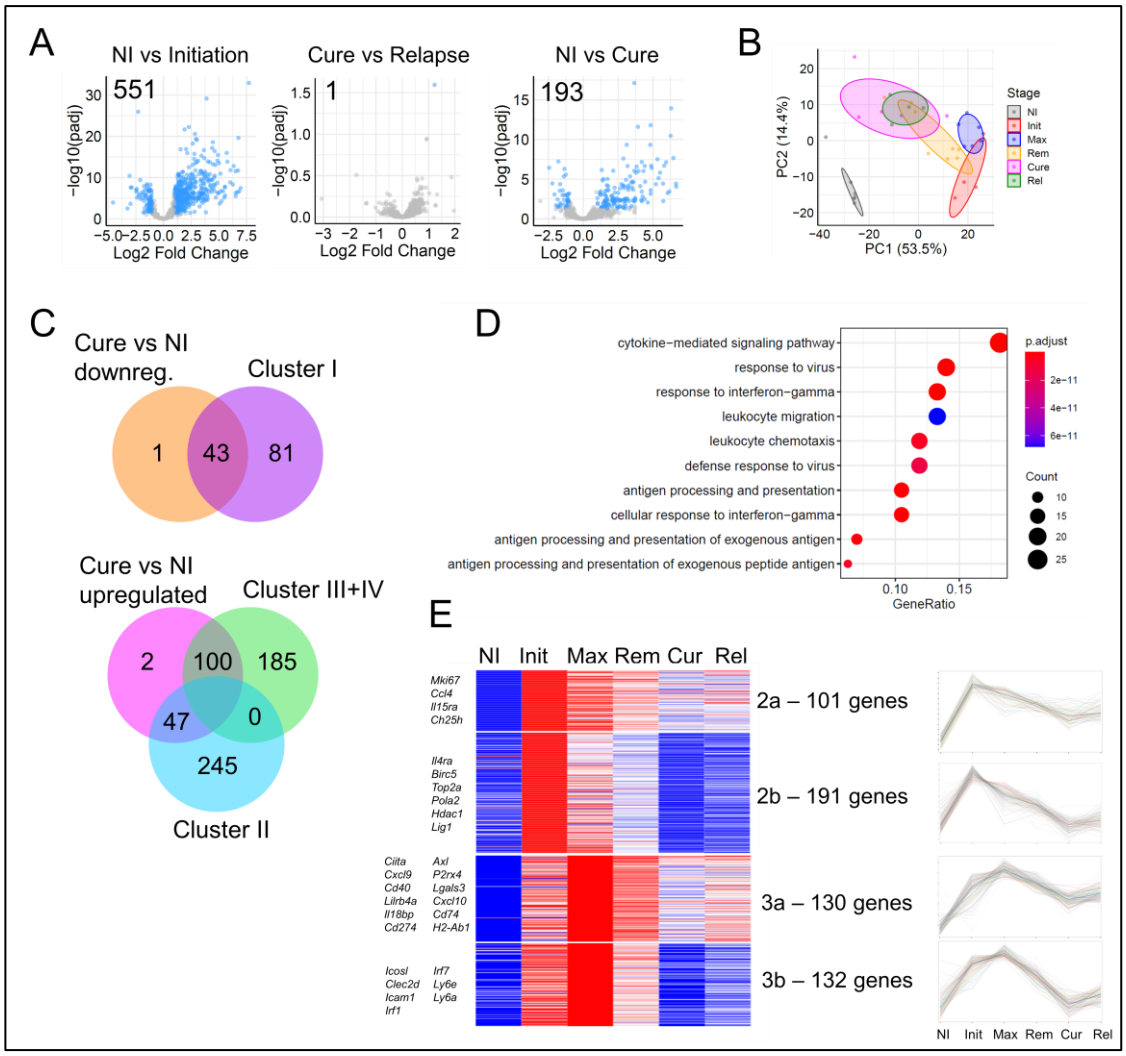

Figure 12. Microglia remain activated upon recovery and do not respond to relapse. **(A)** Volcano plots comparing differentially expressed genes between (left) non-immunized and initiation, (middle) cure vs relapse, and (right) NI vs cure. **(B)** PCA plot of IP HA of all the mice in the stages of RR-EAE. Each dot represents a mouse. Each color represents a different stage of RR-EAE (gray = NI, red = initiation, blue = max, yellow = rem, pink = cure, green = relapse). **(C)** Venn diagrams of lists of genes (UP) downregulated at cure compared to NI (orange, 44 genes) and genes from cluster I (purple, 124 genes) ; (DOWN) upregulated at cure compared to NI (pink, 149 genes), genes from clusters III+IV from figure 2A (green, 285 genes) and genes from cluster II from figure 2A (blue, 292 genes). **(D)** GO analysis of 149 genes upregulated in cure vs NI, showing that immune related pathways are still activated in microglia from cure mice. **(E)** Re-clustering clusters II and III from figure 2A. Right graphs represent the groups of genes in each cluster as z-scores on y axis and disease stages on the x axis.

Microglia depletion delays remission and results in T cell accumulation

To independently investigate contribution of microglia to the RR-EAE disease course we took advantage of a genetic microglia depletion model[15]. TAM treatment of *Cx3cr1*^{CreER}*:Rosa26*^{iDTR} mice results in expression of the Diphtheria Toxin Receptor (DTR) on microglia, rendering them sensitive to depletion by Diphtheria Toxin (DTx)[15]. Eight weeks post TAM treatment, we challenged *Cx3cr1*^{CreER}*:Rosa26*^{iDTR} F1 (B6*SJL) mice with PLP to induce RR-EAE, and treated the animals with either DTx, or PBS (as control), from day 3 post immunization and onwards, every other day throughout the disease course (**Figure 13A**). While the initial course of the disease was not significantly different between groups, mice treated with DTx fail to recover, as compared to controls (**Figure 13B**). This corroborated the earlier notion that microglia are not actively involved in the induction of the disease, but rather suggests that they might play a role in remission. Flow cytometry analysis confirmed partial but significant microglia depletion (50%) in brains and spinal cords of DTx-treated mice at day 25 post immunization (**Figure 13C**). Flow cytometry analysis of the immune infiltrates, incl. monocytes, macrophages, neutrophils, T and NK cells, revealed that only $CD4^+$ T cells were significantly accumulated in the brains of DTx treated mice (**Figure 13D**). Interestingly, $CD4^+$ T cell and microglia cell-numbers displayed an inverse correlation (**Figure 13E**) suggesting that microglia might play a role in the recovery from EAE, by controlling the $CD4^+$ T cell compartment.

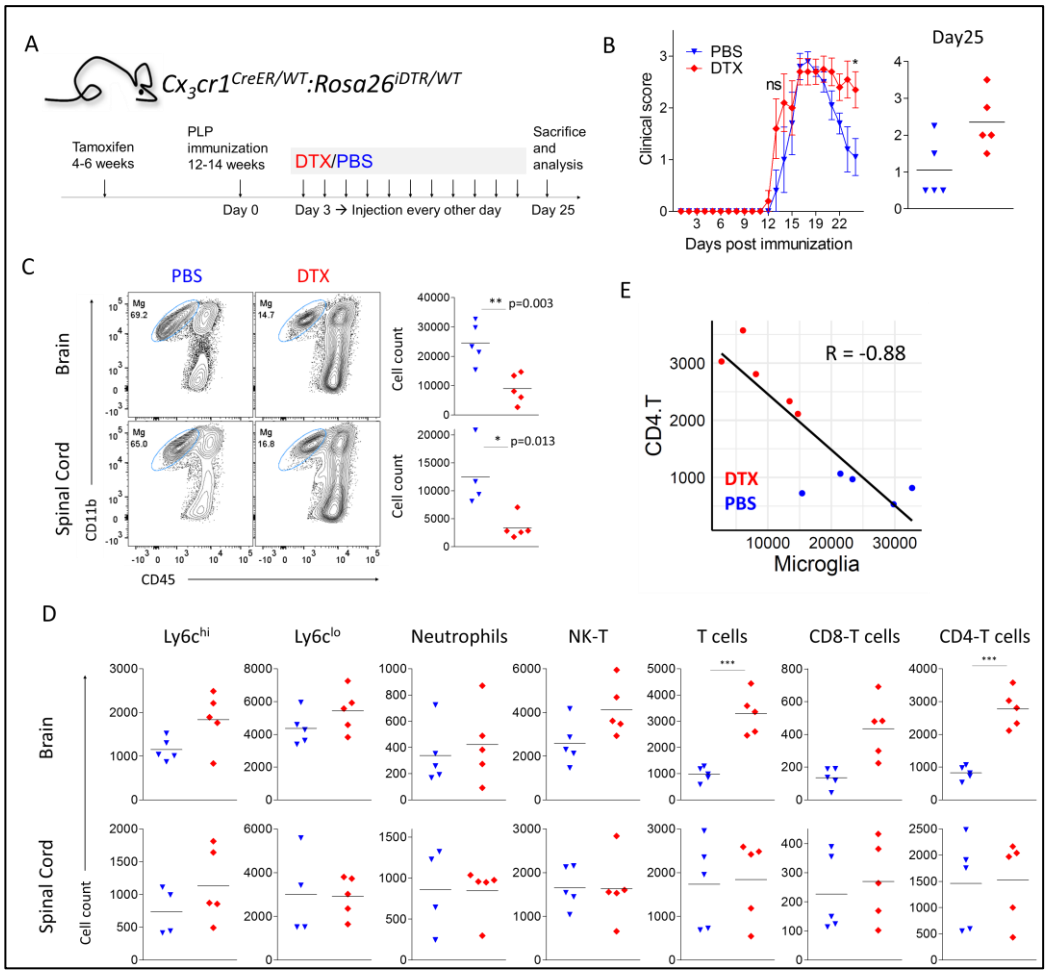

Figure 13. Depletion of microglia leads to T cell accumulation and delayed remission in RR-EAE. **(A)** Scheme describing mouse model used and DTx treatment. **(B)** Clinical scores of PBS vs DTX treated mice, showing delayed remission in DTX treated mice (left). Clinical scores of individual mice at day 25. **(C)** Representative FACS plots gated on live CD45+GR1- (left) and quantification of microglia counts (right panels) in PBS (blue triangles) and DTX (red diamonds) treated mice in brain (upper panels) and spinal cord (lower panels) at day 25 (from B). **(D)** Quantification of immune infiltrates in brain (upper panels) and spinal cord (lower panels) in PBS (blue triangles) and DTX (red diamonds) treated mice at day 25. **(E)** Correlation between microglia and CD4+T cell numbers in PBS (blue) and DTX treated mice showing negative correlation between microglia and T cell numbers R = -0.88. n=5 in each group. This is a representative experiment of 2 repeats.

Microglia closely interact with T cells

The translatome analysis and the result of the depletion experiment suggested that microglia might affect T cell numbers in the brain. To directly probe for microglia-T cell interactions, we performed immunohistochemistry analysis of brain sections of EAE diseased animals at the max stage. We found $CD3^+$ T cells to closely interact with $IBA1^+$ macrophages, either in the form of clusters of T cells surrounded by dense $IBA1^+$ networks, or individual $IBA1^+$ cells reaching out with their dendrites to T cells (**Figure 14A**). IBA1 is a generic macrophage marker and labels monocyte-derived macrophages as well[124]. To verify that some of the cells we saw interacting with T cells are indeed microglia, we resorted to the fate map feature of our RiboTag approach and stained for HA. Indeed, some of the $IBA1^+$ cells that interact with T cells expressed also HA-tagged ribosomes (**Figure 14B**), indicating that they are bona fide long-lived microglia that were targeted by TAM treatment before the onset of EAE.

The close Mg-T interactions raise the question whether they are functionally significant. Could this be a cognate immune interaction that affects T cell phenotype and ultimately influences the outcome of the disease? In support of this notion, we could visualize in tissue sections, that microglia (defined as $IBA1^+TMEM119^+$ or $IBA1^+HA^+$) interact with $CD3^+$ T cells, with focal MHC-II in the interface between the cells (**Figure 14C**).

Interestingly, using image stream analysis, that combines flow cytometry and imaging features, we noted that the $CD11b^+CD45^{hi}$ population is composed of ~50% doublets, as indicated by lower aspect ratio and larger area of the cells (**Figure 14D, left**). In contrast, $CD11b^+CD45^{int}$ microglia and $CD11b^-CD45^{hi}$ lymphocytes comprised only ~5% doublets (**Figure 14D, left**). The doublets of the $CD11b^+CD45^{hi}$ population contained microglia ($CD45^{int}CD11b^+GR1^-$) and $CD4^+$ T cells ($CD45^{hi}$ $TCRb^+$ $CD4^+$), termed here Mg-T (**Figure 14D, right**). These Mg-T doublets were enriched with focal ICAM1, MHC-II and CD4 in the immune synapse between the cells, suggesting that this is indeed a real immune interaction that existed in the tissue context and survived the isolation steps.

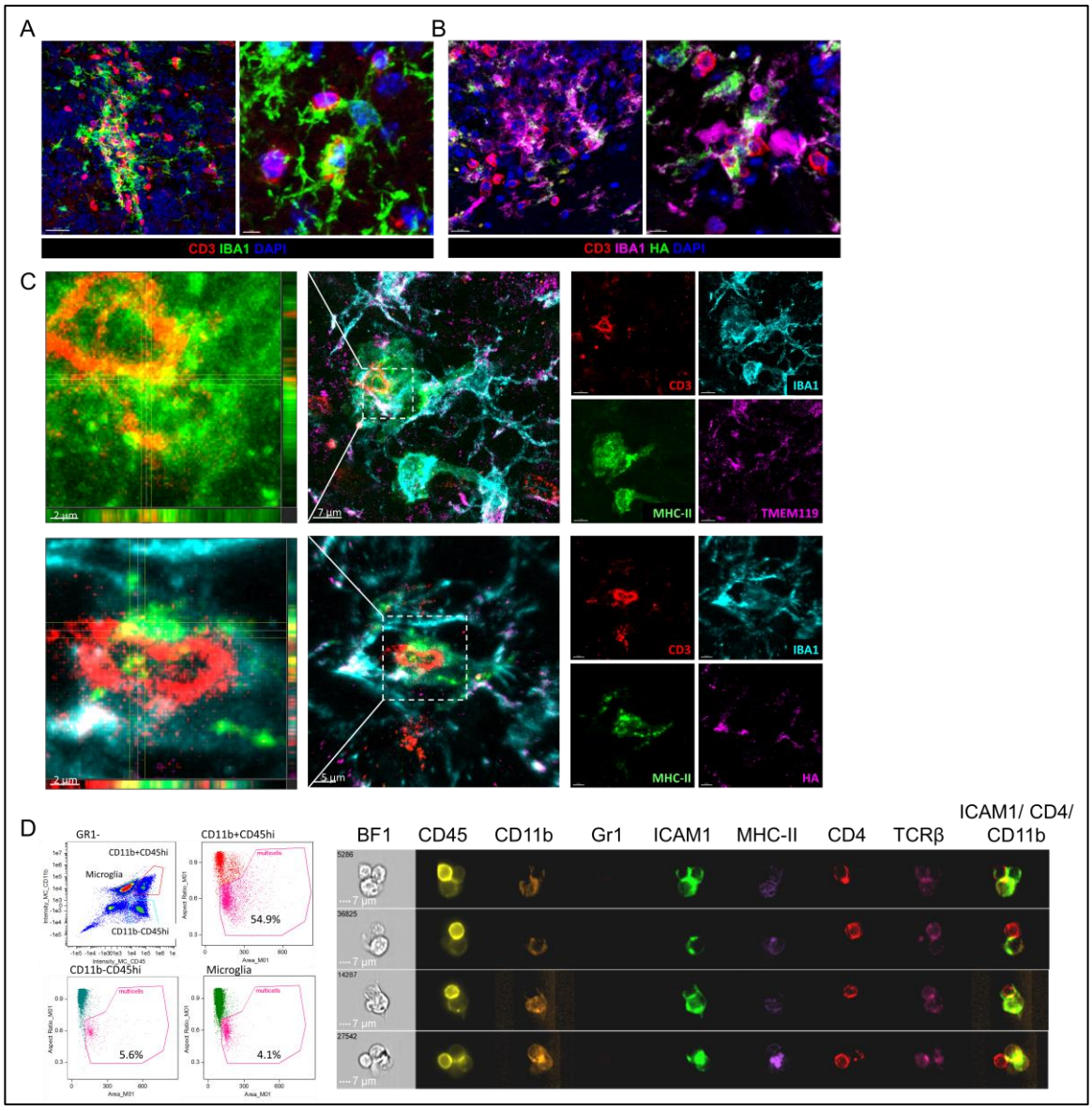

Figure 14. Microglia closely interact with T cells in the tissue. Immunofluorescent staining of **(A)** CD3 (red), IBA1 (green) and DAPI (blue), and **(B)** CD3 (red), IBA1 (magenta), HA (green) and DAPI (blue), sowing HA+ microglia interacting with T cells, in brain at Max stage. **(C)** Immunofluorescent staining of CD3 (red), IBA1 (cyan), TMEM119 (up) or HA (down, magenta) and MHC-II (green) in brain at Max stage. Right panels are single stains, middle panel is composite and left panel is a magnification of the dotted square in the middle panel. Upper magnification is only MHC-II (green) and CD3 (red). **(D)** Image stream pictures of doublets of cells that are composed of microglia ($CD45^{int}CD11b^{+}GR1^{-}$) and $CD45^{hi}CD4^{+}TCRb^{+}$ T cells, with ICAM1 and MHCII at the immune synapse.

Mg-T doublets could be an artifact formed ex-vivo. To investigate this possibility, we performed a mixing experiment in which we took brains from a whole body GFP and a whole body TdTomato (B6*SJL) F1 mice at max stage of RR-EAE and processed them together throughout the entire isolation protocol (enzymatic digestion, percoll, etc.) (**Figure 15A**). In case of a perfect 50:50 mix of green:red cells, statistically, spurious doublet formation would expectedly be anywhere between 0 and 50%, indicating either no ex-vivo random formation or a complete random formation of doublets, respectively. Flow cytometry analysis showed that from the entire "single cells" gate, the ratio of total GFP+:TdTomato+ cells was approximately 30:70. Statistical calculations of this ratio indicated that the expected percent of completely random mixed pairs would be 42% (**Figure 15C**). Our flow cytometry analysis revealed that the GFP^+ $TdTomato^+$ doublets comprised only ~3% of the $CD45^+$ $Gr1^-$ cell population, 0.8% of microglia, and ~5% of $CD4^+$ T cells alone (**Figure 15B**). In contrast, when gating on $CD11b^{hi}$ $CD45^{hi}$ $CD4^+$ $TCRb^+$ events (reflecting T cells interacting with $CD11b^+$ microglia or macrophages), 15% of this population were GFP^+ $TdTomato^+$ (**Figure 15C**). These data suggest that doublets, that were found mostly in the $CD11b^+$ $CD45^{hi}$ gate, are not formed completely randomly (which would show 42%), but that *ex vivo* formation probably also contributes to some extent. Of note, in this analysis we cannot discriminate between microglia and monocyte-derived macrophages due to restriction of fluorophores. In addition, since each of the single populations (microglia or CD4+T cells) essentially did not form ex-vivo doublets, we assumed that even though there is little ex-vivo formation of doublets, it is biologically relevant due to the affinity of the two cell types for each other.

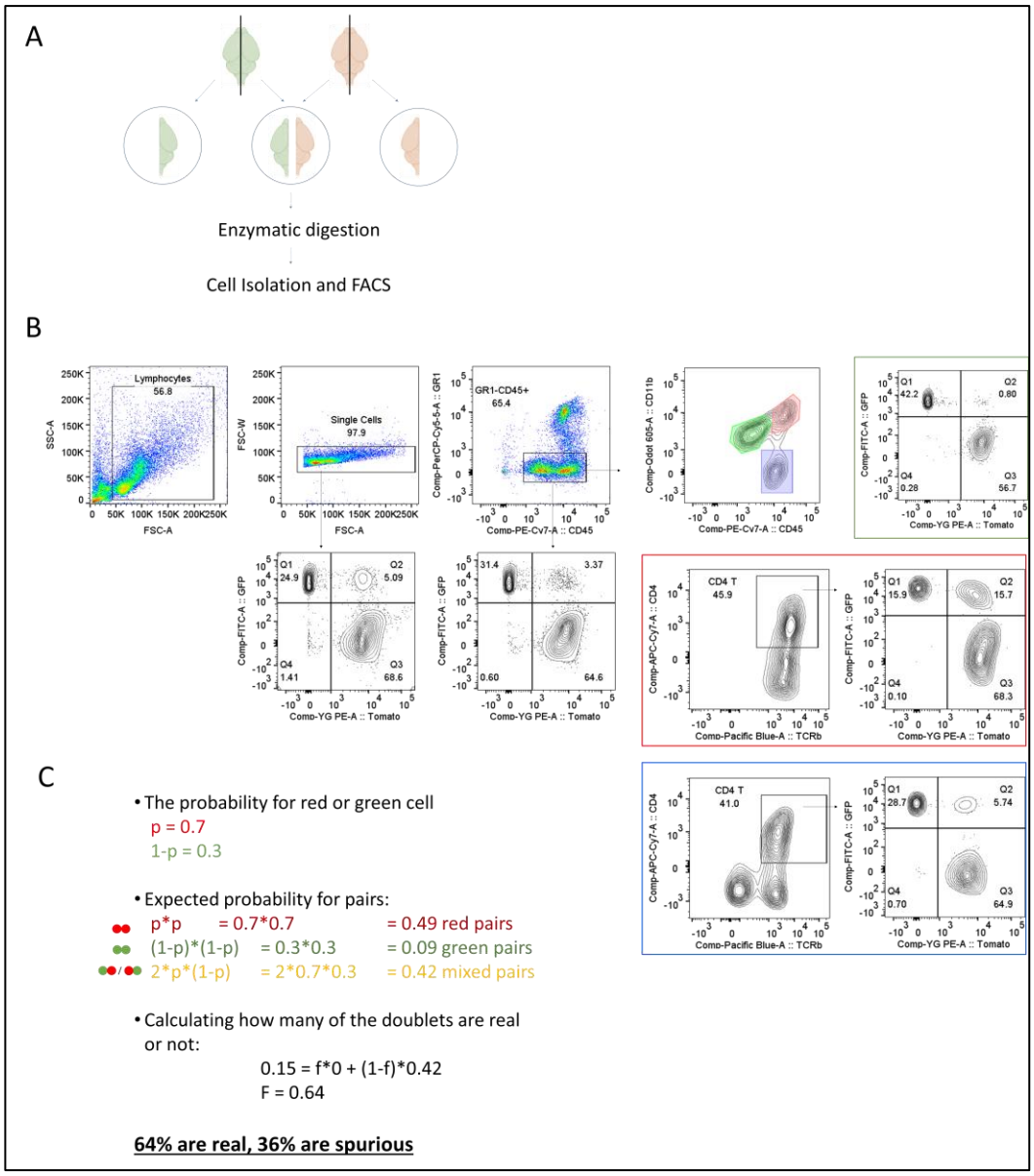

Figure 15. Probing the extent of ex-vivo Microglia-T cell doublet formation. **(A)** Scheme describing the mixing experiment where brains from a whole body GFP or whole body TdTomato mice were mixed together or isolated separately. Mixed brains went through enzymatic digestion and cell isolation process together. **(B)** Gating strategy showing the extent of GFP/TdTomato cells from each population. **(C)** Calculation of the probability to receive spurious vs real doublets, showing that most of the doublets are not spurious (with kind help of Shalev Itzkovitz, WIS).

We next tested whether the formation of Mg-T doublets was stage-dependent. Using flow cytometry analysis we defined Mg-T cells as $CD45^{hi}$ $TCRb^{+}$ $CD4^{+}$ $CD11b^{+}$ $TMEM119^{+}$ events, and singlet T cells as $CD45^{hi}$ $TCRb^{+}$ $CD4^{+}$ $CD11b^{-}$ $TMEM119^{-}$ events (gating strategy in **Figure 16A**). In order to quantify them uniformly and not have them bias each other, we quantified both populations as percent of the live $CD45^{+}$ $Gr1^{-}$ population that includes all immune cells (except monocytes and neutrophils). For this reason, the percent of cells is not high, but our focus was on the kinetics, rather than the percent. We found that while the proportion of singlet T cells peaked at the initiation, very few Mg-T doublets were seen at this stage (**Figure 16B**). However, the proportion of doublets raised with the progression of the disease (at max) and stayed high at remission, while in parallel the proportion of singlet T cells gradually decreased. Such stage-dependent kinetics of T vs Mg-T subsets would be compatible with the assumption of an influential relationship between the formation of Mg-T and the decrease of singlet T cells in the tissue.

Flow cytometry analysis of MHC-II, ICAM-1 and PDL-1 at the different stages showed that microglia ($TMEM119^{+}$ HA^{+}) upregulate these molecules with the progression of EAE (**Figure 16C**), in correlation to the RiboTag data and to the formation of Mg-T doublets (**Figure 16B**). Interestingly, Mg-T doublets expressed higher levels of these markers compared to microglia alone (**Figure 16C,** red vs purple histograms). The fact that microglia that interact with T cells express higher MHC-II, ICAM-1 and PDL1 suggests that microglia indeed interact with $CD4^{+}$ T cells in an cognate TCR-mediated fashion via MHC-II and ICAM-1, and potentially have inhibitory effect via PDL1.

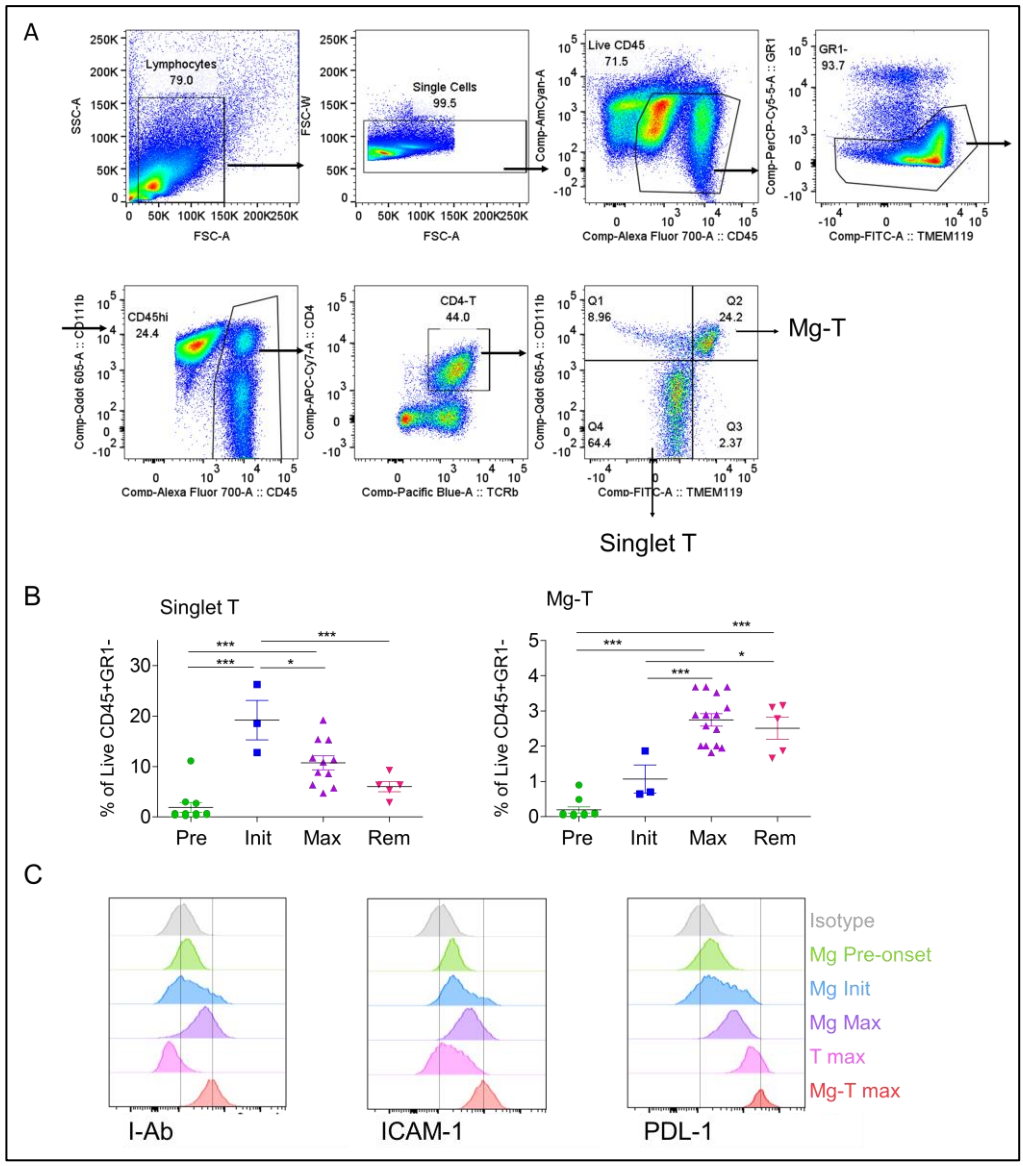

Figure 16. Mg-T doublet formation peaks at Max stage. **(A)** gating strategy to quantify singlet T cells vs. Mg-T doublets. **(B)** Quantification by flow cytometry of singlet T cells (left) and Mg-T doublets (right) as percent of Live CD45+GR1- population (as gated in A), at different stages of RR-EAE (pre = pre onset, init = initiation, max = score ~3). Each dot represents an individual mouse, results are combination of 4 individual experiments. Line represents mean and error bars are SEM. Significance was calculated with one-way ANOVA and bonferroni multiple comparison test. **(C)** Flow cytometry analysis of I-Ab (left), ICAM-1 (middle), and PDL-1 (right) on microglia (Mg) at different stages (green = pre onset, blue = initiation, purple = max), and on T (pink) or Mg-T (red) at max stage.

Next we investigated which $CD4^+$ T cells do microglia interact with, and whether there is a temporal preference for a specific subset. Image stream analysis showed that both $Foxp3^+$ and $ROR\gamma t^+$ T cell subsets are found in the doublets and hence can interact with microglia (**Figure 17A**). Flow cytometry analysis revealed that at both the max and the remission stages, the Mg-T population was enriched with Treg cells, as compared to the singlet T cell compartment (**Figure 17B**), suggesting a preferred interaction of microglia with regulatory T cells.

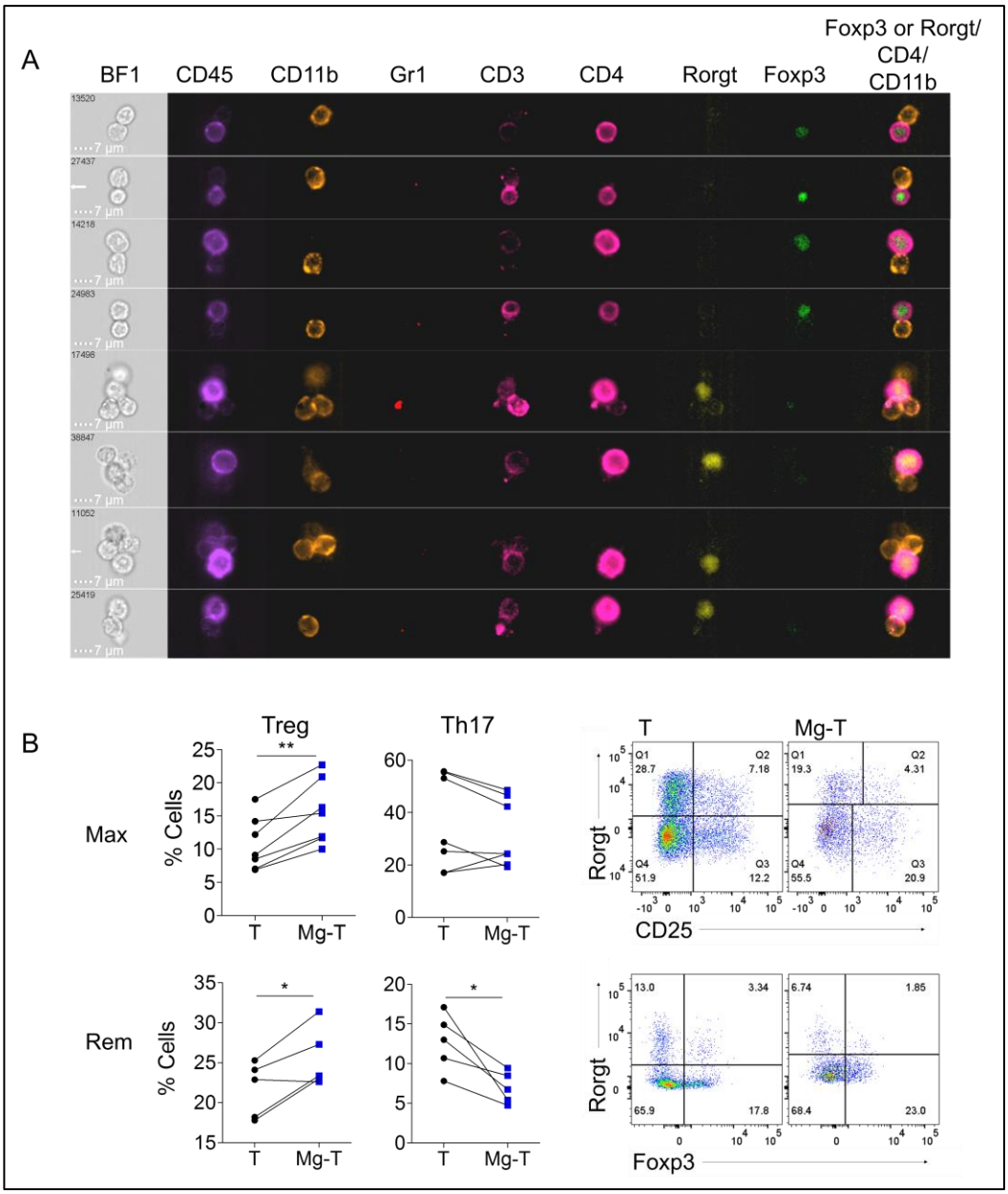

Figure 17. Microglia-T doublets are enriched in regulatory T cells at max and remission. **(A)** Image stream analysis showing doublets of microglia (CD45loCD11b+GR1-) and CD45hiCD3+CD4+ cells that are either Foxp3+ or RORγt+, showing microglia interacting with both Tregs and Th17 cells. **(B)** Quantification of Treg vs Th17 cells from T or Mg-T populations (left) and representative FACS plots (right), at max stage (up) or remission (down), showing enrichment of Tregs within Mg-T compared to singlet T.

Together these results indicate that microglia interact with T cells in the brain, forming cognate immune synapses through MHC-II, in a stage dependent manner with interactions peaking at max and rem, strong enough to survive the cell isolation procedure. Our data further suggest that microglia can interact with both Th17 and Treg cells, but prefer to do so with the latter.

Probing the CXCL9:CXCR3 axis

Mechanistically, in order to interact with T cells, the first step for microglia would be to secrete chemokines to attract T cells. According to our RiboTag data, one of the chemoattractants microglia expressed was *Cxcl9*. Interestingly, the CXCL9 receptor CXCR3, was shown to be critical for the recovery from different injury models by controlling the recruitment of Treg cells to the injured tissue[125,126]. We therefore focused our attention on CXCL9. Despite the established role of CXCR3 in Th1 response and its link to other pathologies[127], mice lacking CXCR3 not only successfully develop EAE, but succumb to a more severe disease[128,129], presumably due to decreased recruitment of regulatory cells[129].

To verify that microglia, but not other macrophages, indeed express *Cxcl9*, we performed a qPCR analysis for *Cxcl9* on various populations sorted from healthy and diseased brains (gated on live $GR1^-$): $CD11b^+$ $CD45^{int}$ microglia, $CD11b^+$ $CD45^{hi}$ double positive (DP, macrophages), $CD11b^-CD45^{hi}$ lymphocytes and double negative (DN) cells (**Figure 18A**). qPCR of the sorted populations showed that in NI brains none of the cells expressed *Cxcl9*, however at max stage both microglia and the DP population, but not lymphocytes or DN cells, expressed *Cxcl9* (**Figure 18B**). However, post sort analysis revealed that the DP population "breaks down" into microglia and lymphocytes after sorting (**Figure 18C**). We then applied a different gating strategy for sorting, by gating on $CD11b^+$ cells from which we sorted either $TMEM119^+$ $CD44^-$ (microglia) or $TMEM119^-$ $CD44^+$ (macrophage singlets, referred to as Mf-s), excluding double positive cells (**Figure 18D**). qPCR for *Cxcl9* in these populations demonstrated that microglia, but not macrophages express *Cxcl9* at the max stage. When probing for the receptor, *Cxcr3*, in the same sorted populations, we found the mirror picture, i.e. *Cxcr3* transcripts were detected in lymphocytes and in the DP population, but not in microglia or 'Mf-s' (**Figure 18F**). Taken together, these results demonstrate that the DP population, that we showed previously to include Mg-T interacting cells, is positive for both *Cxcl9* and *Cxcr3* transcripts, which arise solely from microglia and lymphocyte, respectively. This could suggest that *Cxcl9* expressing microglia might indeed attract $Cxcr3^+$ lymphocytes to interact with them.

In order to probe if this attraction axis is essential for Mg-T interactions and for recovery from EAE, we treated F1 mice with a chemical antagonist for CXCR3, AMG 487[130], here termed AMG, and followed the progression of RR-EAE. Mice were treated with either AMG or vehicle every day, from day 10 post immunization, prior to disease onset, and throughout the experiment. We found no significant difference between the groups, suggesting that although

microglia might use the CXCL9-CXCR3 axis to attract T cells, it is likely not the only mechanism. However, the experiment lacked a positive control that the inhibitor worked and thus will for a final conclusion have to be repeated.

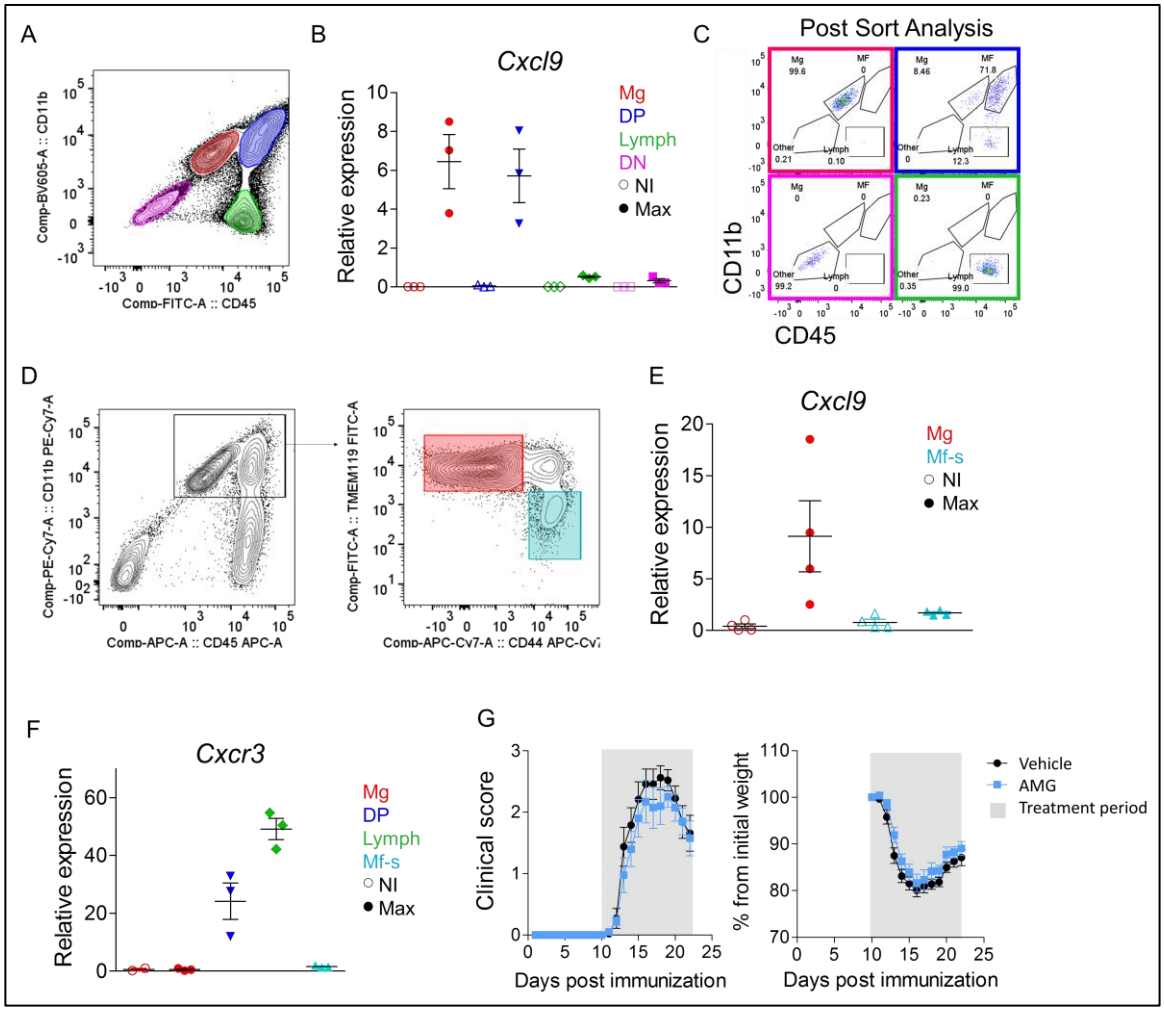

***Figure 18. Microglia-T doublets, but not macrophages, co-express Cxcl9 and Cxcr3 - a potential mechanism of T cell attraction by microglia*.** **(A)** FACS plot presenting sorted populations, gated on live GR1-. Red = CD11bhiCD45int (microglia), blue = CD11bhiCD45hi (double positive, DP), green = CD11b-CD45hi (lymphocytes), pink = CD11b-CD45- (double negative). **(B)** qPCR for Cxcl9 in sorted populations from A. Mg = microglia, red circles; DP = double positive, blue triangles; Lymph = lymphocytes, green diamonds; DN = double negative, pink squares. Empty shapes = NI mice, filled shapes = max, sorted from brain tissue. **(C)** Post-sort analysis of sorted populations from (A), showing microglia and T cells in the "DP" sorted cells. Color coding as in (A). **(D)** Gating strategy for microglia (red, CD11b+TMEM119+CD44-) and macrophages (turquoise, CD11b+TMEM119-CD44hi), gating out double positive cells. **(E)** qPCR for Cxcl9 in sorted populations from (D); Mg = microglia, red circles; Mf-s = macrophages singlets, turquoise triangles. Empty shapes = NI mice, filled shapes = max, both sorted from brain tissue. **(F)** qPCR for Cxcr3 in all populations sorted from (A) and (D). Mg = microglia, red circles; DP = double positive, blue triangles; Lymph = lymphocytes, green diamonds; Mf-s = macrophages singlets, turquoise triangles. Empty shapes = NI mice, filled shapes = max, both sorted from brain tissue. **(G)** Clinical scores (left) and % of initial weight (right) summary of mice treated with CXCR3 chemical blocker or vehicle from day 10 during RR-EAE (n=12 mice per group). This is a representative experiment out of 3 independent repeats.

A Wiskott Aldrich Syndrom Protein (WASP) deficiency in microglia leads to delayed recovery from RR-EAE

Our translatome data, as well as the results of the microglia depletion and histology suggest that microglia might affect the balance of effector and regulatory T cells at the advanced stages of EAE. To further dissect the contribution of microglia to RR-EAE and their potential effect on T cells, we decided to specifically perturb microglia function. For that, we generated animals that harbor a Wiskott Aldrich Syndrome (*WAS*) gene deletion specifically in microglia.

Wiskott Aldrich Syndrome (WAS) is a rare x-linked genetic syndrome, which leads to severe immunodeficiency due to its specificity to the hematopoietic cell lineage[131]. Wiskott Aldrich Syndrome Protein (WASp) is a major regulator of actin polymerization that is crucial for all actin dependent processes in hematopoietic cells, such as migration, phagocytosis, and also immune interaction [132]. Specifically, cells deficient in WASp cannot organize their immune synapse and neither can they form the cuff for cell-cell interaction, affecting the efficiency of cell-cell contact and antigen presentation[133]. WASp contribution to peripheral immunity and its role in T cell biology, as well as dendritic cells and macrophages has been described in depth[132]. However the specific role of WASp in microglia has not been addressed yet, including its importance in MS models. Patients harboring a complete loss of WASp function often die within the first years of life due to recurrent infections, unless treated by BMT[134]. However even upon a successful BMT, that cures the patients, these individuals likely retain some WAS-deficient microglia, since these cells are relatively radio- and chemoresistant[19]. Therefore the elucidation of the role of microglial WASp in pathology is not only mechanistically interesting but also clinically relevant.

Here, we studied the contribution of WASp in microglia to our RR-EAE model in (B6*SJL) H-$2^{b/s}$ F1 hybrids. Specifically, we crossed *Cx3cr1*$^{CreER/CreER}$:*Rpl22*$^{HA/HA}$:*Was* $^{fl/wt}$ B6 females to WT SJL males, and used their *Cx3cr1*$^{CreER/WT}$:*Rpl22*$^{HA/WT}$:*Was*$^{fl/y}$ F1 male offsprings (referred to here as $Mg^{\Delta WAS}$), as well as littermate controls (*Cx3cr1*$^{CreER/WT}$:*Rpl22*$^{HA/WT}$, **Figure 19A**). Notably, since *Was* is an X-linked gene, males have only one copy. Immunization with PLP peptide and adjuvants induced EAE in both $Mg^{\Delta WAS}$ mice and controls (**Figure 19B**). We found no significant difference in the clinical score at induction and the max stage of the mice, neither did the day of onset or weight loss at the initiation and at max stage differ between the two groups (**Figure 19B, 19D-F**). However, at the remission stage, while littermate control mice were in the process of recovery, $Mg^{\Delta WAS}$ mice failed to recover (**Figure 19B**). At day 30 post immunization there was a significant difference in clinical scores and weight loss: $Mg^{\Delta WAS}$

mice could not recover from paralysis, nor did they gain their original weight back, as opposed to littermate controls (**Figure 19B, 19C**). This result reinforces the previous finding that microglia are dispensable for the induction of EAE[94], and supports the notion of a role for microglia in recovery, in accordance with our depletion experiment data.

Analysis of singlet T and Mg-T at the max stage revealed that there was no significant difference in the formation of Mg-T between the groups (**Figure 19G**), but there were more T cells in $Mg^{\Delta WAS}$ mice compared to controls (**Figure 19H**). At remission there was a slight elevation in Mg-T doublets, but no difference in singlet $CD4^+$ T cells. Examination of the $CD4^+$ T cell subpopulations (specifically $ROR\gamma t^+$ and $Foxp3^+$ cells) showed that in remission (but not in max) there is accumulation of $Foxp3^+$ cells in brains of $Mg^{\Delta WAS}$ mice compared to controls (**Figure 19I**). These results indicate that the WASp deficiency in microglia does not result in changes in the formation of doublets, but does affect the fate of $CD4^+$T cells in the brain, and ultimately the recovery from RR-EAE.

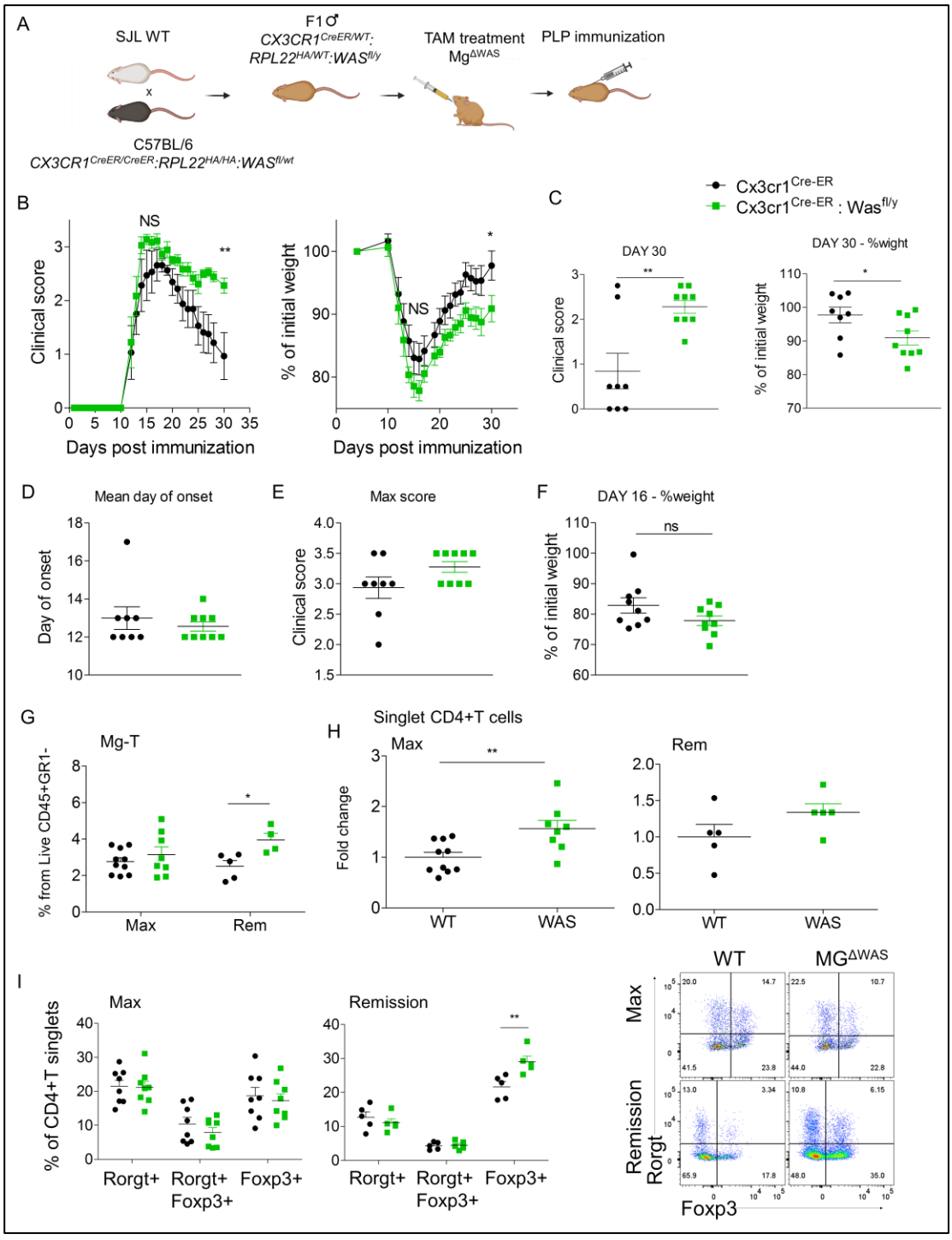

Figure 19. WASp is crucial for microglia-mediated recovery from RR-EAE through impact on T cells. (A) Scheme of mice cross. **(B)** Clinical scores (left) and weight loss (right) of Cx3cr1CreER (black circles) vs Cx3cr1CreER:Wasfl/y ($Mg^{\Delta WAS}$, green squares), showing that $Mg^{\Delta WAS}$ do not recover and to not return to steady state weight by day 30 compared to WT controls. Representative experiment of 3 repeats. N = 8 (WT), 9 ($Mg^{\Delta WAS}$). Lines represent mean, error bars are SEM, significance was calculated using t-test. **(C)** Clinical scores (left) and % of initial weight (right) of individual mice at day 30 post immunization from B, Lines represent mean, error bars are SEM, significance was calculated using t-test. Mean day of onset **(D)**, maximal scores **(E),** and % of initial weight at day16 **(F)** of individual mice. **(G)** Mg-T doublets percent form live CD45+GR1- population at max and rem. Significance calculated using two-way Anova. **(H)** Singlet CD4+T cells fold change over control of the % of CD4+T cells from live CD45+GR1- population. **(I)** The percent of T cell subpopulations from CD4+T singlets (CD45hiCD4+TCRb+CD11b-TMEM119-), at max (left graph) and remission (right graph), and a representative FACS plot for each condition on the right most. Combination

of 2 independent experiments. Each dot is an individual mouse. Lines represent mean, error bars are SEM, significance was calculated using two-way ANOVA and Bonferroni multiple comparison test.

MHC-II deficiency in microglia in RR-EAE

WASp deficiency in microglia halted remission through an impact on CD4+T cells. However, since actin regulation hinders a broad spectrum of cellular activity, we chose to further focus on a more specific $CD4^+$ T cell-related activity, i.e. antigen presentation.

Thymic T regulatory cells infiltrate into the CNS, proliferate locally and are selected for specific TCR chain, ultimately leading to resolution of EAE[78,79]. TCR signaling is essential for regulatory T cells to exert their suppressive functions[80,81]. However the cues driving this phenomena in the CNS are not known.

Our RiboTag data showed upregulation of antigen-presentation-related genes at peak (**Figure 11B, 11C**), and our histology images show that microglia present MHC-II to T cells (**Figure 14C**). Microglial MHC-II is dispensable for the induction of EAE[94], but its contribution to recovery was not explored. The use of F1 hybrids is limiting due to lack of floxed or even KO alleles in the SJL strain. For that reason we decided to use the CRISPR-CAS9 system to generate H2-Ab1 KO SJL mice. The rationale was to cross H2-$Ab1^{KO}$ SJL to *Cx3cr1*$^{CreER/CreER}$*:H2-Ab1*$^{flox/WT}$ C57BL/6 mice and to use the *Cx3cr1*$^{CreER/WT}$*:H2-Ab1*$^{flox/KO}$ F1 (H-$2^{b(fl)/-}$) offspring (hereby referred to as $Mg^{\Delta MHC\text{-}II}$) and their *Cx3cr1*$^{CreER/WT}$*:H2-Ab1*$^{WT/KO}$ (H-$2^{b/-}$) littermate controls in the RR-EAE paradigm (**Figure 20G**). Since the genome of SJL mice is not available, we first amplified and sequenced the region of interest using primers located in conserved regions among 16 different strains. Accordingly, we designed two guide-RNAs spanning the promoter and first exon region of the H2-Ab1 locus (detailed in the method section). A considerable number of SJL mice (11 mice) with a homozygous deletion of ~300bp of the promoter and first exon of the H2-Ab1 gene were successfully generated (detailed in the methods section). Surprisingly, and in contrast to C57BL/6 H2-Ab1 KO mice, which are when kept in an SPF facility healthy and fertile, SJL H2-Ab1 KO mice displayed signs of pathology and skin disorders (**Figure 20C**), and eventually died within a few weeks. Analysis of the blood of H2-Ab1 KO SJL mice showed that the animals were devoid of $CD4^+$ T cells (in line with reports from C57BL/6 H2Ab1 KO mice) (**Figure 20A**, up). On top of that, the blood of H2-Ab1 KO SJL mice was enriched in myeloid cells ($CD11b^+$), specifically with monocytes and neutrophils (**Figure 20A**, down). qPCR analysis of the white blood cells of these mice showed undetectable H2-Ab1 transcripts (**Figure 20B)**, confirming the successful deletion of the gene. These results demonstrate that we successfully disrupted the H2-Ab1 gene

of the SJL strain, in a way that let to abrogation of the mRNA and resulted in depletion of $CD4^+$ T cells, accumulation of monocytes and neutrophils and finally death of the KO animals. We eventually succeeded to obtain four SJL offsprings from one of the H2-Ab1 KO SJL animals. Genotyping surprisingly showed only the WT, but not the KO band in those pups (**Figure 20D**). Flow cytometry analysis of their blood B cells showed a heterozygous expression of $H\text{-}2^s$ (**Figure 20F**). The heterozygosity of the protein expression but the lack of a KO bend in the genotyping suggested the presence of a bigger deletion in one allele. A PCR reaction designed for a larger area (~1200bp) picked up the mutated allele (~900bp) in these pups (**Figure 20E**). These animals were further crossed either to each other to generate mice with homozygous deletion, or to BL6 MHC-II flox animals to generate F1 $Mg^{\Delta MHC\text{-}II}$ mice.

Flow cytometry analysis of blood B cells in F1 pups from the cross of *H2-Ab1*$^{KO/WT}$ SJL to BL6 *Cx3cr1*$^{CreER/CreER}$*:H2-Ab1*$^{flox/WT}$ (**Figure 20G**) mice showed either co-expression of the $H\text{-}2^s$ (the SJL haplotype) and $H\text{-}2^b$ (the BL6 haplotype) or only $H\text{-}2^b$, representing mice harboring the WT or KO $H\text{-}2^s$ allele respectively (**Figure 20H**). At the time of writing we had a group of $Mg^{\Delta MHCII}$ mice treated with TAM and we are ready to perform the RR-EAE experiment 6 weeks after TAM treatment. Other than $Mg^{\Delta MHCII}$ mice we have littermate controls that are $H\text{-}2^{s/b(fl)}$, $H\text{-}2^{-/b}$ and $H\text{-}2^{s/b}$, therefore we will know the effect of each allele on the disease course.

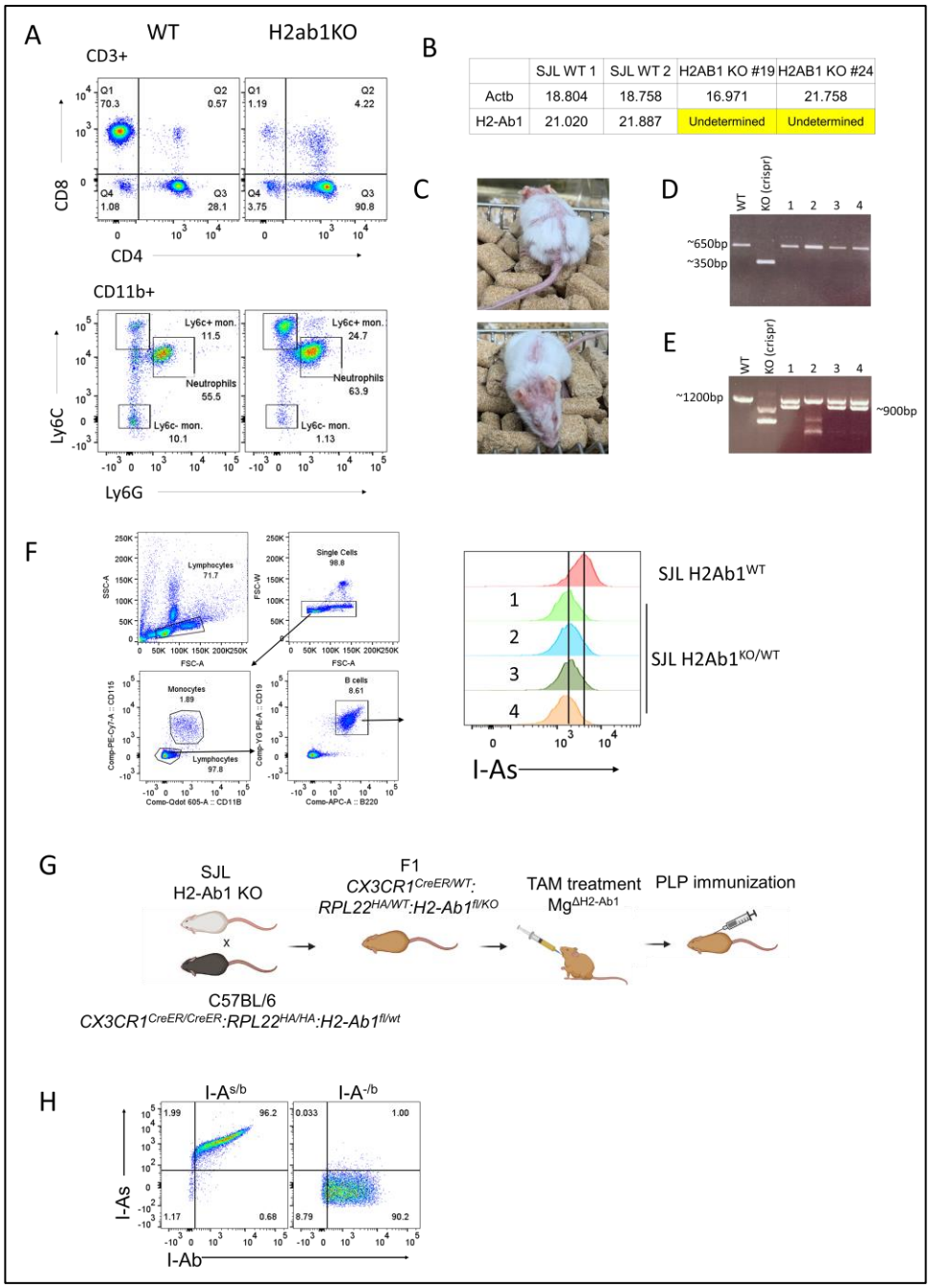

	SJL WT 1	SJL WT 2	H2AB1 KO #19	H2AB1 KO #24
Actb	18.804	18.758	16.971	21.758
H2-Ab1	21.020	21.887	Undetermined	Undetermined

Figure 20. Generation of SJL H2-Ab1 KO mice. **(A)** Flow cytometry analysis of blood of WT and H2-Ab1 KO SJL mice. Upper plots are CD3+ T cells, and lower plots are myeloid CD11b+ cells, left are WT and right are H2-AB1 KO, showing depletion of CD4+T cells and accumulation of monocytes and neutrophils. **(B)** qPCR analysis of H2-Ab1 and Actin (actb) from whole white blood cells extracted using ACK lysis of RBCs, in SJL H2AB1 KO and WT. **(C)** Images of SJL H2AB1 KO mice generated with Crispr-Cas9 showing poor condition of these mice. **(D+E)** genotype analysis of the pups of the crispr founder crossed to WT mouse, genotyped with short product primers **(D)**, or with long product primers **(E)** showing KO bend only with the long-product primers. **(F)** Flow cytometry analysis of B cells in the blood of pups of the crispr founder showing heterozygous expression of the I-As. **(G)** scheme of crossing mice to generate F1 mice with specific MHC-II deletion in microglia. **(H)** Flow cytometry analysis for I-As and I-Ab in F1 pups generated as in G, showing KO of the SJL haplotype.

Interferon Gamma Receptor (IFNγR1) deficiency in microglia in RR-EAE

To further investigate the mechanisms controlling microglial response in RR-EAE, we turned to the interferon gamma (IFNγ) response. The interferon response was prominently activated in microglia according to our RiboTag data, as reflected by the of IFNγ response genes, such as *Irf1*, *H2-Ab1* and *Cxcl9* (**Figure 11**).

IFNγ is secreted by myelin-specific encephalitogenic Th1 cells that infiltrate into the CNS[62,135]. IFNγ is considered a pathogenic cytokine in MS since the injection of IFNγ to MS patients exacerbated symptoms[136]. IFNγ concentration in the CSF and serum of MS patients is increased compared to healthy controls and has been detected in active areas of MS lesions[137,138]. Animal studies support this notion as injection of IFNγ to the blood or CNS of healthy animals resulted in an inflammatory pathology resembling EAE[66,67]. However surprisingly, worsened symptoms of EAE were seen upon the administration of IFNγ blocking antibodies[139], as well as in IFNγ or IFNγR deficient animals[68–71,140], indicating a complex role of IFNγ in EAE and MS. Indeed it was suggested that IFNγ might play distinct roles at different stages of EAE[72,73], as injection of IFNγ prior to EAE onset worsened the disease, but its administration after onset was protective, and depended on IFNγR signaling[141]. Cell-specific contributions of IFNγ and IFNγR in RR-EAE has not been addressed. Here we aimed to dissect the specific contribution of microglial IFNγ-response to RR-EAE.

Similarly to the case of MHC-II, we first had to generate IFNGR1 KO mice (**Figure 21**). We first sequenced the 5' end of the SJL *Ifngr1* gene and designed two guide RNAs that span the promoter and first exon (detailed in the method section). Using the CRISPR/Cas9 approach we successfully deleted ~200bp that included the promoter and first exon of the *Ifngr1* gene (**Figure 21B, 21C**, for details see methods section). Flow cytometry of blood monocytes of the respective B6*SJL F1 hybrids and controls confirmed reduced expression of IFNγR1 (**Figure 21E**). At the time of the writing, we have established TAM treated $Mg^{\Delta IFN\gamma R1}$ mice as well as littermate controls that will be challenged with RR-EAE.

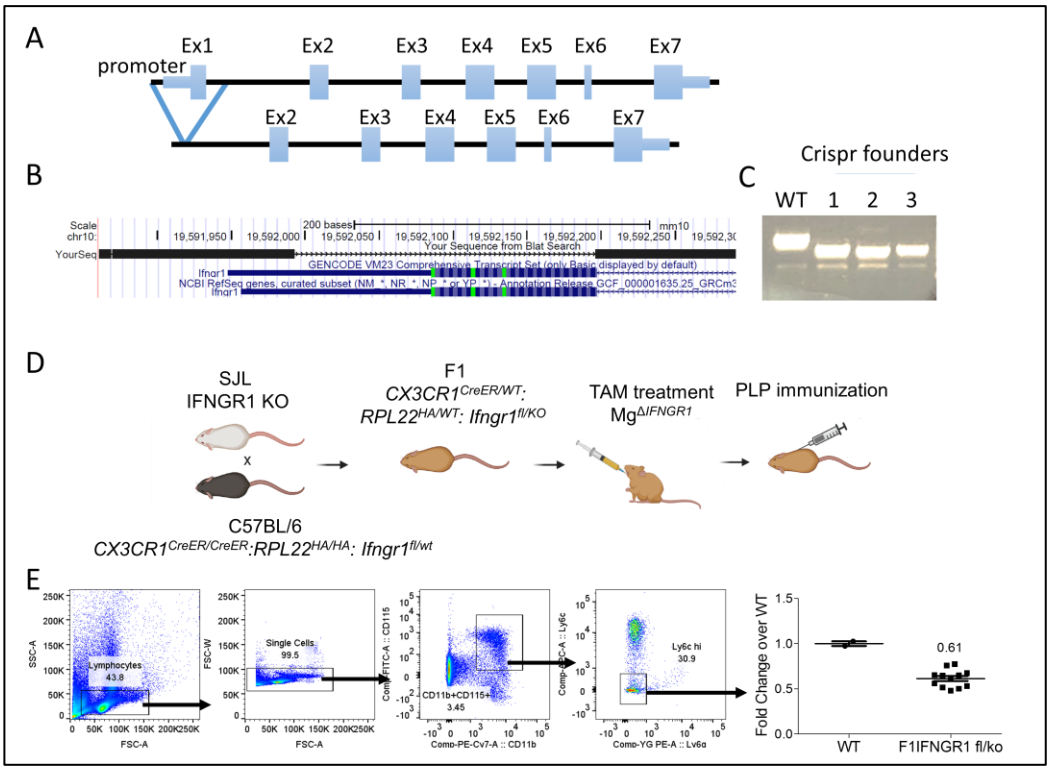

Figure 21. Generation of IFNGR1 KO SJL mice. **(A)** Scheme of the IFNGR1 gene (up) and the deletion design (down). **(B)** sequencing of the deleted allele (black) aligned with WT IFNGR1 gene using UCSC genome browser. **(C)** genotyping of crispr founders showing ~200bp deletion. **(D)** Scheme of crossing SJL and BL6 mice to generate F1 $Mg^{\Delta IFN\gamma R1}$ mice. **(E)** Flow cytometry analysis of blood monocytes from F1 mice showing heterozygous expression of IFNGR1.

Discussion

The main topic of this thesis was the study of microglia in their physiological brain context, including contributions of these cells to physiology and pathophysiology. In a first set of experiments (Part I) I compared experimental approaches to retrieve microglia expression signatures from brains of untreated and challenged animals. Specifically, we defined strengths and weaknesses of the classical cell isolation- and sort-based protocols and the RiboTag strategy[107], that relies on poly-ribosome-attached-mRNA immunoprecipitation from crude tissue extracts. In Part II of my thesis, I then utilized the advantages of the RiboTag in combination with a murine remitting-relapsing MS model to dissect microglia-specific contributions to the RR-EAE disease course. Below I review the pros and cons of the respective microglia profiling techniques, and will then discuss our new insights into the role of microglia in EAE and MS pathology.

The RiboTag strategy was originally introduced by McKnight and colleagues and applied to expression profiling of neurons and Sertoli cells[107]. Cell type-specificity of the approach depends on the accuracy of the Cre-drivers that is combined with the *Rpl22*^{HA} allele. This aspect is highlighted in our study by the side-by-side comparison of *Cx3cr1*^{Cre} and *Cx3cr1*^{CreER} animals, which revealed the superiority of the inducible system to achieve brain macrophage specificity and exclude neurons. As in the case of *Cx3cr1*^{Cre} animals reported here, *LysM*^{Cre} mice that were assumed to be myeloid cell-specific also target neurons[112], as were *Sall1*^{CreER} animals[115 139]. However, as reported earlier and confirmed in this study, even *Cx3cr1*^{CreER} mice not only target microglia, but also non-parenchymal macrophages[114]. In situations where subpopulations can be phenotypically discriminated, as in the case of CD45^{int} microglia and CD45^{hi} perivascular macrophages, sort-based approaches, potentially combined with a RiboTag analysis like in this study, can hence be advantageous. This emphasizes the need for the development of novel Cre transgenic lines targeting microglia, including combinatorial approaches, such as the split-Cre strategy[142] (*Kim et al, in press*), to improve cell type- or lineage-specificity. Importantly, current tests for accuracy of Cre transgenic lines are based on their combination with reporter alleles and the analysis of resulting double transgenic animals by flow cytometry. Our results, and a follow up study that revealed the promiscuity of the Sall^{CreER} model[115], demonstrate that the RiboTag approach provides a useful complementary

method to determine Cre line specificity, in particular for cell types, such as neurons and endothelial cells that are notoriously difficult to isolate for flow cytometric analysis.

Transcriptome profiling either of bulk populations or more recently single cells, has been widely used to infer on protein expression and functional states of specific cell types, as well as to define responses to stimuli. It should be noted that macrophage expression signatures tend to be contaminated by material that the phagocytes ingested from their surroundings[118]. Since the RiboTag strategy only retrieves mRNAs that are associated with HA-epitope tagged host cell ribosomes, it excludes such exogenous material, and hence allows identification of *bona fide* macrophage mRNAs.

Not all transcripts in a cell are translated, but a considerable fraction is now known to be retained in incompletely spliced form in nuclei, or sequestered until further use in membrane-less organelles, called P bodies or 'stress granules'[101,121]. In collaboration with the Ulitzky team at the Weizmann Institute, we could show that the RiboTag approach efficiently excludes these sequestered mRNAs, that otherwise contaminate the whole cell transcriptome.

Ribosome-associated mRNAs, as retrieved by the RiboTag approach are considered to reflect the translatome. Interestingly though, the microglial response to LPS using an analog experimental system, showed that mRNAs induced by the challenge can be associated with ribosomes but prevented from translation by binding of a splicing factor to their 3'UTRs[143]. Like other emerging layers of posttranscriptional expression control, this mechanism, which was revealed by a combined transcriptome and peptidome analysis on immunoprecipitated ribosomes, requires however further study.

Above we listed advantages of the RiboTag approach, but an inherent weakness of this protocol is the fact that for confident assessment of gene expression in the targeted population, the method relies on an enrichment of the specific mRNA over the input, i.e. the whole tissue extract. The RiboTag approach hence precludes statements on the expression of genes that are equally expressed in the target cells and the surrounding tissue. For the assessment of these co-expressed genes, sort-based strategies might be superior, although these also bear caveats, as outlined below.

Side-by-side comparison of the translatomes isolated by IP from crude tissue extracts and from sorted microglial cells with whole cell transcriptomes revealed a number of short-comings of the latter. First, we noted a prominent activation signature that is presumably introduced during the process of cell extraction from their tissue context. This artifact comprised proinflammatory genes, such as *Cd86, Tlr4* and *Tlr7*, and will have to be considered in

microglia profiling studies. Importantly, this robust and reproducible artifact could not be discerned when control and test samples were processed similarly. Rather we found that the isolation procedure had a differential impact on microglia retrieved from either challenged or unchallenged animals. Of note, artifacts like the ones we report here that are introduced during the isolation procedure, were shown to be significantly reduced, when the transcription inhibitor actinomycin D (ActD) was included during the cell preparation[106,144].

Taken together, the first part of our study shows that cell isolation coupled with sort-based methods and the RiboTag approach both have strengths and weaknesses, which should be considered when experiments are designed and conclusions are drawn. Cell isolation bears the risk of artifacts that might significantly confound transcriptome-based studies, including single cell analysis. Our study should hence caution experimentalists and make them aware of the 'observer effect' that is well established in physics[145], but often less appreciated in biology.

In the second part of my thesis we decided to address a major question in microglia research, i.e. to what extend these cells are able to interact as antigen presenting cells and shape T cell immunity, for instance in the setting of autoimmune encephalitis. Specifically, we resorted to a model of relapsing-remitting EAE, which better resembles the clinical course and histopathology of RR-MS lesions and might share relevant mechanisms of immune regulation. Unlike the monophasic chronic model in C57BL/6 mice, the (SJL*B6) H-$2^{s/b}$ model enables to study mechanism that are involved in recovery or relapse, on top of induction. In addition, it allows to relate mechanisms and changes in gene or protein expression to clinical outcome, and to deduce mechanisms contributing to pathology and recovery. In contrast, mouse models lacking recovery, but also human *post mortem* histopathology analysis, lack temporal and potential future clinical consequences, thus are limited with respect to functional implications deduced from gene expression or protein staining.

We took advantage of the combination of fate mapping and advanced translatomics features of the RiboTag to dissected microglia specific contributions to RR-EAE. The exact role of microglia in the EAE course remains debated and challenging to address due to the high resemblance of microglia and infiltrating monocyte-derived cells. As we established earlier[110], the TAM-inducible *Cx3cr1*^{CreER} system allows to exclude monocytes and their derivatives. The *Cx3cr1*^{CreER} system however also targets barrier associated macrophages (BAM), some of which are long lived[102,114]. While the exact kinetics of BAM replacement under EAE are not known, BAM are probably replaced by monocyte-derived ‘WT’ cells that are not labeled with

HA. Moreover, even if some BAM remained labeled, they represent a very low percentage of the HA^+ population (<10%), and our translatomes probably largely reflect microglia.

Although microglial turnover was broadly studied in steady state[22,146], microglia half lives in pathology are less known. Studies show that microglia are replaced from CNS internal pools with low turnover rates in steady state. During demyelination microglia undergo apoptosis and repopulation to enable recovery[147,148]. Here we show by the persistent HA tag that microglia are a stable population even upon EAE pathology. While it is possible that the cells undergo a major turnover, which is suggested by the *proliferation signatures* we observed, it seems that dying cells are replenished solely from internal pools by local proliferation – not only in steady state – but in pathology as well.

The response of microglia for the first induction of EAE included marked downregulation of microglia signature genes and activation of proliferation, a previously described phenotype in EAE[18,85]. At the initiation, microglia also upregulate genes related to immune response e.g. MHC-II, ICAM-1 and CD40, the expression of which peaks at the maximal stage of the disease. Since our analysis is at the population- but not single-cell level, it is possible that the gene upregulation we observe is not uniform throughout the entire population, but rather represents a mixture of responding and non-responding cells. Flow cytometric analysis of microglial MHC-II, ICAM-1 and PDL1 showed that indeed, at the initiation there is a wide range of expression levels of these surface molecules by microglia. However, at the max stage all microglia expressed a uniform high level of these molecules.

The timing of the expression of molecules that are related to T cell priming and immune cell activation is interesting. The expression was minimal at pre-onset but peaked at the max stage, potentially implying that these molecules are not likely to prime pathogenic T cells but maybe more likely to be involved in recovery. This would be in line with evidence form our group that microglia are dispensable as APC for the local restimulation of autoreactive T cells[94], which is supplied by monocyte-derived cells[149].

Interestingly, one of the mice we analysed at the initiation showed gene expression levels resembling the max stage, and also clustered with max in the PCA plot. Indeed, certain individual mice develop only a mild disease and recover. It is tempting to speculate that mice whose microglia express high levels of immune-related molecules might have developed decreased pathology and earlier recovery.

Upon recovery from EAE, even though mice were clinically healthy, microglial translatomes did not return to steady-state levels. Microglia signature genes remained low and

genes related to *antigen presentation* and *IFNγ response* decreased to some extent, but did not reach steady-state levels. One possible reason for this could be that the BBB might still be compromised, allowing immune cell infiltrates and microglial exposure to serum proteins, such as fibrin that is known to activate microglia[150]. The BBB is known to be impaired in B6 EAE[151], but no data are available for the RR-EAE disease course of the (SJL*B6) H-$2^{s/b}$ model. We are therefore in the process to investigate BBB integrity at the remission stage by measuring the leakage of different sized dextran conjugates into the parenchyma following their intravenous injection.

Surprisingly, upon relapse the microglial expression pattern remains essentially unaltered with no significantly changed genes from cure to relapse. It seems that microglia are inert to the second response, potentially since they are at an intermediate activated or exhausted state. This also strongly suggests that as in the initiation, microglia are not the cause of the relapse, rather they are bystanders. We did not follow the disease beyond the second relapse, and thus do not know whether in our model under our animal facility conditions, mice experience a second recovery following relapse. It is intriguing whether the lack of the responsiveness of microglia to the second relapse correlates with the lack of a second recovery.

Microglia *de novo* upregulate MHC-II expression in EAE, albeit to a lesser extent than professional APCs, such as dendritic cells (DC)[152,153]. The ligation of low MHC-II levels to T cell receptor (TCR) was suggested to have a regulatory role in anergizing T cells rather than priming them[154]. Indeed, ex-vivo activation of microglia by low doses of IFNγ induced low levels of MHC-II, that when incubated with naïve CD4+T cells, lead to the generation of regulatory T cells[155]. Such in-vitro assays should however be taken with a grain of salt, since microglia lose their identity once out of their physiological environment[156].

For efficient T cell priming, APCs require both MHC-II molecules and co-stimulatory molecules such as CD80, CD86 and CD40, the absence of which can alternatively cause T cell apoptosis or anergy[157]. Interestingly, our RiboTag RNA-seq data showed that microglial expression of CD80 and CD86 was very low, below our cut off value of 50 reads, and was not upregulated upon disease (data not shown). In contrast, the expression of CD40 and the adhesion molecule ICAM1 reached high levels at the max stage. In addition, ICOSL – a co-stimulatory molecule important for the priming of regulatory T cells was also highly expressed by microglia.

Locally produced cytokines mediate inflammatory, anti-inflammatory and immune modulatory properties through complex interactions within microenvironment-specific cellular networks. We did not find evidence for microglial expression of cytokines that are essential for controlling pathogenic Th cell fate, such as IL-4, IL-6, IL-22, IL-23 or IL-10. Interestingly, the only cytokine components we could find to be significantly expressed by microglia at high levels were *Ebi3*, encoding the IL27b subunit of IL-27 (and of IL-35), and *Il-16*. The development of tissue-induced Treg cells was shown to be dependent on IL-27[158,159]. IL-16 role in the attraction of Treg cells has been described[160], and suggested that at sites of inflammation IL-16 may contribute to the expansion of Treg cell through the preferential induction of a migratory response from existing Treg cells, as well as by the induction of *de novo* generation of Foxp3^{+} cells.

Interestingly, we also found microglia to express IL-18 binding protein *(Il18bp)*, ILT3 *(Lilrb4a)* and PDL1 *(CD274)* which are known as inhibitory molecules that promote anergy of T cells and prevent T cell proliferation as well as cytotoxic functions[161,162,163]. In cancer research these molecules are described to be expressed on myeloid-derived suppressor cells and to play a central role as immune checkpoint inhibitors by regulating T cell mediated responses[164,165,166].

Altogether the expression profile of microglia, i.e. relatively low MHC-II levels, partial expression of co-stimulatory molecules, as well as expression of inhibitory molecules and cytokines related to Treg attraction and stimulation, suggest that microglia might act as regulatory cells. Rather than restimulating pathogenic effector T cells, microglia might promote the differentiation of CNS-resident regulatory T cells, enhance their attraction and local proliferation. Interestingly, the expression of these molecules peaked at the max stage and gradually decreased and remained low in cure and relapse. One could speculate that these molecules might aid to resolve the damage at the max stage and lead to remission, while low expression at the later stages might enable to unleash the 2nd response.

Following the detailed examination of the microglial expression profile that suggest a tolerogenic potential, it was not surprising that their depletion resulted in a prominent halt of recovery from EAE and in the accumulation of CD4^{+} T cells. Previous studies of microglia depletion in EAE yielded controversial results due to different depletion strategies. Chemical inhibition of CSF1R (that results in microglia depletion) in EAE from day 7 post immunization in C57BL6 mice resulted in attenuation of EAE, suggesting a pathogenic role for microglia[167]. Quite the reverse, a similar depletion method although in NOD mice (that succumb to RR-EAE)

from day 20 onwards – showed an exacerbated relapse with increased levels of $CD4^+$T cells – indicating a protective role of microglia[168]. However, it was recently shown that CSF1 receptor antagonists are not specific for microglia, but have confounding systemic effects on hematopoiesis and macrophage functions[169]. Acute depletion prior to or post EAE induction using the iDTR system in the chronic model was shown to result in increased disease and increased mortality[170]. However, the significance of an acute depletion is not clear as microglia quickly repopulate once the depleting agent is withdrawn[15,171]. Moreover, cell ablation experiments always bear the risk of collateral damage[172]. Overall, the results of microglia depletion experiments in EAE remain contradictory. Nonetheless, our results would be in line with the work of the Yamashita group, which proposed that microglia suppress the secondary progression of autoimmune encephalomyelitis by influencing the $CD4^+$ T cell compartment in a comparable RR-EAE model to ours[168].

The relationship between microglia and T cells was further reinforced by our finding of intimate interactions of these cells in the tissue, either in the form of clusters or by individual cell-cell interactions, mediated through focal MHC-II centred in the contact area between the cells. Microglia-T cell nodules have been described previously in brain tissue from patients, and were proposed to be pre-active lesions due to activation of STAT1 in those cells[87]. However, *post mortem* analysis precluded conclusions on functional contributions. Here we propose that the timing of the formation of Mg-T doublets has a pro-recovery effect and clinical significance: At the initiation, although there were many T cells in the tissue, not many Mg-T cells were formed – rather the frequency of Mg-T doublets peaked at the max stage, coinciding with: (1) the anergizing expression profile of microglia, (2) the decreased abundance of tissue T cells, and (3) with the subsequent recovery. Therefore, we propose that Mg-T conjugate formation might contribute to regulation of the pathology. Although some of the observed doublets were probably generated during the ex-vivo isolation procedure, such a stage- and cell-state-dependent formation of Mg-T doublets argues against a mere artifact; rather it implies a biologically relevant interaction between microglia and T cells that potentially contributes to recovery.

Such a scenario, would also be supported by our finding that *Cxcl9* expressing microglia are in association with *Cxcr3* expressing lymphocytes, suggestive of chemoattraction of T cells by microglia. Supported by the literature describing the role of $CXCR3^+$ Treg cells[126,173–175], we speculated that a chemical blockade will recapitulate previous finding[128,129]. However, this was not the case, potentially due to the fact that the chemical delivery to the CNS might be

inefficient. A repeat of this experiment, would have to include controls for proper delivery and activity of the chemical in the brain to verify the activity of the inhibitor. A more precise way to address the question of Treg CXCR3 involvement would be to genetically target microglial Cxcl9 or a Treg specific deletion of Cxcr3. This will however require generation of the respective *floxed* or KO SJL animals.

Of note, in our analysis of *Cxcl9* expression we excluded monocytes and neutrophils. Recently, a pathogenic $CXCL9^+$ $CXCL10^+$ monocyte subset in EAE was described[176]. It is intriguing why two cell types with different effects on pathogenicity will express the same cytokine. One possibility would be a competitive attraction of pathogenic T cells by monocytes and microglia, when one recruits (and/or primes) pathogenic T cells, while the other would interact to anergize them.

Further analysis of T cell subsets in the Mg-T doublets revealed that Treg cells were enriched in the Mg-T doublets compared to their frequencies among singlet T cells, suggesting a preferred interaction of microglia with Treg cells. $Foxp3^+$ Treg cells can be generated in the thymus (tTreg) or induced peripherally (pTreg) in lymphoid or non-lymphoid tissues where they acquire tissue-specific suppressive programs[76]. In EAE, tTreg cells migrate to the CNS, become activated in a TCR-dependent manner, expand, and acquire suppressive Treg effector functions[78,79]. Their effector regulatory phenotype is regulated by the transcription factor Blimp1, which stabilizes Foxp3 expression and controls IL-10 expression[77]. Loss of Blimp1 in Treg cells leads to exacerbated EAE[77]. However what controls tissue specific TCR selection and clonal proliferation of Treg cells in EAE remains unknown. Here we propose that microglia, due to their regulatory expression profile discussed above, might be the missing link as the local APC that drive Treg attraction, priming and expansion.

Somewhat counterintuitively, we found that mice that harbor WAS deficient microglia ($Mg^{\Delta WAS}$) accumulated $FOXP3^+$ Tregs, even though they failed to recover from EAE. It is possible that the accumulating Treg cells did not acquire effector functions and thus are dysfunctional. Like other WAS deficient APCs, which fail to form a functional immune synapse[133], also WAS deficient microglia might fail to present antigen to T cells and mediate their anergizing functions. This could lead to accumulation of immature Foxp3+ cells that cannot be locally primed to differentiate into effector regulatory cells that express Il-10 and control inflammation. To address this, Treg effector phenotypes should be analysed including

the expression of BLIMP1, GITR, ICOS, OX40, IL-10 and even a global transcriptome analysis of Treg cells isolated form brains of WT and $Mg^{\Delta WAS}$ mice.

Another Treg cell type that was described, does not express Foxp3 but rather depends on the transcription factor Foxa1, which is induced by IFNβ and requires IFNAR signalling[177]. $FoxA1^{+}$ Treg cells develop and proliferate locally in the CNS. It is not known whether these cells depend on TCR signalling or what are the cues that drive their expansion in the CNS. However, the effect of microglial defects on the generation and function of $FoxA1^{+}$ Treg cells would be interesting to test.

Treg cells depend on TCR signalling to exert their regulatory functions and a lack of TCR results in loss of the effector regulatory phenotype[80,81]. To specifically dissect an effect of microglia on CD4+ T cells in the context of MHC-II and TCR interactions, one will require an experimental system that allows microglia-specific MHC-II deletion. Since MHC-II deletion in microglia has no impact on generation of pathogenic T cells[94], we speculate that it might be important to mediate TCR dependent transition of regulatory cells to effector cells and might be involved in TCR selection and clonal expansion of Treg cells.

To address this question we generated a new line of H2-Ab1 deficient SJL mice. We are in the process to generate (SJL*B6) $H\text{-}2^{s/b}$ hybrids that harbor a floxed B6 $H\text{-}2^{b}$ allele and a mutant SJL $H\text{-}2^{s}$ allele, which will ,in combination with the *Cx3cr1*^{CreER} transgene, allow the conditional microglia-specific MHC-II ablation. An important question to answer is whether the deletion of the $H\text{-}2^{s}$ haplotype of the SJL strain will impact the disease course of the (SJL*B6) $H\text{-}2^{s/b}$ F1 mice and generate the relapsing and remitting model as we have seen until now. If this is the case, we will be able to address whether cognate interactions of microglia and Treg cells are critical for the remission.

Surprisingly, we noticed that MHC-II KO SJL mice generated by the CRISPR/Cas9 technology did not survive past few months of age and developed signs of a spontaneous autoimmune disease. At the cellular level, the mice displayed massive accumulation of monocytes and neutrophils, as well as CD8+ T cells in the blood. Also crosses of the following SJL generations did not result in a mice harboring homozygous deletion of MHC-II, suggesting that the MHC-II mutation in this strain could be lethal, as oppose to the C57BL/6 strain. This potentially opens up a new field of study addressing the basic questions of strain specificity effect of gene deletion on hematopoiesis.

To summarize, we implement the RiboTag method to microglia research that enabled us to focus on translated mRNA, screening out artifacts. We further performed longitudinal analysis of microglial translatome throughout the course of RR-EAE. We provide evidence that microglia display a tolerogenic expression profile and interact with T cells, suggesting that microglia are involved in the recovery from RR-EAE. The underlying specific mechanisms remain to be studied, such as the role of MHC-II and its inducer – the IFNγ response.

Hopefully this study will give rise to more studies yet to come that will approach the question of cell-specific contributions to EAE and MS. Such detailed analyses will provide a more comprehensive understanding of the immune-modulatory mechanisms that control pathologies like MS and will allow the development of more specific drugs and intervention strategies. For example, broad spectrum immunosuppressant drugs or the targeting of specific immune related functions that induce the immune modulatory effect can impair the beneficial response of immune regulatory cells. A better understanding of the mechanisms will allow to develop better immune modulatory drugs to treat pathologies like MS and others.

Methods

Animals. Mice were maintained on a 12 hr light/dark cycle, and food and water were provided ad libitum. Animals for RiboTag calibration of the first part were on C57BL/ 6JOlaHsd background, for RR-EAE experiments SJL/J purchased from Harlan were crossed to relevant C57BL/ 6JOlaHsd mouse strain as described for each section. All mice were maintained in specific pathogen-free (SPF) conditions and handled according to protocols approved by the Weizmann Institute Animal Care Committee (IACUC), as per international guidelines. The strains used included: *Cx3cr1*^{Cre} mice (JAX stock # 025524; B6J.B6N(Cg)-*Cx3cr1*$^{tm1.1(cre)Jung}$/J); *Cx3cr1*^{CreER} mice (JAX stock # 020940; B6.129P2(C)-Cx3cr1$^{tm2.1(cre/ERT2)Jung}$/J) ; *RPL22*$^{HA/HA}$ (JAX stock # 011029; B6N.129-*Rpl22*$^{tm1.1Psam}$/J); Rosa26-YFP reporter mice ; *Ifngr1*$^{fl/fl}$ (JAX stock # 025394; C57BL/6N-*Ifngr1*$^{tm1.1Rds}$/J) and *H2-Ab1fl*/fl (JAX stock # 013181; B6.129X1-*H2-Ab1*^{tm1Koni}/J). *WAS*$^{fl/fl}$ mice were a kind gift from the lab of Fabio Candotti (Lausanne, Switzerland). The presented Ribotag data were generated with animals homozygote for the *Rpl22*^{HA} allele and heterozygote for the modified *Cx3cr1* alleles. RR-EAE experiments were done on heterozygote mice for the *Rpl22*^{HA} allele.

Generation of SJL KO mice using CRISPR-Cas9. CRISPR guides were chosen using several design tools, including: the MIT CRISPR design tool[178] and sgRNA Designer, Rule set 2[179], in the Benchling implementations (www.benchling.com), SSC[180], and sgRNAscorer[181], in their websites. Guides for H2ab1 gene: upstream: GACTCCGAAAGTAAGTGCCG, downstream: TTACAAAGGCTCTCTATGCG. Guides for Ifngr1 gene: upstream: CTAGTCGCCAAGTCCGCAAG, downstream: GGCTCGGAGAGATTACCCGA. All mouse experiments were approved by the Weizmann Institute's IACUC committee and were carried out in accordance with their approved guidelines. Ifngr1 and H2-Ab1 KO SJL mice were generated at the Weizmann Institute of Science, Rehovot, Israel, using CRISPR-Cas9 genome editing in one-cell embrys[182], obtained via in vitro fertilization (IVF)[183] on the SJL background. crRNA and tracrRNA and Cas9 protein were purchased from IDT - Integrated DNA Technologies, Inc. RNPs were delivered to one-cell embryos via electroporation using the Biorad Genepulser. See **Table 3** for genotyping primers, followed by DNA sequences of KO animals.

Tamoxifen (TAM) treatment. Five grams of Tamoxifen were dissolved in 5ml of 100% Ethanol, vortexed and supplemented to 50ml with corn oil (Sigma), warmed in 55˚C for several hours until completely dissolved, aliquoted and kept in -20 till use. To induce gene recombination in CreER transgenic mice, TAM was administered orally via gavage 50µl/dose for four times every other day. All animals were TAM-treated at 4-6 weeks of age. Each oral application was of 5mg at a concentration of 0.1 mg / µl. Mice were examined 8 weeks following treatment. For the LPS treatment, mice were injected intraperitoneally (i.p.) with a single dose of LPS [2.5 mg/kg; E. coli 0111:B4; Sigma]; controls received or the same volume of vehicle solution (PBS).

EAE induction and assessment. For EAE induction, mice were injected (day 0) subcutaneously on both sides of the body with 100 µL of emulsion containing a 1:1 ratio of 2 mg/mL $PLP_{139-151}$ peptide (HCLGKWLGHPDKF) (GeneScript, USA) in PBS and Complete Freund's Adjuvant (Sigma) (composed of Incomplete Freund's Adjuvant supplemented with killed *M. tuberculosis* (BD) at 10mg/ml). Mice were supplemented with 200 ng pertussis toxin (Sigma) administered i.p. on day 0 and 2. For WAS experiments, the emulsion was prepared as above with the following modifications: Complete Freund's Adjuvant (Sigma) supplemented with killed *M. tuberculosis* (BD) at 2mg/ml and pertussis toxin 50ng of per injection. EAE was assessed according to accepted assessment index[51]. The mice were weighed and monitored daily by being held at the base of the tail. The index is as follows: 0—no symptoms; 0.5— limp tail; 1—complete tail paralysis; 1.5—limp gait reflex; 2—loss of gait reflex; 2.5—one hind limb paralysis; 3—complete hind limb paralysis; 3.5—one forelimb paralysis; 4—complete fore limb paralysis, mice are sacrificed due to humane reasons.

Administration of Chemicals to mice. (+/-)-AMG 487 (Tocris, Cat#4487) was dissolved in 45% (2-Hydroxypropyl)- beta-cyclodextrin solution (Sigma) and injected at 5mg/kg in 20% (2-Hydroxypropyl)- beta-cyclodextrin in PBS solution every day intraperitoneally. Vehicle was 20% (2-Hydroxypropyl)- beta-cyclodextrin in PBS at same volume to weight ratio as AMG. For microglia depletion using diphtheria toxin, $Cx3cr1^{CreER}$ iDTR mice were treated intraperitoneally with diphtheria toxin (sigma, cat# D0564) 500ng/mouse in PBS from day 3 post immunization, every other day until termination of experiment. PBS injections served as control.

Microglia isolation protocols. Mice were anesthetized with Pental (1:2 in PBS) and were perfused with PBS. Brains were dissected, crudely chopped and incubated for 20 min at 37°C in a 1 ml HBSS solution containing 2% BSA, 1 mg/ml Collagenase D (Sigma) and 50µg/ml DNase1 (Sigma). In the middle of incubation homogenates were pipetted for further dissociation. Next, the homogenates were filtered through a 150µm mesh, washed with cold FACS buffer (2% FCS, 1mM EDTA, 0.05% Sodium Azide in PBS-/-) and centrifuged at 2200 RPM, at 4°C, for 5 min. For the enrichment of microglia, the cell pellet was re-suspended with 3ml of 40% percoll solution and centrifuged at 2200 RPM, no acceleration and breaks, at RT for 15 min. Next, the cell pellet was resuspended in FACS buffer, passed through 80µm mesh, washed with 5ml FACS buffer and centrifuged at 1400 RPM at 4°C for 5 min, followed by antibody (Ab) labeling and flow cytometry analysis. For the protocol excluding the digest, brains were chopped and then filtered through a 150µm mesh. The subsequent steps were as above, but without the enzymatic digest.

Flow cytometry, cell sorting and Image Stream. Antibodies against CD11b (M1/70), Ly6C/G (Gr-1) (RB6-8C5), CD45 (30-F11), CD4 (GK1.5) TCRb (H57-597) Foxp3 (MF-14) RORγt (B2D), I-Ak (10-3.6), I-Ab (AF6-120.1), ICAM1/Cd54 (YN1/1.7.4), PDL1/CD274 (10F.9G2), TMEM119 (106-6), IFNGR1/CD119 (2E2 or GR20), HA.11 (16B12) purchased from Biolegend, eBioscience, BD or Abcam were used. For intracellular transcription factor staining True-Nuclear™ Transcription Factor Buffer Set (Biolegend) was used according to manufacture instructions. Flow cytometric analysis was done on LSR Fortessa 4 lasers (BD). Samples were flow sorted using AriaIII (BD Biosciences, BD Diva Software) cell sorter. Analysis was performed on Fortessa (BD Biosciences, BD Diva Software) and analyzed with FlowJo software (Treestar). For Image Streatm, single-cell suspension was resuspended in ~30µl FACS buffer and acquired in ImageStreamX Flow Imager system with 5 lasers. Data analysis was done using IDEAS 6.2 software.

Immunofluorescence. Mice were anesthetized with Pental (1:2) and were perfused with PBS. Brains excised and fixed overnight in 2% paraformaldehyde. Brains were incubated for 72 hours in 30% sucrose prior to OCT (TissueTek) imbedding and freezing. Brains were sectioned to 30 µm and were kept as floating sections in PBS-Azide till use. For staining sections were put on a slide, let dry to adhere. For staining, slides were blocked in 5% donkey serum 0.5% Triton in PBS for 1.5 hours and incubated overnight in room temp with the primary antibody. The next day slides were washed 3 times in PBSX1 and conjugated with secondary antibody for 1 hour in room temp. Before covering samples were washed 3 times and incubated for 3 minutes with Hoechst 1:10,000. Sections were analyzed by confocal laser scanning microscope Zeiss 880. Image acquisition was processed by Imaris software. The following antibodies were used: Mouse anti-HA.11 (1:100, Covance), Goat polyclonal anti-Iba1 (1:200, Abcam), I-A/I-E-Alexa Fluor 594 (clone M5/114.15.2, 1:100, biolegend), anti CD3ε-PE (clone 145-2C11, 1:100, biolegend), Rat anti Foxp3 (FJK-16s, eBioscience), Rabbit anti TMEM119 (28-3, Abcam) and Hoechst 33342 (1:10,000, Invitrogen).

Ribosome Immunoprecipitation (IP). Samples were extracted from mice, flash-frozen in liquid nitrogen and stored at −80 °C until use. Samples were homogenized on ice in ice-cold homogenization buffer (50 mM Tris, pH 7.4, 100 mM KCl, 12 mM MgCl2, 1% NP-40, 1 mM DTT, 1:100 protease inhibitor (Sigma), 200 units/ml RNasin (Promega) and 0.1 mg/ml cycloheximide (Sigma) in RNase free DDW) 10% w/v with a Dounce homogenizer (Sigma) until the suspension was homogeneous. To remove cell debris, 1 ml of the homogenate was transferred to an Eppendorf tube and was centrifuged at 10,000g and 4°C for 10 min. Supernatants were transferred to a fresh Eppendorf tube on ice, then 10µl was removed for 'input' analysis and 10µg of anti-HA.7 antibody (H9658, Sigma) or 10µg of mouse monoclonal IgG1 antibody (Merck, Cat# PP100) was added to the supernatant, followed by 4 h of incubation with slow rotation in a cold room at 4 °C. Meanwhile, Dynabeads Protein G (Thermo Fisher Scientific), 100 µl per sample, were equilibrated to homogenization buffer by washing three times. At the end of 4 h of incubation with antibody, beads were added to each sample, followed by incubation overnight in cold room at 4 °C. After up to 12 h, samples were washed three times with high-salt buffer (50 mM Tris, 300 mM KCl, 12 mM MgCl2, 1% NP-40, 1 mM DTT, 1:200 protease inhibitor, 100 units/ml RNasin and 0.1 mg/ml cycloheximide in RNase free DDW), 5 min per wash in a cold room on a rotator. At the end of the washes, beads were magnetized and excess buffer was removed, 100µl Lysis Buffer was added to the beads and RNA was extracted with Dynabeads mRNA Direct purification kit (Thermo Fisher). RNA was eluted in 6µl H_2O and taken for RNA sequencing. For Sort-IP samples (RiboTag IP after sorting), ~50-100*10^3 cells were sorted into cold PBS, centrifuged 400g for 5 min at 4°C. Supernatant was removed and the pellet was re-suspended in 1ml of lysis buffer, the rest of IP was continued as above.

RNA sequencing. RNA-Seq of populations was performed as described previously (Lavin 2014). In brief, 5,000 microglia cells were sorted into 50µl of Lysis Buffer (Life Technologies) and stored at -80°C. mRNA was captured with Dynabeads oligo(dT) (Life Technologies) according to manufacturer's guidelines. We used a derivation of MARS-seq[184]. Library concentration was measured with a Qubit fluorometer (Life Technologies) and mean molecule size was determined with a 2200 TapeStation instrument. RNA-Seq libraries were sequenced using Illumina NextSeq-500.

Data Analysis. Raw reads were mapped to the genome (NCBI37/mm9) using hisat (version 0.1.6). Only reads with unique mapping were considered for further analysis. Gene expression levels were calculated using the HOMER software package (analyzeRepeats.pl rna mm9 -d <tagDir> -count exons -condenseGenes -strand + -raw). Normalization and differential expression analysis was done using the DESeq2 R-package. Differential expressed genes were selected using a 2-fold change cutoff between at least two populations and adjusted pValue for multiple gene testing < 0.05. Gene expression matrix was clustered using k-means algorithm (matlab function kmeans) with correlation as the distance metric. Heatmaps were generated using GeneE software.

Analysis of Gene Features. For comparison of features between genes in cluster IIb and other genes, we used gene models from GENCODE vM13. Splicing efficiency was computed as by Tilgner and colleagues[185] using polyA+ RNA-seq data from microglia[186]. Cytoplasmic/nuclear expression levels in liver and MIN6 cells were obtained using RNA-seq data from Bahar Halpern and colleagues[123] quantified using RSEM with GENCODE vM13 gene models. Cytoplasmic/nuclear ratios were computed using DESeq2s.

Statistical Analysis. In all experiments, data are presented as mean ± standard deviation, if not stated otherwise. Statistical tests were selected based on appropriate assumptions with respect to data distribution and variance characteristics. Statistical significance was defined as $P<0.05$. Sample sizes were chosen according to standard guidelines. Number of animals is indicated as 'n'. Of note, the sizes of the tested animal groups were also dictated by availability of the transgenic strains and litter sizes, allowing littermate controls. Pre-established exclusion criteria are based on IACUC guidelines. Animals of the same age, sex and genetic background were randomly assigned to treatment groups. The investigator was not blind to the mouse group allocation, although tested samples were assayed blindly.

qPCR. mRNA was captured with Dynabeads oligo(dT) (Life Technologies) according to manufacturer's guidelines. mRNA was reverse transcribed using the High-Capacity cDNA Reverse Transcription Kit (Applied Biosystems). PCR was performed with a SYBR Green PCR Master Mix kit (Applied Biosystems). Quantification of the PCR signals of each sample was performed by comparing the cycle threshold (Ct) values, in triplicates, of the gene of interest with the Ct values of the β-actin. See **Table 2** for primers used for qPCR.

Table 2. qPCR primers

Gene	Forward (5'→3')	Reverse (5'→3')
H2-Ab1	GACTGCCATTACCTGTGCCT	GCGTCCCGTTGGTGAAGTA
Actb	GGAGGGGGTTGAGGTGTT	TGTGCACTTTTATTGGTCTCAAG
Cxcl9	CGAGGCACGATCCACTACAA	AGGCAGGTTTGATCTCCGTT
Cxcr3	GCCATGTACCTTGAGGTTAGTGA	ATCGTAGGGAGAGGTGCTGT

Table 3. Genotyping primers

Gene	Forward (5'→3')	Reverse (5'→3')	WT size	KO size
SJL H2-Ab1 Del1	AGTTGTCTATACTTCACGCACT	CCGTTTATATGTCAGGCTCGC	649	355
SJL H2-Ab1 Del2	TTAACCACATCACACTGCTCT	AGGTTTCTTGGTCACTGGCT	1217	~900
SJL IFNGR1	GAGATTGCGTATTGGTCCCG	CGCTGCCGTGGAAACTAACT	593	400

SJL IFNGR1 KO sequence:
TCCGCCCCTGAGAGCTGCCTTTTAACCCTTTGCCCCGTGAGGCTCCGCCTCCCACTTAAGCCACGCCCCTCAGT
CCCAGGCTGGTCTCTCAAGCTTTGGTTTTGGCCCCACCCAGCTCCCCGGCAGGCCGCTTGGTAATCTCTCCGAG
CCGCTGCGGGCTGGGGCGGGAGGCCAGGCCGGAGGCGCCGGGCTGGGAAGTCCCTGCGTTCCTGCTGCGCCGC
CCTGGGCAAGGCAGCCCCAAGGGGCCCCGGGGGCTCCGCGGTTTACACGCCGCTTTCGCCTCTTCTTTGCCGAC
ACAACACAAATCTGTGGTCTGTTTTACAGTTAGTTTCCACGGCAGCG

SJL H2-Ab1 Del1:
GGCAGTCTGCAGTTTgGAAAAGTTTACTCTGTAACTGAGAGGAGCAGTCACCTCAAACaTTCATCCAGTGGGGC
TCATGAAGAAACAGACCATGCCaCGCACCAGGGGCAGGGCTCTCCAGAGCCAGCACTCTGGGGGTCGTGTTCT
GAGGGACCCTGGGGACTCTGGGATGTGGGAGGGGGTGGCAAAATCCTGATTTTACTATAGATTTCCTTTCTCTG
AAGAGAGAGTGAGACTCCATTCTCACTTCTGTGTTCTAATATTGAGTTAGGATGGTGCCGCCGCCGGTGCGAGC
CTGACATATAAACGG

SJL H2-Ab1 Del2:
GGGAACATGGCTTGCATTTTACAAAGAGAAGTCCAGGATTAGAAAGAGGCTCAGCGACTCCCCAAGAACTCTG
CTTTCTCACCTGAGGCACCCCAGATGGTCAGATGTAACAAAACATGATTTCTCTGTCTCCTAATACATGTCACA
CTCATTTCTCCCACTACAACCTCAAGTGTAAGAACAGTAGATTTGAAATAATTATCCCAAAGTTGTCTATACTT
CACTCACTTTTCTCTTTAAACCCCAAACACAGGCAGTCTGCAGTTTGGAAAAGTTTACTCTGTAACTGAGAGGA
GCAGTCACCTCAAACATTCATCCAGTGGGGCTCATGAAGAAACAGACCATGCCACGCAATAGAGAGCCTTTGT
AAACAAAGTCTACCCAGAGACAGATGACAGGCTTCAGCTCCAATGCTGATTGGTTCCTCACTTGGGACCAACC
CTGACACTCTGGGATTTCAGATCACTCTAGGCTACAGAACTTTGCTTTCTGAAGGGGGCACAGCAGGTGTGAGT
CCTGGTGACTGCCATTACCTGTGCCTTAGAGATGGCTCTGCAGATCCCCAGCCTCCTCCTCTCGGCTGCTGTGG
TGGTGCTGATGGTGCTGAGGAGGAGGAGGAGGAGGCGGCAGAGTTTAAATTGACCACCAAAGATAAGGGTTG
TGCATGGGGAGACAGCAGGGCTTACAATACCAGTGCCCCCACCCCACCCCGTACATTGTCTGGAGGAAATGCC
AGATTCTGAAGTGGGGAAACAGACCAGCGATGGTCTGTGGTCCCGATGTTTGCGGACAACTCCTCATGTGGAG
TGGAGGTTTAAGAGAGCGAACTCTA

References

1. Prinz, M., Jung, S. & Priller, J. Microglia Biology: One Century of Evolving Concepts. *Cell* **179**, 292–311 (2019).
2. Nimmerjahn, A., Kirchhoff, F. & Helmchen, F. Resting Microglial Cells Are Highly Dynamic Surveillants of Brain Parenchyma in Vivo — Resting Microglial Cells Are Highly Dynamic Surveillants of Brain Parenchyma in Vivo — Supporting Online Material. **308**, 1314–1319 (2005).
3. Davalos, D. *et al.* ATP mediates rapid microglial response to local brain injury in vivo. *Nat. Neurosci.* **8**, 752–758 (2005).
4. Ueno, M. *et al.* Layer V cortical neurons require microglial support for survival during postnatal development. *Nat. Neurosci.* **16**, 543–551 (2013).
5. Cunningham, C. L., Martinez-Cerdeno, V. & Noctor, S. C. Microglia Regulate the Number of Neural Precursor Cells in the Developing Cerebral Cortex. *J. Neurosci.* **33**, 4216–4233 (2013).
6. Mattei, D. *et al.* Maternal immune activation results in complex microglial transcriptome signature in the adult offspring that is reversed by minocycline treatment. *Transl. Psychiatry* **7**, (2017).
7. Knuesel, I. *et al.* Maternal immune activation and abnormal brain development across CNS disorders. *Nat. Rev. Neurol.* **10**, 643–660 (2014).
8. Paolicelli, R. C. *et al.* Synaptic Pruning by Microglia Is Necessary for Normal Brain Development. *Science (80-.).* **333**, 1456–1458 (2011).
9. Frost, J. L. & Schafer, D. P. Microglia: Architects of the Developing Nervous System. *Trends Cell Biol.* **26**, 587–597 (2016).
10. Kierdorf, K. *et al.* Microglia emerge from erythromyeloid precursors via Pu.1- and Irf8-dependent pathways. *Nat. Neurosci.* **16**, 273–280 (2013).
11. Schulz, C. *et al.* A lineage of myeloid cells independent of myb and hematopoietic stem cells. *Science (80-.).* **335**, 86–90 (2012).
12. Ginhoux, F. *et al.* Primitive Macrophages. *Science (80-.).* **701**, 841–845 (2010).
13. Alliot, F., Godin, I. & Pessac, B. Microglia derive from progenitors, originating from the yolk sac, and which proliferate in the brain. *Dev. Brain Res.* **117**, 145–152 (1999).
14. Ajami, B., Bennett, J. L., Krieger, C., Tetzlaff, W. & Rossi, F. M. V. Local self-renewal can sustain CNS microglia maintenance and function throughout adult life.

Nat. Neurosci. **10**, 1538–1543 (2007).

15. Bruttger, J. *et al.* Genetic Cell Ablation Reveals Clusters of Local Self-Renewing Microglia in the Mammalian Central Nervous System. *Immunity* **43**, 92–106 (2015).
16. Ginhoux, F. & Guilliams, M. Tissue-Resident Macrophage Ontogeny and Homeostasis. *Immunity* **44**, 439–449 (2016).
17. Bain, C. C. *et al.* Constant replenishment from circulating monocytes maintains the macrophage pool in the intestine of adult mice. *Nat. Immunol.* **15**, 929–937 (2014).
18. Ajami, B., Bennett, J. L., Krieger, C., McNagny, K. M. & Rossi, F. M. V. Infiltrating monocytes trigger EAE progression, but do not contribute to the resident microglia pool. *Nat. Neurosci.* **14**, 1142–1149 (2011).
19. Shemer, A. *et al.* Engrafted parenchymal brain macrophages differ from microglia in transcriptome, chromatin landscape and response to challenge. *Nat. Commun.* **9**, 1–16 (2018).
20. Bennett, F. C. *et al.* A Combination of Ontogeny and CNS Environment Establishes Microglial Identity. *Neuron* **98**, 1170-1183.e8 (2018).
21. Stence, N., Waite, M. & Dailey, M. E. Dynamics of microglial activation: A confocal time-lapse analysis in hippocampal slices. *Glia* **33**, 256–266 (2001).
22. Tay, T. L. *et al.* A new fate mapping system reveals context-dependent random or clonal expansion of microglia. *Nat. Neurosci.* **20**, 793–803 (2017).
23. Olah, M. *et al.* Identification of a microglia phenotype supportive of remyelination. *Glia* **60**, 306–321 (2012).
24. Popescu, B. F. G. & Lucchinetti, C. F. Pathology of demyelinating diseases. *Annu. Rev. Pathol. Mech. Dis.* **7**, 185–217 (2012).
25. Lampron, A. *et al.* Inefficient clearance of myelin debris by microglia impairs remyelinating processes. *J. Exp. Med.* **212**, 481–495 (2015).
26. Bolmont, T. *et al.* Dynamics of the microglial/amyloid interaction indicate a role in plaque maintenance. *J. Neurosci.* **28**, 4283–4292 (2008).
27. Meyer-Luehmann, M. *et al.* Rapid appearance and local toxicity of amyloid-β plaques in a mouse model of Alzheimer's disease. *Nature* **451**, 720–724 (2008).
28. Kuhlmann, T. *et al.* An updated histological classification system for multiple sclerosis lesions. *Acta Neuropathol.* **133**, 13–24 (2017).
29. Lassmann, H., Van Horssen, J. & Mahad, D. Progressive multiple sclerosis: Pathology and pathogenesis. *Nat. Rev. Neurol.* **8**, 647–656 (2012).

30. Guerrero, B. L. & Sicotte, N. L. Microglia in Multiple Sclerosis: Friend or Foe? *Front. Immunol.* **11**, 1–8 (2020).
31. Bickford, P. C., Flowers, A. & Grimmig, B. Aging leads to altered microglial function that reduces brain resiliency increasing vulnerability to neurodegenerative diseases. *Exp. Gerontol.* **94**, 4–8 (2017).
32. Hickman, S. E., Allison, E. K. & El Khoury, J. Microglial dysfunction and defective β-amyloid clearance pathways in aging alzheimer's disease mice. *Journal of Neuroscience* **28**, 8354–8360 (2008).
33. Marschallinger, J. *et al.* Lipid-droplet-accumulating microglia represent a dysfunctional and proinflammatory state in the aging brain. *Nat. Neurosci.* **23**, 194–208 (2020).
34. Haney, M. S. *et al.* CD22 blockade restores homeostatic microglial phagocytosis in ageing brains. *Nature* doi:10.1038/s41586-019-1088-4
35. Compston, A. & Coles, A. Multiple sclerosis. *Lancet* **372**, 1502–1517 (2008).
36. Kearney, H. *et al.* Cervical cord lesion load is associated with disability independently from atrophy in MS. *Neurology* **84**, 367 LP – 373 (2015).
37. Lublin, F. D. & Reingold, S. C. Defining the clinical course of multiple sclerosis. *Neurology* **46**, 907 LP – 911 (1996).
38. Frischer, J. M. *et al.* neurodegeneration in multiple sclerosis brains. (2009). doi:10.1093/brain/awp070
39. Beecham, A. H. *et al.* Analysis of immune-related loci identifies 48 new susceptibility variants for multiple sclerosis. *Nat. Genet.* **45**, 1353–1362 (2013).
40. IMSGC. A high-density screen for linkage in multiple sclerosis. *Am. J. Hum. Genet.* **77**, 454–467 (2005).
41. Schaapveld, M. *et al.* Risk Alleles for Multiple Sclerosis Identified by a Genomewide Study. *N. Engl. J. Med.* **373**, 2499–2511 (2015).
42. Belbasis, L., Bellou, V., Evangelou, E., Ioannidis, J. P. A. & Tzoulaki, I. Environmental risk factors and multiple sclerosis: An umbrella review of systematic reviews and meta-analyses. *Lancet Neurol.* **14**, 263–273 (2015).
43. Lossius, A. *et al.* High-throughput sequencing of TCR repertoires in multiple sclerosis reveals intrathecal enrichment of EBV-reactive CD8+ T cells. *Eur. J. Immunol.* **44**, 3439–3452 (2014).
44. Münz, C., Lünemann, J. D., Getts, M. T. & Miller, S. D. Antiviral immune responses:

Triggers of or triggered by autoimmunity? *Nat. Rev. Immunol.* **9**, 246–258 (2009).

45. Hauser, S. L. *et al.* B-cell depletion with rituximab in relapsing-remitting multiple sclerosis. *N. Engl. J. Med.* **358**, 676–688 (2008).
46. Barr, T. A. *et al.* B cell depletion therapy ameliorates autoimmune disease through ablation of IL-6-producing B cells. *J. Exp. Med.* **209**, 1001–1010 (2012).
47. Haghikia, A., Hohlfeld, R., Gold, R. & Fugger, L. Therapies for multiple sclerosis: Translational achievements and outstanding needs. *Trends Mol. Med.* **19**, 309–319 (2013).
48. Ben-Nun, A. & Cohen, I. R. Vaccination against autoimmune encephalomyelitis (EAE): Attenuated autoimmune T lymphocytes confer resistance to induction of active EAE but not to EAE mediated by the intact T lymphocyte line. *Eur. J. Immunol.* **11**, 949–952 (1981).
49. Mendel, I., de Rosbo, N. K. & Ben-Nun, A. A myelin oligodendrocyte glycoprotein peptide induces typical chronic experimental autoimmune encephalomyelitis in H-2b mice: Fine specificity and T cell receptor Vβ expression of encephalitogenic T cells. *European Journal of Immunology* **25**, 1951–1959 (1995).
50. Ji, Q. & Goverman, J. Experimental autoimmune encephalomyelitis mediated by CD8+ T cells. *Ann. N. Y. Acad. Sci.* **1103**, 157–166 (2007).
51. Stromnes, I. M. & Goverman, J. M. Active induction of experimental allergic encephalomyelitis. *Nat. Protoc.* **1**, 1810–1819 (2006).
52. Barkauskas, D. S. *et al.* Focal transient CNS vessel leak provides a tissue niche for sequential immune cell accumulation during the asymptomatic phase of EAE induction. *Exp. Neurol.* **266**, 74–85 (2015).
53. Owens, T., Tran, E., Hassan-Zahraee, M. & Krakowski, M. Immune cell entry to the CNS - A focus for immunoregulation of EAE. *Res. Immunol.* **149**, (1998).
54. Caravagna, C. *et al.* Diversity of innate immune cell subsets across spatial and temporal scales in an EAE mouse model. *Sci. Rep.* **8**, 1–16 (2018).
55. Miller, S. D., Karpus, W. J. & Davidson, T. S. Experimental autoimmune encephalomyelitis in the mouse. *Curr. Protoc. Immunol.* (2010). doi:10.1002/0471142735.im1501s77
56. Croxford, A. L. *et al.* The Cytokine GM-CSF Drives the Inflammatory Signature of CCR2+ Monocytes and Licenses Autoimmunity. *Immunity* **43**, 502–514 (2015).
57. Komuczki, J. *et al.* Fate-Mapping of GM-CSF Expression Identifies a Discrete Subset

of Inflammation-Driving T Helper Cells Regulated by Cytokines IL-23 and IL-1β. *Immunity* **50**, 1289-1304.e6 (2019).

58. Skundric, D. S. *et al.* Distinct immune regulation of the response to H-2b restricted epitope of MOG causes relapsing-remitting EAE in H-2b/s mice. *J. Neuroimmunol.* **136**, 34–45 (2003).
59. Hirota, K. *et al.* Fate mapping of IL-17-producing T cells in inflammatory responses. *Nat. Immunol.* **12**, 255–263 (2011).
60. Codarri, L. *et al.* RORγ3t drives production of the cytokine GM-CSF in helper T cells, which is essential for the effector phase of autoimmune neuroinflammation. *Nature Immunology* **12**, 560–567 (2011).
61. Tzartos, J. S. *et al.* Interleukin-17 production in central nervous system-infiltrating T cells and glial cells is associated with active disease in multiple sclerosis. *Am. J. Pathol.* **172**, 146–155 (2008).
62. Olsson, T. Cytokines in neuroinflammatory disease: role of myelin autoreactive T cell production of interferon-gamma. *J. Neuroimmunol.* **40**, 211–218 (1992).
63. Langrish, C. L. *et al.* IL-23 drives a pathogenic T cell population that induces autoimmune inflammation. *J. Exp. Med.* **201**, 233–240 (2005).
64. Kroenke, M. A., Carlson, T. J., Andjelkovic, A. V. & Segal, B. M. IL-12- and IL-23-modulated T cells induce distinct types of EAE based on histology, CNS chemokine profile, and response to cytokine inhibition. *J. Exp. Med.* **205**, 1535–1541 (2008).
65. Jäger, A., Dardalhon, V., Sobel, R. A., Bettelli, E. & Kuchroo, V. K. Th1, Th17, and Th9 Effector Cells Induce Experimental Autoimmune Encephalomyelitis with Different Pathological Phenotypes. *J. Immunol.* **183**, 7169–7177 (2009).
66. Sethna, M. P. & Lampson, L. A. Immune modulation within the brain: recruitment of inflammatory cells and increased major histocompatibility antigen expression following intracerebral injection of interferon-γ. *Journal of Neuroimmunology* **34**, 121–132 (1991).
67. Simmons, R. D. & Willenborg, D. O. Direct injection of cytokines into the spinal cord causes autoimmune encephalomyelitis-like inflammation. *J. Neurol. Sci.* **100**, 37–42 (1990).
68. Willenborg, D. O., Fordham, S., Cowden, W. B., Ramshaw, I. A. & Bernard, C. C. A. IFN-γ Plays a Critical Down-Regulatory Role in the Induction and Effector Phase of Myelin Oligodendrocyte Glycoprotein-Induced Autoimmune Encephalomyelitis. *J.*

Immunol. **157**, 3223–3227 (1996).

69. Tran, E. H., Prince, E. N. & Owens, T. IFN-γ Shapes Immune Invasion of the Central Nervous System Via Regulation of Chemokines. *The Journal of Immunology* **164**, 2759–2768 (2000).
70. Ferber, I. A. *et al.* Mice with a disrupted IFN-gamma gene are susceptible to the induction of experimental autoimmune encephalomyelitis (EAE). *J. Immunol.* **156**, 5–7 (1996).
71. Krakowski, M. & Owens, T. Interferon-γ confers resistance to experimental allergic encephalomyelitis. *European Journal of Immunology* **26**, 1641–1646 (1996).
72. Arellano, G., Ottum, P. A., Reyes, L. I., Burgos, P. I. & Naves, R. Stage-specific role of interferon-gamma in experimental autoimmune encephalomyelitis and multiple sclerosis. *Front. Immunol.* **6**, (2015).
73. Ottum, P. A., Arellano, G., Reyes, L. I., Iruretagoyena, M. & Naves, R. Opposing roles of interferon-gamma on cells of the central nervous system in autoimmune neuroinflammation. *Front. Immunol.* **6**, 1–8 (2015).
74. Kohm, A. P., Carpentier, P. A., Anger, H. A. & Miller, S. D. Cutting Edge: CD4 + CD25 + Regulatory T Cells Suppress Antigen-Specific Autoreactive Immune Responses and Central Nervous System Inflammation During Active Experimental Autoimmune Encephalomyelitis . *J. Immunol.* **169**, 4712–4716 (2002).
75. Lowther, D. E. *et al.* Th1 not Th17 cells drive spontaneous MS-like disease despite a functional regulatory T cell response. *Acta Neuropathol.* **126**, 501–515 (2013).
76. Scheinecker, C., Göschl, L. & Bonelli, M. Treg cells in health and autoimmune diseases: New insights from single cell analysis. *J. Autoimmun.* **110**, 102376 (2020).
77. Garg, G. *et al.* Blimp1 Prevents Methylation of Foxp3 and Loss of Regulatory T Cell Identity at Sites of Inflammation. *Cell Rep.* **26**, 1854-1868.e5 (2019).
78. O'Connor, R. A., Malpass, K. H. & Anderton, S. M. The Inflamed Central Nervous System Drives the Activation and Rapid Proliferation of Foxp3 + Regulatory T Cells. *J. Immunol.* **179**, 958–966 (2007).
79. Korn, T. *et al.* Myelin-specific regulatory T cells accumulate in the CNS but fail to control autoimmune inflammation. *Nat. Med.* **13**, 423–431 (2007).
80. Vahl, J. C. *et al.* Continuous T Cell Receptor Signals Maintain a Functional Regulatory T Cell Pool. *Immunity* **41**, 722–736 (2014).
81. Levine, A. G., Arvey, A., Jin, W. & Rudensky, A. Y. Continuous requirement for the

TCR in regulatory T cell function. *Nat. Immunol.* **15**, 1070–1078 (2014).

82. Korn, T. & Kallies, A. T cell responses in the central nervous system. *Nat. Rev. Immunol.* **17**, 179–194 (2017).
83. Mildner, A. *et al.* CCR2+Ly-6Chi monocytes are crucial for the effector phase of autoimmunity in the central nervous system. (2009). doi:10.1093/brain/awp144
84. Wolf, Y. *et al.* Autonomous TNF is critical for in vivo monocyte survival in steady state and inflammation. *J. Exp. Med.* **214**, 905–917 (2017).
85. Yamasaki, R. *et al.* Differential roles of microglia and monocytes in the inflamed central nervous system. *J. Exp. Med.* **211**, 1533–1549 (2014).
86. Luo, C. The role of microglia in multiple sclerosis. *Brain and Nerve* **69**, 975–984 (2017).
87. Tröscher, A. R. *et al.* Microglial nodules provide the environment for pathogenic T cells in human encephalitis. *Acta Neuropathol.* **137**, 619–635 (2019).
88. Butovsky, O. & Weiner, H. L. Microglial signatures and their role in health and disease. *Nat. Rev. Neurosci.* **19**, 622–635 (2018).
89. Bogie, J. F. J., Stinissen, P. & Hendriks, J. J. A. Macrophage subsets and microglia in multiple sclerosis. *Acta Neuropathol.* **128**, 191–213 (2014).
90. Zrzavy, T. *et al.* Loss of 'homeostatic' microglia and patterns of their activation in active multiple sclerosis. *Brain* **140**, 1900–1913 (2017).
91. Goldmann, T. *et al.* A new type of microglia gene targeting shows TAK1 to be pivotal in CNS autoimmune inflammation. *Nat. Neurosci.* **16**, 1618–1626 (2013).
92. Voet, S. *et al.* A20 critically controls microglia activation and inhibits inflammasome-dependent neuroinflammation. *Nat. Commun.* **9**, (2018).
93. Dong, Y. & Yong, V. W. When encephalitogenic T cells collaborate with microglia in multiple sclerosis. *Nat. Rev. Neurol.* **15**, (2019).
94. Wolf, Y. *et al.* Microglial MHC class II is dispensable for experimental autoimmune encephalomyelitis and cuprizone-induced demyelination. *European Journal of Immunology* **48**, 1308–1318 (2018).
95. Mathys, H. *et al.* Temporal Tracking of Microglia Activation in Neurodegeneration at Single-Cell Resolution. *Cell Rep.* **21**, 366–380 (2017).
96. Mrdjen, D. *et al.* High-Dimensional Single-Cell Mapping of Central Nervous System Immune Cells Reveals Distinct Myeloid Subsets in Health, Aging, and Disease. *Immunity* **48**, 380-395.e6 (2018).

97. Masuda, T., Sankowski, R., Staszewski, O. & Prinz, M. Microglia Heterogeneity in the Single-Cell Era. *Cell Rep.* **30**, 1271–1281 (2020).
98. Tay, T. L., Sagar, Dautzenberg, J., Grün, D. & Prinz, M. Unique microglia recovery population revealed by single-cell RNAseq following neurodegeneration. *Acta Neuropathol. Commun.* **6**, 87 (2018).
99. Sousa, C. *et al.* Single-cell transcriptomics reveals distinct inflammation-induced microglia signatures. *EMBO reports* **19**, (2018).
100. Li, Q. *et al.* Developmental Heterogeneity of Microglia and Brain Myeloid Cells Revealed by Deep Single-Cell RNA Sequencing. *Neuron* **101**, 207-223.e10 (2019).
101. Hubstenberger, A. *et al.* P-Body Purification Reveals the Condensation of Repressed mRNA Regulons. *Mol. Cell* **68**, 144-157.e5 (2017).
102. Haimon, Z. *et al.* Re-evaluating microglia expression profiles using RiboTag and cell isolation strategies /631/1647/2017 /631/1647/2017/2079 technical-report. *Nat. Immunol.* **19**, 636–644 (2018).
103. AlJanahi, A. A., Danielsen, M. & Dunbar, C. E. An Introduction to the Analysis of Single-Cell RNA-Sequencing Data. *Mol. Ther. - Methods Clin. Dev.* **10**, 189–196 (2018).
104. Mereu, E. *et al.* Benchmarking single-cell RNA-sequencing protocols for cell atlas projects. *Nat. Biotechnol.* **38**, 747–755 (2020).
105. Van Den Brink, S. C. *et al.* Single-cell sequencing reveals dissociation-induced gene expression in tissue subpopulations. *Nat. Methods* **14**, 935–936 (2017).
106. Wu, Y. E., Pan, L., Zuo, Y., Li, X. & Hong, W. Detecting Activated Cell Populations Using Single-Cell RNA-Seq. *Neuron* **96**, 313-329.e6 (2017).
107. Sanz, E. *et al.* Cell-type-specific isolation of ribosome-associated mRNA from complex tissues. *Proc. Natl. Acad. Sci. U. S. A.* **106**, 13939–13944 (2009).
108. Heiman, M. *et al.* A Translational Profiling Approach for the Molecular Characterization of CNS Cell Types. *Cell* **135**, 738–748 (2008).
109. Jung, S. *et al.* Analysis of fractalkine receptor CX(3)CR1 function by targeted deletion and green fluorescent protein reporter gene insertion. *Mol Cell Biol* **20**, 4106–4114 (2000).
110. Yona, S. *et al.* Fate Mapping Reveals Origins and Dynamics of Monocytes and Tissue Macrophages under Homeostasis. *Immunity* **38**, 79–91 (2013).
111. Zhang, Y. *et al.* An RNA-Sequencing Transcriptome and Splicing Database of Glia,

Neurons, and Vascular Cells of the Cerebral Cortex. *J. Neurosci.* **34**, 11929–11947 (2014).

112. Orthgiess, J. *et al.* Neurons exhibit Lyz2 promoter activity in vivo: Implications for using LysM-Cre mice in myeloid cell research. *Eur. J. Immunol.* **46**, 1529–1532 (2016).
113. Kim, K. W. *et al.* In vivo structure/function and expression analysis of the CX 3C chemokine fractalkine. *Blood* **118**, 156–167 (2011).
114. Goldmann, T. *et al.* Origin, fate and dynamics of macrophages at central nervous system interfaces. *Nat. Immunol.* **17**, 797–805 (2016).
115. Chappell-maor, L. *et al.* Comparative analysis of CreER transgenic mice for the study of brain macrophages – a case study. 1–10 (2019). doi:10.1002/eji.201948342
116. Van Hove, H. *et al.* Identifying the variables that drive tamoxifen-independent CreERT2 recombination: Implications for microglial fate mapping and gene deletions. *European Journal of Immunology* **50**, 459–463 (2020).
117. Zeisel, A. & Muñoz-Manchado, A. B. Cell types in the mouse cortex and hippocampus revealed by single-cell RNA-seq. *Science (80-.).* **347**, 1138–1141 (2015).
118. A-Gonzalez, N. *et al.* Phagocytosis imprints heterogeneity in tissue-resident macrophages. *J. Exp. Med.* **214**, 1281–1296 (2017).
119. Derrien, T. *et al.* The GENCODE v7 catalogue of human long non-coding RNAs : Analysis of their structure , evolution and expression. *Genome Res.* **22**, 1775–1789 (2012).
120. Braunschweig, U. *et al.* Widespread intron retention in mammals functionally tunes transcriptomes. *Genome Res.* **24**, 1774–1786 (2014).
121. Khong, A. *et al.* The Stress Granule Transcriptome Reveals Principles of mRNA Accumulation in Stress Granules. *Mol. Cell* **68**, 808-820.e5 (2017).
122. Tebaldi, T. *et al.* Widespread uncoupling between transcriptome and translatome variations after a stimulus in mammalian cells. *BMC Genomics* **13**, 220 (2012).
123. Bahar Halpern, K. *et al.* Nuclear Retention of mRNA in Mammalian Tissues. *Cell Rep.* **13**, 2653–2662 (2015).
124. Nakamura, R. *et al.* Availability of a microglia and macrophage marker, Iba-1, for Differential diagnosis of spontaneous malignant reticuloses from astrocytomas in rats. *J. Toxicol. Pathol.* **26**, 55–60 (2013).
125. Erhardt, A. *et al.* CXCR3 Deficiency Exacerbates Liver Disease and Abrogates

Tolerance in a Mouse Model of Immune-Mediated Hepatitis. *J. Immunol.* **186**, 5284–5293 (2011).

126. Paust, H. J. *et al.* CXCR3+ regulatory T cells control TH1 responses in crescentic GN. *J. Am. Soc. Nephrol.* **27**, 1933–1942 (2016).
127. Groom, J. R. & Luster, A. D. CXCR3 in T cell function. *Exp. Cell Res.* **317**, 620–631 (2011).
128. Liu, L. *et al.* Severe Disease, Unaltered Leukocyte Migration, and Reduced IFN-γ Production in CXCR3 −/− Mice with Experimental Autoimmune Encephalomyelitis . *J. Immunol.* **176**, 4399–4409 (2006).
129. Müller, M. *et al.* CXCR3 Signaling Reduces the Severity of Experimental Autoimmune Encephalomyelitis by Controlling the Parenchymal Distribution of Effector and Regulatory T Cells in the Central Nervous System. *J. Immunol.* **179**, 2774–2786 (2007).
130. Pradelli, E. *et al.* Antagonism of chemokine receptor CXCR3 inhibits osteosarcoma metastasis to lungs. *Int. J. Cancer* **125**, 2586–2594 (2009).
131. Candotti, F. Clinical Manifestations and Pathophysiological Mechanisms of the Wiskott-Aldrich Syndrome. *J. Clin. Immunol.* **38**, 13–27 (2018).
132. Rivers, E. & Thrasher, A. J. Wiskott-Aldrich syndrome protein: Emerging mechanisms in immunity. *European Journal of Immunology* **47**, 1857–1866 (2017).
133. Malinova, D. *et al.* WASp-dependent actin cytoskeleton stability at the dendritic cell immunological synapse is required for extensive, functional T cell contacts. *J. Leukoc. Biol.* **99**, 699–710 (2016).
134. Massaad, M. J., Ramesh, N. & Geha, R. S. Wiskott-Aldrich syndrome: A comprehensive review. *Ann. N. Y. Acad. Sci.* **1285**, 26–43 (2013).
135. Baron, J. L., Madri, J. A., Ruddle, N. H., Hashim, G. & Janeway, C. A. Surface expression of α4 integrin by CD4 T cells is required for their entry into brain parenehyma. *J. Exp. Med.* **177**, 57–68 (1993).
136. Panitch, H. S., Haley, A. S., Hirsch, R. L. & Johnson, K. P. Exacerbations of Multiple Sclerosis in Patients Treated With Gamma Interferon. *Lancet* **329**, 893–895 (1987).
137. Beck, J. *et al.* Increased production of interferon gamma and tumor necrosis factor precedes clinical manifestation in multiple sclerosis: Do cytokines trigger off exacerbations? *Acta Neurol. Scand.* **78**, 318–323 (1988).
138. Arellano, G. *et al.* Th1 and Th17 cells and associated cytokines discriminate among

clinically isolated syndrome and multiple sclerosis phenotypes. *Front. Immunol.* **8**, 1–10 (2017).

139. Billiau, A. *et al.* Enhancement of experimental allergic encephalomyelitis in mice by antibodies against IFN-gamma. (1988).
140. Carter, S. L., Müller, M., Manders, P. M. & Campbell, I. L. Induction of the genes for Cxcl9 and Cxcl10 is dependent on IFN-γ but shows differential cellular expression in experimental autoimmune encephalomyelitis and by astrocytes and microglia in vitro. *Glia* **55**, 1728–1739 (2007).
141. Naves, R. *et al.* The Interdependent, Overlapping, and Differential Roles of Type I and II IFNs in the Pathogenesis of Experimental Autoimmune Encephalomyelitis. *J. Immunol.* **191**, 2967–2977 (2013).
142. Hirrlinger, J. *et al.* Split-Cre complementation indicates coincident activity of different genes in vivo. *PLoS One* **4**, 1–10 (2009).
143. Boutej, H. *et al.* Diverging mRNA and Protein Networks in Activated Microglia Reveal SRSF3 Suppresses Translation of Highly Upregulated Innate Immune Transcripts. *Cell Rep.* **21**, 3220–3233 (2017).
144. Van Hove, H. *et al.* A single-cell atlas of mouse brain macrophages reveals unique transcriptional identities shaped by ontogeny and tissue environment. *Nat. Neurosci.* **22**, 1021–1035 (2019).
145. Buks, E., Schuster, R., Heiblum, M., Mahalu, D. & Umansky, V. Dephasing in electron intererence by a 'which path' detector. *Nat.* **391**, 871 (1998).
146. Askew, K. *et al.* Coupled Proliferation and Apoptosis Maintain the Rapid Turnover of Microglia in the Adult Brain. *Cell Rep.* **18**, 391–405 (2017).
147. Miron, V. E. Microglia-driven regulation of oligodendrocyte lineage cells, myelination, and remyelination. *J. Leukoc. Biol.* **101**, 1103–1108 (2017).
148. Lloyd, A. F. *et al.* Central nervous system regeneration is driven by microglia necroptosis and repopulation. *Nat. Neurosci.* **22**, 1046–1052 (2019).
149. Keller, C. W. *et al.* CYBB/NOX2 in conventional DCs controls T cell encephalitogenicity during neuroinflammation. *Autophagy* **00**, 1–15 (2020).
150. Ryu, J. K. *et al.* Fibrin-targeting immunotherapy protects against neuroinflammation and neurodegeneration. *Nat. Immunol.* **19**, 1212–1223 (2018).
151. Bennett, J. *et al.* Blood-brain barrier disruption and enhanced vascular permeability in the multiple sclerosis model EAE. *J. Neuroimmunol.* **229**, 180–191 (2010).

152. Lewis, N. D., Hill, J. D., Juchem, K. W., Stefanopoulos, D. E. & Modis, L. K. RNA sequencing of microglia and monocyte-derived macrophages from mice with experimental autoimmune encephalomyelitis illustrates a changing phenotype with disease course. *J. Neuroimmunol.* **277**, 26–38 (2014).
153. Vainchtein, I. D. *et al.* In acute experimental autoimmune encephalomyelitis, infiltrating macrophages are immune activated, whereas microglia remain immune suppressed. *Glia* **62**, 1724–1735 (2014).
154. Mirshahidi, S. & Huang, C. Anergy in Peripheral Memory CD4 ♀ T Cells Induced by Low Avidity Engagement of T Cell Receptor. **194**, (2001).
155. Ebner, F. *et al.* Microglial Activation Milieu Controls Regulatory T Cell Responses. *J. Immunol.* **191**, 5594–5602 (2013).
156. Bohlen, C. J. *et al.* Diverse Requirements for Microglial Survival, Specification, and Function Revealed by Defined-Medium Cultures. *Neuron* **94**, 759-773.e8 (2017).
157. Kishimoto, H. & Sprent, J. Strong TCR ligation without costimulation causes rapid onset of Fas-dependent apoptosis of naive murine CD4+ T cells. *J. Immunol.* **163**, 1817–26 (1999).
158. Do, J. *et al.* Treg-specific IL-27Rα deletion uncovers a key role for IL-27 in Treg function to control autoimmunity. *Proceedings of the National Academy of Sciences of the United States of America* **114**, 10190–10195 (2017).
159. Hall, A. O. H. *et al.* The Cytokines Interleukin 27 and Interferon-γ Promote Distinct Treg Cell Populations Required to Limit Infection-Induced Pathology. *Immunity* **37**, 511–523 (2012).
160. McFadden, C. *et al.* Preferential Migration of T Regulatory Cells Induced by IL-16. *J. Immunol.* **179**, 6439–6445 (2007).
161. Suciu-Foca, N. & Cortesini, R. Central role of ILT3 in the T suppressor cell cascade. *Cell. Immunol.* **248**, 59–67 (2007).
162. Millward, J. M., Løbner, M., Wheeler, R. D. & Owens, T. Inflammation in the Central Nervous System and Th17 Responses Are Inhibited by IFN-γ–Induced IL-18 Binding Protein. *The Journal of Immunology* **185**, 2458–2466 (2010).
163. Wilcox, R. A. *et al.* B7-H1 (PD-L1, CD274) suppresses host immunity in T-cell lymphoproliferative disorders. *Blood* **114**, 2149–2158 (2009).
164. de Goeje, P. L. *et al.* Immunoglobulin-like transcript 3 is expressed by myeloid-derived suppressor cells and correlates with survival in patients with non-small cell lung

cancer. *Oncoimmunology* **4**, 1–11 (2015).

165. Context-dependent role of IL-18 in cancer biology and counter-regulation by IL-18BP.pdf.
166. Lu, C., Redd, P. S., Lee, J. R., Savage, N. & Liu, K. The expression profiles and regulation of PD-L1 in tumor-induced myeloid-derived suppressor cells. *Oncoimmunology* **5**, 1–13 (2016).
167. Nissen, J. C., Thompson, K. K., West, B. L. & Tsirka, S. E. Csf1R inhibition attenuates experimental autoimmune encephalomyelitis and promotes recovery. *Exp. Neurol.* **307**, 24–36 (2018).
168. Tanabe, S., Saitoh, S., Miyajima, H., Itokazu, T. & Yamashita, T. Microglia suppress the secondary progression of autoimmune encephalomyelitis. *Glia* **67**, 1694–1704 (2019).
169. Lei, F. *et al.* CSF1R inhibition by a small-molecule inhibitor is not microglia specific; affecting hematopoiesis and the function of macrophages. *Proc. Natl. Acad. Sci.* **0**, 201922788 (2020).
170. Rubino, S. J. *et al.* Acute microglia ablation induces neurodegeneration in the somatosensory system. *Nat. Commun.* **9**, 4578 (2018).
171. Elmore, M. R. P. *et al.* Colony-Stimulating Factor 1 Receptor Signaling Is Necessary for Microglia Viability, Unmasking a Microglia Progenitor Cell in the Adult Brain. *Neuron* **82**, 380–397 (2014).
172. Ruedl, C. & Jung, S. DTR-mediated conditional cell ablation—Progress and challenges. *European Journal of Immunology* **48**, 1114–1119 (2018).
173. Kornete, M. *et al.* Th1-like ICOS+ Foxp3+ Treg cells preferentially express CXCR3 and home to β-islets during pre-diabetes in BDC2.5 NOD mice. *PLoS ONE* **10**, (2015).
174. Tan, T. G., Mathis, D. & Benoist, C. Singular role for T-BET+CXCR3+ regulatory T cells in protection from autoimmune diabetes. *Proc. Natl. Acad. Sci. U. S. A.* **113**, 14103–14108 (2016).
175. Hasegawa, H. *et al.* Therapeutic effect of CXCR3-expressing regulatory T cells on liver, lung and intestinal damages in a murine acute GVHD model. *Gene Ther.* **15**, 171–182 (2008).
176. Giladi, A. *et al.* Cxcl10 + monocytes define a pathogenic subset in the central nervous system during autoimmune neuroinflammation. *Nat. Immunol.* **21**, 525–534 (2020).
177. Liu, Y. *et al.* FoxA1 directs the lineage and immunosuppressive properties of a novel

regulatory T cell population in EAE and MS. *Nat. Med.* **20**, 272–282 (2014).

178. Hsu, P. D. *et al.* DNA targeting specificity of RNA-guided Cas9 nucleases. *Nat. Biotechnol.* **31**, 827–832 (2013).
179. Doench, J. G. *et al.* Optimized sgRNA design to maximize activity and minimize off-target effects of CRISPR-Cas9. *Nat. Biotechnol.* **34**, 184–191 (2016).
180. Xu, H. *et al.* Sequence determinants of improved CRISPR sgRNA design. *Genome Res.* **25**, 1147–1157 (2015).
181. Chari, R., Mali, P., Moosburner, M. & Church, G. M. Unraveling CRISPR-Cas9 genome engineering parameters via a library-on-library approach. *Nat. Methods* **12**, 823–826 (2015).
182. Gertsenstein, M. & Nutter, L. M. J. Engineering Point Mutant and Epitope-Tagged Alleles in Mice Using Cas9 RNA-Guided Nuclease. *Current protocols in mouse biology* **8**, 28–53 (2018).
183. Takeo, T., Sztein, J. & Nakagata, N. The CARD Method for Mouse Sperm Cryopreservation and In Vitro Fertilization Using Frozen-Thawed Sperm. in *Microinjection: Methods and Protocols* (eds. Liu, C. & Du, Y.) 243–256 (Springer New York, 2019). doi:10.1007/978-1-4939-8831-0_14
184. Jaitin, D. A. *et al.* Massively Parallel Single-Cell RNA-Seq for Marker-Free Decomposition of Tissues into Cell Types. *Science (80-.).* **343**, 776–779 (2014).
185. Tilgner, H. *et al.* Deep sequencing of subcellular RNA fractions shows splicing to be predominantly co-transcriptional in the human genome but inefficient for lncRNAs. *Genome Res.* **22**, 1616–1625 (2012).
186. Gosselin, D. *et al.* Environment drives selection and function of enhancers controlling tissue-specific macrophage identities. *Cell* **159**, 1327–1340 (2014).